

**Magnezyum alařımlarının dűřük sıcaklık deformasyon
kabiliyetinin geliřtirilmesi**

**Enhancement of the low temperature deformation ability
of magnesium alloys**

VAHİD ATTARI

Thesis

Submitted to the Office of Graduate Studies

In partial fulfillment of the requirements for the degree of

MASTER OF SCIENCE

In

Mechanical Engineering Department

Hacettepe University

2012

Enhancement of the low temperature deformation ability of magnesium alloys

Vahid Attari

ABSTRACT

In general, magnesium alloys exhibit the attractive combinations of low densities (1.74 g/cm^3 versus 2.7 g/cm^3 for Al) and high specific strength values (comparable or greater than that of precipitation strengthened Al alloys), along with good damping capacity, castability, weldability, and machinability. Conventional magnesium alloys can be divided into five main groups (Mg-Al-Zn, Mg-Zn-Zr, Mg-Rare Earth-Zr, Mg-Th-Al, Mg-Li-Al) and among these alloys, those developed from the Mg-Al-Zn ternary system (i.e. coded as AZ alloys) have found great interest and the vast number of industrial applications.

The main objective of this thesis is to enhance the mechanical properties of AZ31 and AZ91 Mg alloys. AZ31 and AZ91 magnesium alloy plates with 3% and 9% aluminum respectively were purchased from Turkey and China. AZ31 and AZ91 samples were homogenized at 400°C for 2 hours and at 425°C for 15 minutes respectively to break up the casting microstructure and to eliminate chemical inhomogeneity.

Both alloys were aged at $150\text{-}200\text{-}250^\circ\text{C}$ for 1-5-10-24-50-100 hours to see the effect of aging on the microstructural evolution and its influence on the evolution of mechanical properties of these alloys.

Furthermore, aging under stress experiments were performed at the same temperature for one hour, by applying constant stress values (20, 40, 60 and 80 MPa) which are in the elastic range of the alloys. The influence of these thermo-mechanical processes on the evolution of microstructures and mechanical properties was investigated and compared with the aged samples.

Aging heat treatments were performed using a tabletop furnace and aging under stress experiments were performed using an environmental chamber which was designed and manufactured for this study. Strain measurements were performed using high temperature extensometer with ceramic rods.

The samples were analyzed with XRD¹ to examine the phase characterizations, and furthermore were investigated by SEM/EDS². Also tensile tests were conducted at room temperature to understand the evolution of the mechanical properties after thermo-mechanical and aging processes. The effect of formation and growth of the β -Mg₁₇Al₁₂ precipitates was investigated in the aged samples and the influence of the 3rd parameter (stress) was further examined in the age-tensioned samples.

Investigation of the aged samples for both of the alloys shows that the amounts of the precipitates were increased by increasing the temperature and the aging time. SEM and optical microscopy results revealed the precipitate distribution in the matrix of both alloys.

Aging under stress treatments caused a considerable increase in the strength and ductility of AZ91. A smooth increase in the ductility and strength values of AZ31 was observed after short period thermo-mechanical treatments. It was also shown that 100 hours of aging periods were not necessary for further improvements in the strength and ductility.

Keywords: Magnesium alloys, Aging, Aging under stress, quantitative characterization, Microstructure, Mechanical properties, XRD, SEM

Advisor: Assistant Prof. Dr. Benat Kockar, Hacettepe University, Mechanical Engineering Dept.

¹ X-Ray Power Diffraction method

² Scanning Electron Microscopy/Energy Dispersive Spectroscopy

Magnezyum alařımlarının dūřuk sıcaklık deformasyon kabiliyetinin geliřtirilmesi

Vahid Attari

ÖZ

Magnezyum alařımları ok dūřuk bir yoęunluęa (1.74 g/cm^3) sahip olmakla beraber, alūminyum benzeri alařımlarla (Al: 2.7 g/cm^3) neredeyse aynı ve/veya daha yūksel oęgūl mukavemete sahiptirler. Ayrıca magnezyum alařımları iyi sōnūmlene kapasitesine sahiptirler ve ūstelik kaynak, dōkūm ve ikincil malzeme iřlemleri de yapılmaktadır. Konvansiyonel olarak kullanılan magnezyum alařımları, beř ana gruba (Mg-Al-Zn, Mg-Zn-Zr, Mg-Toprak Metaller-Zr, Mg-th-Al, Mg-Li-Al) ayrılmaktadırlar ve bunlar arasında Mg-Al-Zn alařımları (AZ alařımları olarak kodlanmıřtır) olduka ōnemli bir yere sahiptir.

Bu tezin ana amacı, AZ31 ve AZ91 alařımlarının mekanik ōzelliklerini geliřtirmektir. AZ31 alařımı %3 alūminyum ierir ve AZ91 alařımı ise %9 alūminyum ierir. alıřma sūresince kullanılan AZ31 malzemesi yerli ūreticiden, AZ91 malzemesi ise yabancı ūreticiden (in) levha řeklinde satın alınmıřtır. AZ31 malzemesinin dōkūm mikroyapısını bozmak iin, 400°C de 2 saat boyunca homojenizasyon ısıl iřlemi yapılmıřtır. AZ91 numunelerine ise daha homojen yapı elde etmek amacıyla, 425°C de 15 dakika boyunca homojenizasyon yapılmıřtır.

Homojenize edilmiř numunelere, 1-5-10-24-50-100 saatlik sūrelerde, ū farklı sıcaklıkta ($150\text{-}200\text{-}250^\circ\text{C}$) yařlandırma ısıl iřlemleri uygulanmıřtır. Yapılan ısıl iřlemlerle, malzemelerdeki mikroyapı deęiřiklikleri ve ardından bu deęiřikliklerin mekanik ōzelliklerinin evrimindeki etkileri incelenmiřtir.

Yařlandırma ısıl iřlemlerinin ardından, literatūrde daha ōnce hi yapılmamıř, bir saat boyunca ve aynı sıcaklıklarda sabit gerilim altında ($20\text{-}40\text{-}60\text{-}80\text{MPa}$) yařlandırma iřlemleri uygulanmıřtır. Bu termo-mekanik iřlemlerin amacı, uygulanan gerilimin mikroyapı ve mekanik ōzellikler ūzerindeki etkisini incelemektir. Bu termo-mekanik iřlemlerin sonrasında elde edilen mekanik ōzelliklerdeki deęiřikliklerle, yařlandırma deneyleri sonrası mekanik ōzelliklerdeki deęiřim karřılařtırılmıřtır.

Yaşlandırma ısı işlemleri Protherm masaüstü fırını ile yapılmıştır. Sabit gerilim altında yaşlandırma deneyleri özel olarak tasarlanmış ve imal edilmiş bir çember fırında yapılmıştır. Gerinim değerleri, yüksek sıcaklığa dayanıklı olan bir seramik çubuklu extensometre ile ölçülmüştür.

Tüm numuneler, faz karakterizasyonu yöntemleri ile (XRD³, SEM/EDS⁴) ve ayrıca oda sıcaklığında çekme testleri ile incelenmiştir. Bütün bu analizler mikroyapı evrimi ve bu evrimin mekanik özelliklere olan etkisini incelemek amacıyla yapılmıştır. β -Mg₁₇Al₁₂ çökeltilerinin oluşması ve büyümelerinin etkisi yaşlandırılmış numunelerde incelenmiştir ve 3. parametre olarak uygulan gerilimin etkisi, sabit gerilim altında yaşlandırılmış numunelerde incelenmiştir.

Yapılan yaşlandırma deneyleri sonucunda, her iki malzemede de sıcaklık ve sürelerin artışı ile β -Mg₁₇Al₁₂ çökeltilerin miktarı artmaktadır. Ayrıca SEM ve optik mikroskop sonuçları çökeltilerin mikroyapıdaki dağılımlarının her iki alaşımda iyi bir şekilde açığa vurmaktadır.

Yapılan termo-mekanik işlemleri sonucunda, AZ91 alaşımlarının, dayanımı ve sünekliğinde büyük bir artış gözlemlenmiştir. AZ31 alaşımında ise daha az bir artış gözlemlenmiştir. Süneklik ve dayanım değerleri, kısa süreli termo-mekanik işlemlerinden sonra önemli bir artış göstermektedirler. Bu sebeple 100 saatlik gibi uzun süreli yaşlandırma ısı işlemlerinin gerekli olmadığı gösterilmiştir.

Anahtar Kelimeler : Magnezyum alaşımları, yaşlandırma , gerilim altında yaşlandırma, karakterizasyon ,mikroyapı, mekanik özellikler , XRD , SEM

Danışman : Yrd. Doç. Dr. Benat Koçkar, Hacettepe Üniversitesi, Makina Mühendisliği Bölümü

³ X-Işını Kırınım yöntemi

⁴ Taramalı Elektron Mikroskobu / Elektron Dağılım Spektroskopisi

To

MY MOTHER SHAMSI SAKKAKI, MY FATHER MANSOUR ATTARI,

MY WIFE NASRIN ATTARI

AND MY ADVISOR DR. BENAT KOCKAR

TO WHOM I OWE MY EDUCATIONAL CAREER.

ACKNOWLEDGEMENTS

I would first like to thank my advisor Dr. Benat Kockar for her support, guidance, friendship and excellent training for experimental and analytical skills. In addition, her incredible vision in the general philosophy of research led me produce results that are worthy of writing this thesis. I would like to thank for her patience and motivating me in my research subjects.

Also I would like to thank all those people who helped me during my studies and made this thesis an unforgettable experience for me. I would like to express my great appreciations for my beloved wife Nasrin who helped me a lot during my M.Sc. studies.

My sincere thanks also goes to my dear friend, Hamed Samandari for his helps and friendship during my stay in Ankara. I hope great successes for him in every aspect of his life and education.

I would also like to thank my fellow labmate, Hande Özcan who helped me in all aspects of my research and living in Ankara. I am hoping great scientific successes for her in the near future.

I take this opportunity to express the profound gratitude from my deep heart to my beloved parents, grandparents, and my siblings for their love and continuous support – both spiritually and materially. Without their support, I could not complete my degree.

Finally, I would like to thank TUBITAK MAG group for supporting the project “110M719” titled as “Enhancement of the Low temperature deformation ability of magnesium alloys”. This thesis was performed as a part of this project.

TABLE OF CONTENTS

ABSTRACT	i
ÖZ	iii
ACKNOWLEDGEMENTS.....	vi
TABLE OF CONTENTS	vii
TABLE OF FIGURES	ix
LIST OF TABLES	xii
1 INTRODUCTION	1
1.1 Motivation.....	1
2 THEORETICAL BACKGROUND.....	3
2.1 Origin and characteristics of Mg chemical element.....	3
2.2 Extraction and production history (Until 1997)	4
2.3 Extraction and production (2010).....	4
2.4 Mg Metal Forming Processes	5
2.5 Magnesium Alloys.....	7
2.5.1 Cast Alloys.....	9
2.5.2 Wrought Alloys.....	10
2.6 AZ31 and AZ91 Alloys	12
2.7 Material strengthening methods.....	15
2.7.1 Age-hardening:	15
2.8 Deformation mechanisms in magnesium	16
2.8.1 Mg Crystal structure.....	16
2.8.2 Slip systems in Magnesium	17
2.8.3 Twinning mechanism in Magnesium.....	19
2.9 Strengthening mechanisms for Mg alloys	20
2.9.1 Dislocation Strengthening.....	20
2.9.2 Solid Solution Hardening	21
2.9.3 Precipitation Strengthening.....	22
2.10 Latest related research	23
3 EXPERIMENTAL PROCEDURE	26
3.1 Materials	26
3.2 Heat treatment	26
3.3 Thermo-mechanical Procedure.....	29
3.3.1 Thermo-mechanical experiment set-up	29
3.3.2 Thermo-mechanical Treatments.....	31
3.4 Microstructural Characterization	33
3.4.1 Surface Microscopy and characterization.....	33

3.4.2	Quantitative X-Ray Diffraction.....	37
3.5	Mechanical Behavior Characterization.....	37
4	RESULTS AND DISCUSSION	40
4.1	Enhancement of AZ31	40
4.1.1	Aging heat treatment	40
4.1.2	Phase study in AZ31.....	48
4.1.3	Aging under stress.....	53
4.1.4	Tensile testing of AZ31	57
4.2	Enhancement of AZ91	62
4.2.1	Aging heat treatment	62
4.2.2	Phase study in AZ91.....	69
4.2.3	Aging under stress.....	70
4.2.4	Tensile testing of AZ91	76
5	Summary of results, conclusions and future works.....	82
5.1	Summary of results and conclusions	82
5.2	Future works and suggestions	84
	References	85
	Curriculum vitae	89

TABLE OF FIGURES

Figure 2.1 General forming processes for AZ31 alloy at POSCO. South Korea [9]	6
Figure 2.2 Some of the main metal forming methods for Mg alloys [9].....	7
Figure 2.3 Liquid solubility of elements in binary magnesium alloys [14, 15]	9
Figure 2.4 Cast and wrought alloys mechanical properties comparison [16].....	11
Figure 2.5 Typical tensile yield strength and elongation to failure values for commercial Mg alloys and some other Mg alloys under investigation [17]	11
Figure 2.6 α -Mg and β -Mg ₁₇ Al ₁₂ in AZ91 (left) and α -Mg and β -Mg ₁₇ Al ₁₂ in AM60 (Right) [1].....	12
Figure 2.7 Mn-Al compounds of different shapes [1]	13
Figure 2.8 Mg ₂ Si particles [1]	13
Figure 2.9 Oxide films and oxide clusters [1].....	13
Figure 2.10 dislocations crossing the precipitates [21]	16
Figure 2.11 Atoms, planes and directions in hcp metals [23]	17
Figure 2.12 CRSS for basal and non-basal slip at room and elevated temperatures [26]	18
Figure 2.13 Slip and twinning in a crystal [21]	19
Figure 3.1 Binary phase diagram of Mg-Al alloy system, showing homogenization points for AZ31 and AZ91 alloys [13]	27
Figure 3.2 Binary phase diagram of Mg-Al alloy system, showing aging points for AZ31 and AZ91 alloys [13]	28
Figure 3.3 Temperature vs. Time schematic for aging heat treatments and the digital image of tabletop furnace.....	28
Figure 3.4 Mounting plots of environmental chambers on the UTM	29
Figure 3.5 a) PID controllers for 3 zones separately b) the data acquisition device connected through USB to PC c) external controller thermocouple and the hole in front of the chamber	30
Figure 3.6 Designed chamber and grips and the final assembly	31
Figure 3.7 Heat treatment procedure for aging under stress experiments	32
Figure 3.8 Cold mounting mold and sample	34
Figure 3.9 Nikon optical microscope	34
Figure 3.10 a) Match! Crystal Impact software b) Rigaku Ultima IV XRD device .	38
Figure 3.11 The Epsilon 3448 high temperature extensometer	38
Figure 3.12 Tension sample and the related dimensions according to ASTM standard	39
Figure 4.1 Microstructure of as-received twin-rolled AZ31 left) 50X right) 500X..	42
Figure 4.2 Microstructure of the homogenized AZ31 right) 500X left) 1000X.....	42
Figure 4.3 Microstructure of aged AZ31 for 1hr at a) 150°C b) 200°C c) 250°C	43
Figure 4.4 Microstructure of aged AZ31 for 24hrs at a) 150°C b) 200°C c) 250°C.	44
Figure 4.5 Investigation of the chemical composition of AZ31 sample aged at 250°C for 1 hour using EDS.....	46
Figure 4.6 Detailed investigation of chemical composition and microstructure of AZ31 which was aged at 250°C for 10hrs	46
Figure 4.7 Microstructural and precipitate evolution after a) 10hrs and b) 24hrs of aging heat treatments at 200C	47
Figure 4.8 Precipitate distribution and shapes at 24H-200°C aging heat treatment a)3000x b)6000x c)22000x.....	47
Figure 4.9 Precipitate distribution and shapes in the AZ31 sample aged at 250°C for 24 hrs a)2500x b)5000x c)16000x.....	48

Figure 4.10 Comparison of the XRD patterns of the samples aged at different temperatures for 1Hour.	49
Figure 4.11 Comparison of the XRD patterns of the samples aged at different temperatures for 5 Hours.	50
Figure 4.12 Comparison of the XRD patterns of the samples aged at 250°C for different aging periods.....	50
Figure 4.13 Comparison of the XRD pattern of the samples aged at different temperatures for 24 Hours	51
Figure 4.14 Applied stress vs Time curves for the samples aged at 250°C under 20, 40, 60 and 80MPa for 1hr.....	54
Figure 4.15 Applied stress vs Time curves for the samples aged at 200°C under 20 and 40MPa for 1hr.....	54
Figure 4.16 Applied stress vs Time curves for the samples aged at 150°C under 20, 40 and 60MPa for 1hr.....	55
Figure 4.17 Temperature vs Time curves for the samples age-tensioned at 150, 200 and 250°C samples.	56
Figure 4.18 Creep behavior and fracture of AZ31 under 80MPa loading	56
Figure 4.19 Tensile test results of the samples aged at 150, 200, 250°C for 1 hr, as-received and homogenized samples.	57
Figure 4.20 Tensile test results of the samples aged at 150°C for 1, 5, 24, 50 and 100hrs under no stress and for 1hr under 20, 40 and 60MPa constant stress levels.	58
Figure 4.21 Tensile test results of the samples aged at 200°C for 1, 5, 24, 50,100 hrs under no stress and for 1 hr under 20 and 40MPa.	59
Figure 4.22 Tensile test results of the samples aged at 250°C for 1, 5, 24, 50,100 hrs under no stress and for 1 hr under 20, 40MPa and 60MPa.....	60
Figure 4.23 AZ91 samples a) before homogenization and b) after homogenization	63
Figure 4.24 Vaporized AZ91 sample which was tried to be homogenized at 450C for 30 Minutes.....	64
Figure 4.25 Microstructure of aged samples for 1 hour at a) 150°C b) 200°C c) 250°C	64
Figure 4.26 Microstructure of aged samples for 24 hours at a) 150°C b) 200°C c) 250°C	65
Figure 4.27 Microstructure of aged samples for 50 hours at a) 150°C b) 200°C c) 250°C	65
Figure 4.28 Precipitate distribution along the grain boundaries of AZ91 samples aged for left) 50hrs at 250°C and for right) 24hrs at 150°C	65
Figure 4.29 The precipitate distribution in the matrix and along the grain boundaries of the AZ91 sample which was aged at 200°C for 24 hrs	66
Figure 4.30 The precipitate distribution in the matrix and along the grain boundaries of the AZ91 sample which was aged at 250°C for 24 hrs.	66
Figure 4.31 Energy Dispersive Spectroscopy of precipitates in AZ91 alloy.....	67
Figure 4.32 Energy Dispersive Spectroscopy of the shown region and presence of “Ca” and “Si” in AZ91 structure.....	68
Figure 4.33 AZ91 XRD pattern comparison for 24 hours aging.....	69
Figure 4.34 Applied stress vs Time curves for the samples aged at 250°C under 20, 40, 60 and 80MPa for 1hr.....	71
Figure 4.35 Applied stress vs Time curves for the samples aged at 200°C under 20, 40 and 60 MPa for 1hr.....	71

Figure 4.36 Applied stress vs Time curves for the samples aged at 150°C under 20, 40 and 60MPa for 1hr.....	72
Figure 4.37 Microstructure of the aged-tensioned sample at 250°C for 1hr under 20Mpa constant stress from the a) sample middle section b) grip section	72
Figure 4.38 Microstructure of the age-tensioned sample at 150°C for 1hr under 40MPa stress from the a) sample middle section b) grip section	73
Figure 4.39 Microstructure of the age-tensioned sample at 200°C for 1hr under 40MPa constant stress from the a) sample middle section b) grip section.....	74
Figure 4.40 Microstructure of the age-tensioned sample at 250°C for 1hr under 40MPa constant stress from the a) sample middle section b) grip section.....	74
Figure 4.41 Microstructure of the age-tensioned samples at 250C for 1hr under a) 40MPa b) 20MPa c) No Stress.....	74
Figure 4.42 The dislocations and the precipitates in the microstructure of the sample which was age-tensioned at 250°C for 1hr under 20MPa constant stress	75
Figure 4.43 Tensile test results of the samples aged at 150, 200, 250°C for 1 hr, as-received and homogenized samples.	77
Figure 4.44 Tensile test results of the samples aged at 150°C for 1,5,24,50 and 100hrs under no stress and for 1hr under 20, 40 and 60MPa constant stress levels.	77
Figure 4.45 Tensile test results of the samples aged at 200°C for 1,5,24,50 and 100hrs under no stress and for 1hr under 20, 40 and 60MPa constant stress levels.	79
Figure 4.46 Tensile test results of the samples aged at 250°C for 1,5,24,50 and 100hrs under no stress and for 1hr under 20, 40 and 60MPa constant stress levels.	79

LIST OF TABLES

Table 2.1 Magnesium production statistics around the world in 2010 [8]	5
Table 2.2 Typical Mg Cast & wrought alloys [13].....	8
Table 2.3 Mechanical properties of AZ31 under different conditions [18, 19]	14
Table 2.4 Mechanical properties of AZ31 & AZ91 at elevated temperatures [18-20]	14
Table 2.5 Slip systems in hcp metals [8]	18
Table 3.1 Chemical compositional of the alloys.....	26
Table 3.2 Protherm Environmental chamber specifications	30
Table 3.3 Thermo-mechanical experiments procedure	32
Table 3.4 Six-step grinding polishing procedure.....	35
Table 3.5 The used etchants for microstructure revealing[13].....	36
Table 4.1 Aging conditions for AZ31 alloy	41
Table 4.2 Crystal structures and phase descriptions.....	48
Table 4.3 Results which are obtained from the XRD patterns of AZ31 samples which are aged at 250°C	52
Table 4.4 Calculated parameters for the AZ31-24Hour-250°C aged sample	52
Table 4.5 AZ31 aging under stress experiments	53
Table 4.6 AZ31 Tensile Properties for 150°C Heat Treatments	60
Table 4.7 AZ31 Tensile Properties for 200°C Heat Treatments	61
Table 4.8 AZ31 Tensile Properties for 250°C Heat Treatments	61
Table 4.9 Aging conditions for AZ91 alloy	63
Table 4.10 AZ91 aging under stress experiments.....	70
Table 4.11 AZ91 Tensile Properties for 150°C Heat Treatments	80
Table 4.12 AZ91 Tensile Properties for 200°C Heat Treatments	80
Table 4.13 AZ91 Tensile Properties for 250°C Heat Treatments	81

1 INTRODUCTION

1.1 Motivation

Magnesium alloys among other metal alloys such as steel and copper can be considered as very promising candidates for different structural applications due to their low weight and high specific strength properties. Good castability and easy machining properties make the Mg alloys a good candidate for the replacement of Al and Fe alloys which are widely used in industries such as aerospace and automotive.

Energy efficiency is currently one of the top concerns in all heavy industries. For the automotive industry, the main goal is to reduce the fuel consumption via decreasing the weight of vehicles. The automotive applications of Magnesium alloys can be traced back to 1960's, but then magnesium alloys were replaced by aluminum alloys due to their high cost. Magnesium alloys have received great attention again nowadays because of the increase in fuel prices and lack of fuel sources in the world. For instance, BMW is using composite magnesium-aluminum crankcases in their I6 engines to achieve the combinations of low weight and efficiency. Mg alloy has the capability to sustain such severe applications owing to the new improvements. Despite the fact that there is an increasing demand in using magnesium alloys, current applications are still limited in comparison to their major rivals steel, aluminum and plastics. For instance, in a GM vehicle, 123 kg aluminum is used against 4 kg magnesium [1, 2].

Magnesium is the lightest structural material among metals because of its low density. Its specific tensile strength and rigidity are comparable to iron and aluminum. The greatest limitation for the usage of magnesium and its alloys is their poor formability at room temperature and this is because of its hexagonal closed packed (HCP) crystal structure. Magnesium alloys have only two independent basal slip systems which can be activated at room temperature therefore they tend to deform with twinning deformation mechanism. However, the ductility of magnesium can be greatly improved at higher temperatures due to the activation of non-basal slip systems. A fine grain structure and texture in desired direction will also improve the strength of magnesium due to the decrease of

volume fraction of twinning and the increase in number of basal slip systems that can be activated respectively.

The present research focuses on the understanding of microstructural evolution in AZ31 and AZ91 magnesium alloys after applying different aging heat treatments and thermo-mechanical treatment such as aging under stress. AZ31 and AZ91 alloys are precipitation hardenable magnesium alloys. Up to date, there is no published study on the aging under stress studies of Magnesium alloys. It was expected that any orientation, size change and distribution of precipitates or the decrease in the grain size due to applied stress during aging, may lead to better mechanical properties in the aforementioned alloys. The tensile tests for the AZ31 and AZ91 aging under stress samples shows a great increase in mechanical properties of these alloys simultaneously. Mechanical properties of the age-tensioned samples were enhanced significantly in comparison with the as-received samples.

This thesis is divided into five chapters including this chapter. A brief introduction and objectives of this research are explained in chapter one and two. A literature review of related researches is presented in chapter two. Experimental procedure is described in chapter three. All the experimental results were discussed and presented in chapter four. The summary of the research is contained in chapter five.

2 THEORETICAL BACKGROUND

In this chapter, magnesium and magnesium alloy's development during recent years and the potential of these alloys as a high strength/density material will be discussed briefly. First of all a brief history of the production and purification of Mg will be explained during the last century and then the crystal structure and effect of it in Magnesium alloys will be discussed. Second, the related publications and recent related works are inscribed as well and the motivation and aim of this research will be discussed.

2.1 Origin and characteristics of Mg chemical element

Magnesium is a chemical element with symbol "Mg" and atomic number 12. It's common oxidation number is "+2" and it is an alkaline earth metal and the eighth most abundant element in the Earth's crust and ninth in the known universe as a whole[3, 4]. Magnesium is the fourth most common element in the Earth as a whole (behind iron, oxygen and silicon), making up 13% of the planet's mass and a large fraction of the planet's mantle. The relative abundance of magnesium is related to the fact that it is easily built up in supernova stars from a sequential addition of three helium nuclei to carbon (which in turn is made from three helium nuclei). Due to magnesium ion's high solubility in water, it is the third most abundant element dissolved in seawater [5].

The usage of magnesium alloys were increased from 1 to ~4 kilogram over the past 10 years in North America per produced vehicle. Even though this value is still relatively low, many more auto parts are being developed these days from magnesium alloys. It has been estimated that over 100 kg of magnesium could be used in each vehicle. Because of its low density, the specific tensile strength and rigidity of magnesium are superior to iron and aluminum.

2.2 Extraction and production history (Until 1997)

After World War II, production of magnesium decreased drastically. Germany was prohibited from producing magnesium. British operators started to close their plants and by 1947 almost there was no magnesium production in the United Kingdom. Some facilities were built in Canada (Alcan) and United States during 1950s and the Korean War, however China had the record of numbers of plants being built during whole the times some of which were closed due to economic reasons. Furthermore, there were lots of other facilities around the world in countries like Japan, Norway , Italy , Brazil , Yugoslavia , Kazakhstan , Ukraine , India , China during this century which some of which are still operating and some were closed due to several economic reasons [6, 7].

During this period, the magnesium industry attempted to develop magnesium for a number of applications, but failed in the most part. The most successful peacetime application for magnesium was in the original German Volkswagen car that was designed by Ferdinand Porsche. The VW Beetle used large magnesium alloy die castings for the crankcase and the transmission housing (both cast in halves) plus a number of smaller castings. Each Beetle contained more than 20 kg of magnesium alloy [6].

2.3 Extraction and production (2010)

The global annual magnesium production in 1999 was around 375,000 metric tons according to statistics from the International Magnesium Association. Table 2.1 shows that 110,000 tons of primary magnesium metal was produced throughout the world in 2010 according to magnesium association industry databases. This database does not include the productions in USA and China. On the other hand, the China Magnesium Association (CMA) reported that 654,000 tons of primary magnesium was produced in 2010 in China. In addition to all these productions, USA produced approximately 45,000 tons of primary magnesium in 2010. Thus, total production of primary magnesium in the world was approximately 809,000 tons in 2010. This shows nearly 215% increase in Mg production since 1999. Therefore, this increase motivated the companies and researchers to focus on the

studies of Mg Alloys production and enhancing the mechanical, physical and chemical properties of these alloys.

Table 2.1 Magnesium production statistics around the world in 2010 [8]

Production Amount in 2010	
Country	Quantity (thousands of tons)
USA	45
Brazil	16
China	654
Israel	30
Kazakhstan	20
Russia	40
Ukraine	2
Serbia	2
Total	809
Annual Change	+24%

2.4 Mg Metal Forming Processes

There are wide varieties of production methods for magnesium alloys which makes Magnesium production special and unlike the other industries. There are over ten different processes for producing magnesium and, there is no particular dominant technology used for most of the world's production.

Basic parameters in the production of Magnesium are listed below and these parameters are the main reason for the difference and variety of production methods.

- Raw materials
- Materials and purification methods
- Production temperatures
- By-products

Two principal production processes for pure magnesium is listed below. Figure 2.1 shows the common production method of AZ31 used at POSCO industries. Almost all of the shape forming methods and processes are applicable to magnesium alloys.

- Electrolysis of molten magnesium chloride
- Thermal reduction of magnesium oxide

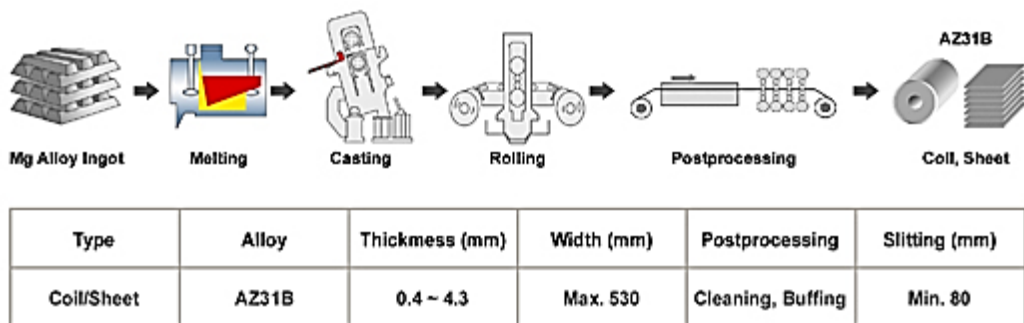


Figure 2.1 General forming processes for AZ31 alloy at POSCO. South Korea [9]

Figure 2.2 shows some of the main metal forming processes for Magnesium alloys. Here is a list of applicable forming methods for magnesium and its alloys:

- Castings (die 70%, sand, permanent mold, and investment)
 - Automobile application of die casting parts 85%
- Extrusions
- Forgings
- Impact extrusions
- Flat-rolled products
- Joining by riveting or any of the commonly used welding methods.
- Machining

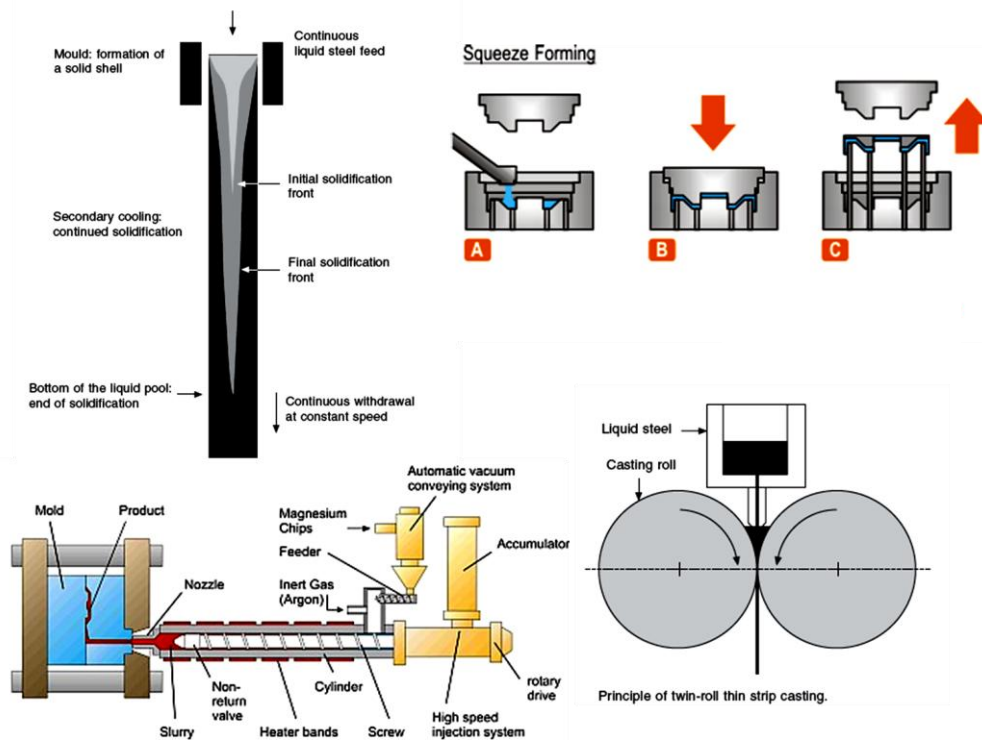


Figure 2.2 Some of the main metal forming methods for Mg alloys [9]

2.5 Magnesium Alloys

Magnesium is the third most commonly used structural metal, following iron and aluminum. It is mentioned for being as the lightest metal which can be used for structural applications. Some of the other applications of magnesium are as following:

- component of aluminum alloys, in die-casting (alloyed with zinc) [10]
- to remove sulfur in the production of iron and steel
- the production of titanium in the Kroll process [11]

Table 2.2 shows some of the most known magnesium cast and wrought alloys. Magnesium must be alloyed with other metals if it is to be employed for engineering applications. There are only about ten elements which can be considered as alloying elements. Those elements are generally expected to modify the ductility and the elastic properties and harden the magnesium by solid solution hardening. Common alloying elements are Al, Ca, Li, Mn, rare earth elements, Si, Ag, Th, Yt, Zn and Zr [12].

Table 2.2 Typical Mg Cast & wrought alloys [13]

<i>Cast Mg alloys</i>	<i>Wrought alloys</i>
AZ81	ZE41ZC71
AZ91	AZ61
AM50	AZ80
ZK51	Elektron 675
ZK61	ZK60
ZE41	M1A
ZC63	HK31
HK31	HM21
HZ32	ZE41
Elektron 21	ZC71

Aluminum is the most commonly used alloying element especially for the die casting process. The maximum solubility of Aluminum in Magnesium is 11.5% (12.7 mass %). Aluminum improves mainly the strength; however, the main advantage to add aluminum is to achieve the optimum combination of strength and ductility. The creep resistance of aluminum added Mg Alloys is limited due to the poor thermal stability of the β -Mg₁₇Al₁₂ phase.

Alloying with calcium is becoming more common in the development of cheap creep resistant alloys due to the replacement of β -Mg₁₇Al₁₂ with Al₁₂Ca since Ca can act as a de-oxidant in the melt or in subsequent heat treatment. It improves the roll ability of sheet but Ca addition higher than 0.3 mass% can reduce the weldability property of the Ca added Mg Alloys.

Manganese is usually not employed alone but with other elements, e.g., Al. In this case compounds MnAl, MnAl₆ or MnAl₄ type of second phases are formed. It reduces the solubility of iron and produces relatively innocuous compounds. It increases the yield strength and improves salt water corrosion resistance of MgAl and MgAlZn alloys. The maximum amount of manganese is 1.5–2 mass percent.

Zinc is one of the most common alloying addition elements. It is used in combination with Al (e.g., AZ91) or with zirconium, thorium or rare earth elements.

In AZ Mg alloy series, “A” stands for aluminum and “Z” stands for Zinc and magnesium is the main alloying element. Since addition of zinc increases the strength and addition of aluminum increases the ductility of these alloys, AZ series are widely preferred as conventional alloys in the automotive and aerospace industries. Decreasing the weight of the structures without sacrificing from the mechanical properties is very important for the decrease in the fuel consumption and CO₂ emission [12].

2.5.1 Cast Alloys

Pure magnesium has a hexagonal closed pack crystal structure with lattice parameters of $a = 0.32092$ nm and $c = 0.52105$ nm [12, 14]. The ideal c/a ratio for close packed spheres is 1.633. For magnesium at room temperature the value is 1.6236. This shows that magnesium has a nearly perfect close packed hexagonal structure with an atomic diameter of 0.32 nm. Figure 2.3 indicates the level of liquid solubility of alloying elements in binary magnesium alloys. When several alloying elements are added, the situation becomes extremely complicated, and it is often observed that the liquid solubility of an element is suppressed by the third or the other elemental additions. Thermodynamically stable intermetallic particles (second phases) suppress the liquid solubility. Even if elements in group 2a, 3a, 3b and 4a of the periodic table generally show a high liquid solubility in magnesium, combinations of these may dramatically reduce the liquid solubility.

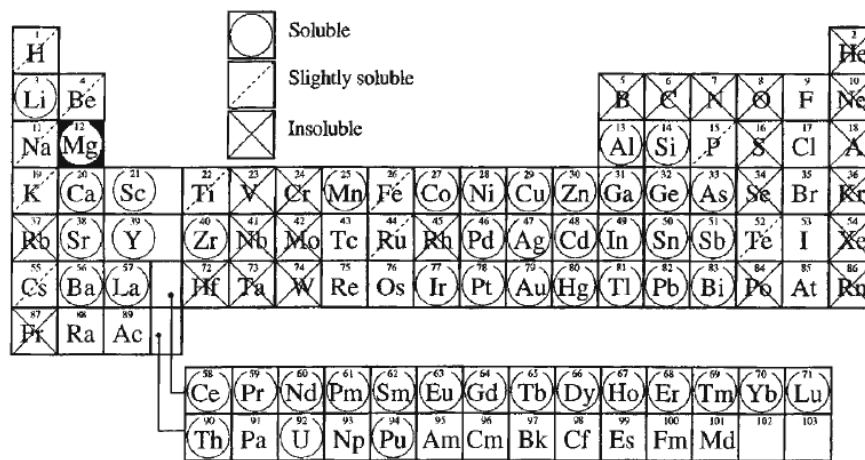


Figure 2.3 Liquid solubility of elements in binary magnesium alloys [14, 15]

Production of cast Mg alloys is a little bit difficult. Magnesium alloys have a high affinity to oxygen and nitrogen in the atmosphere and their vapor pressure of molten metal is high, and the oxide layer formed on the molten metal surface is porous and non-protective.

The standard alloy AZ91D is produced according to the following principles: the basic material is pure magnesium with minimum purity of 99.90%. Mn is added at an elevated temperature to a level exceeding the final specification. Following an addition of Mn, Al and Zn are added, and the temperature of the molten alloy is then lowered to the casting temperature. At the end, Be is added. During the alloying, Mn, Al, and Fe are precipitated as intermetallic compounds that settle to the sludge in the bottom of the furnace.

2.5.2 Wrought Alloys

The capability for plastic deformation is of paramount importance of wrought alloys, whereas cast alloys should be readily pourable and exhibit good mould-filling characteristics. Magnesium has excellent casting properties, but deformation is highly difficult, especially at room temperature. Therefore, conventionally more cast alloys are available than wrought alloys. Hot working mainly is performed by extrusion, rolling, and press forging at 300–500°C. Some main results of workability problems with these alloys are listed below:

- Higher cost
- Lower knowledge about wrought alloys
- Low mechanical properties

On the other hand, wrought magnesium alloys have specific advantages, as an example, excellent mechanical properties can be achieved by some special thermo-mechanical treatment as can be seen in Figure 2.4 and Figure 2.5.

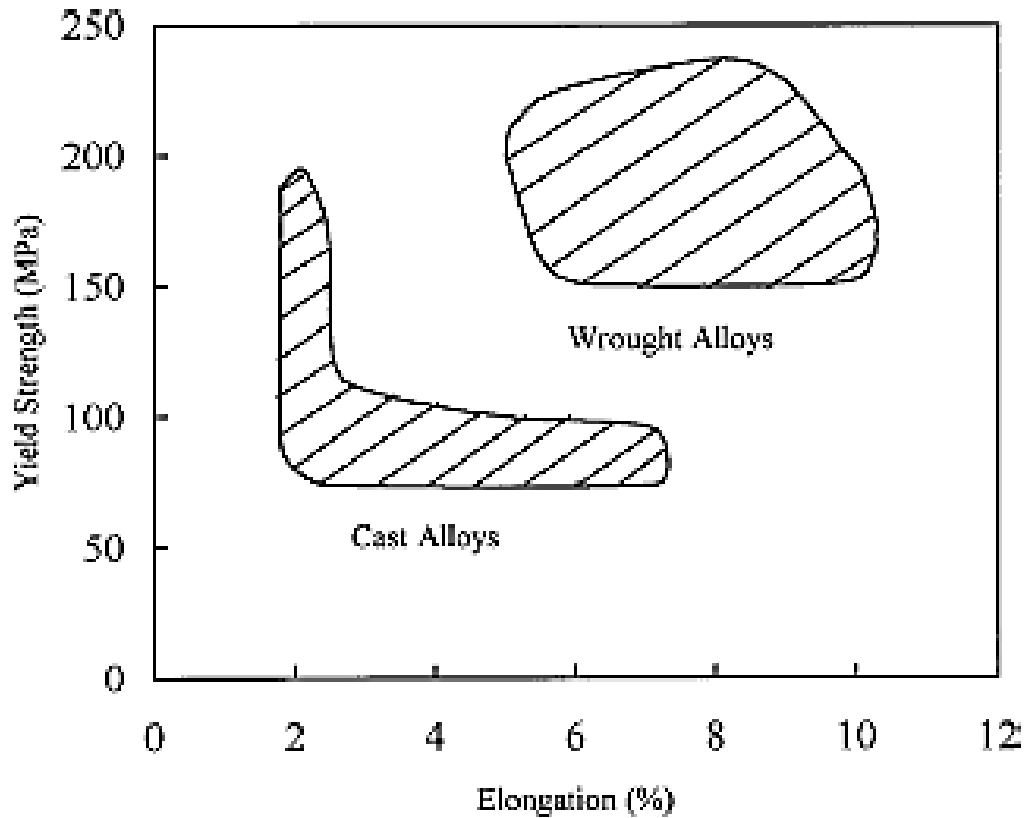


Figure 2.4 Cast and wrought alloys mechanical properties comparison [16]

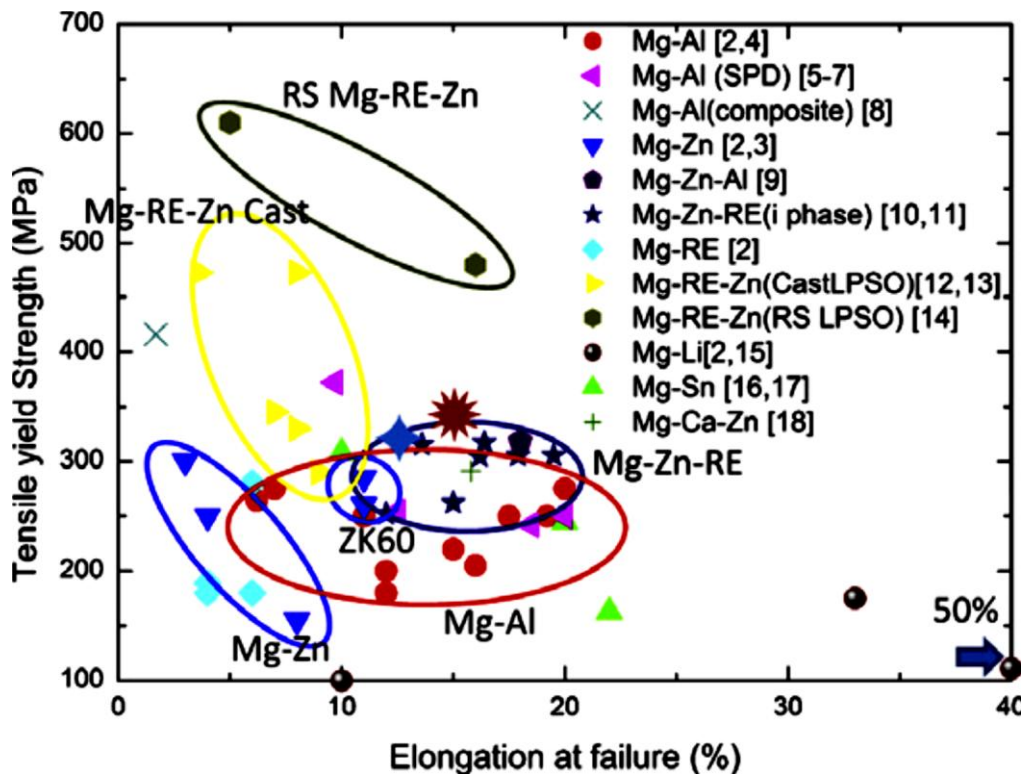


Figure 2.5 Typical tensile yield strength and elongation to failure values for commercial Mg alloys and some other Mg alloys under investigation [17]

2.6 AZ31 and AZ91 Alloys

Magnesium and aluminum are fully soluble in the liquid state, and the eutectic reaction takes place at 437°C, forming a mixture of α (Mg) and β (β -Mg₁₇Al₁₂), as shown in Figure 2.3. The secondary phase Mg₁₇Al₁₂ (β -phase) is brittle, and alloys with a large volume fraction of this secondary phase have reduced practical interest due to their brittleness. The shape and distribution of this β -phase depends on whether the alloy contains zinc or not. If zinc is not present, a massive compound with islands of magnesium solid solution is formed. In alloys with zinc, a completely divorced compound is formed. The precipitation of β from solid solution can be continuous or discontinuous. During cooling of alloys with more than about 8% Al (AZ91), (depending on cooling rate), such precipitation starts at grain boundaries and has a lamellar form which is shown in Figure 2.6.

The microstructure of Magnesium alloys depends on the alloy composition, solidification and cooling rates and patterns, as well as heat treatment. The structure of a die cast alloy with a high solidification rate is much more finely distributed than that of a gravity cast alloy. Figure 2.6, 2.7, 2.8 and 2.9 illustrate the examples for microstructures of the different magnesium alloys after different processes.

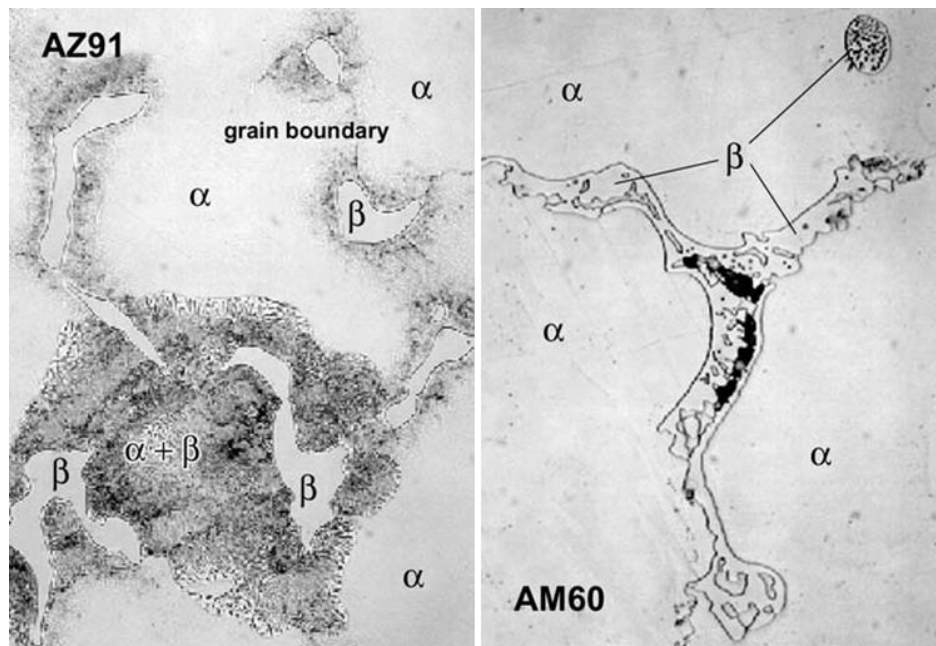


Figure 2.6 α -Mg and β -Mg₁₇Al₁₂ in AZ91 (left) and α -Mg and β -Mg₁₇Al₁₂ in AM60 (Right) [1]

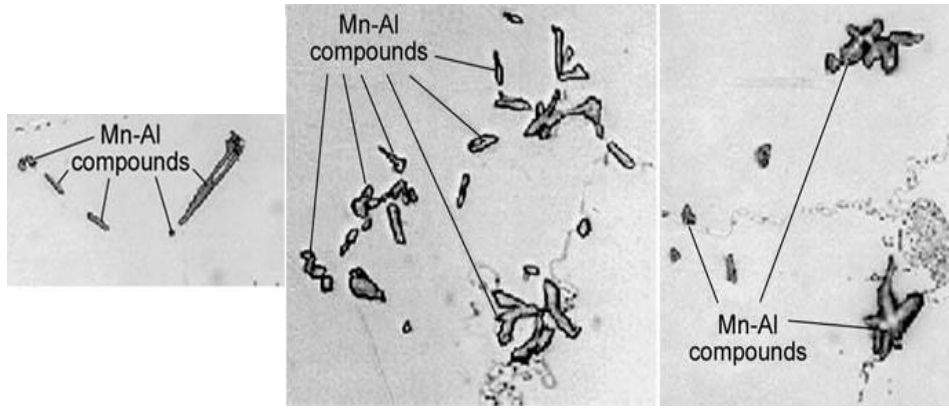


Figure 2.7 Mn-Al compounds of different shapes [1]

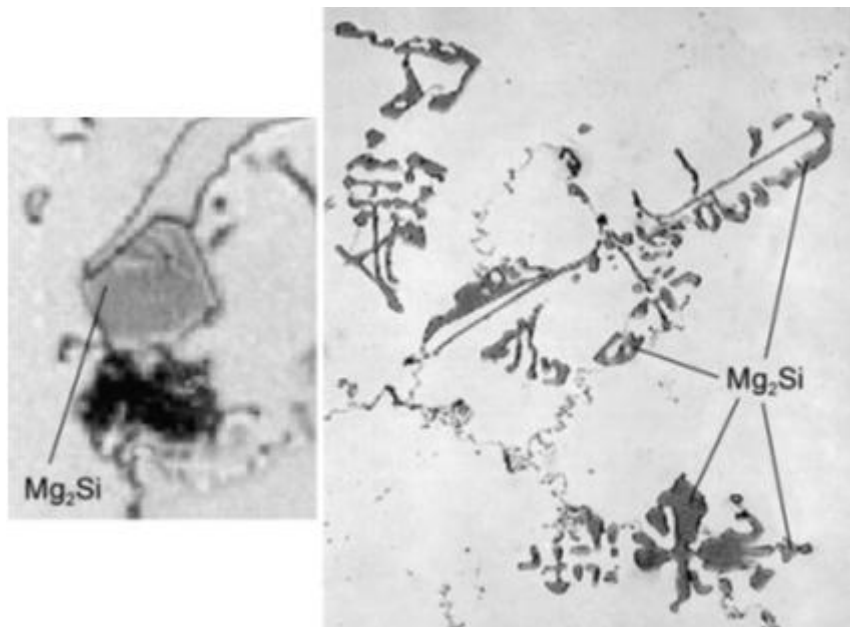


Figure 2.8 Mg₂Si particles [1]

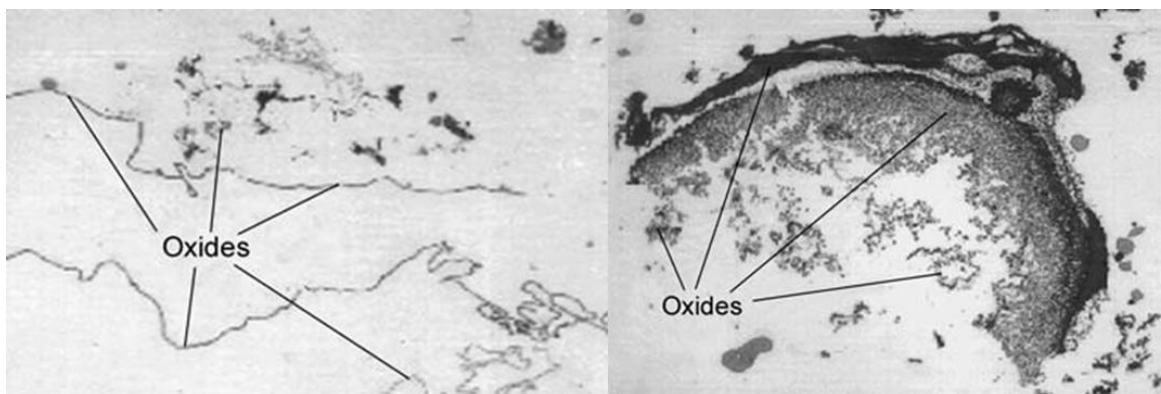


Figure 2.9 Oxide films and oxide clusters [1]

If aluminum is present in the alloy, then zinc is dissolved mainly in the β -phase. If the ratio of zinc to aluminum exceeds 1 to 3 inside the alloy, the $Mg_{17}Al_{12}$ phase is transformed to $Mg_{32}(AlZn)_{49}$. Figure 2.7 and Figure 2.8 show the formation of different intermetallics phases inside magnesium alloy and the possible shape of these precipitates. As it can be seen, the magnesium alloys are highly precipitation hardenable materials and the precipitates in these alloys have different shapes in the matrix. Figure 2.9 shows the possible oxidation phases at the surfaces of the magnesium alloys [12].

Table 2.3 and Table 2.4 shows typical mechanical properties of AZ31 and AZ91 alloys at different conditions and elevated temperatures. It is proven that the properties of these alloys are decreasing highly at elevated temperatures. Table 2.4 shows the mechanical properties of twin roll casting AZ31 obtained from recent works on this alloy.

Table 2.3 Mechanical properties of AZ31 under different conditions [18, 19]

Mechanical properties of twin roll casting AZ31 under different conditions				
		Tensile Strength (MPa)	Yield Strength (MPa)	Elongation (%)
Nakaura et. al. [18]	As-Manufactured	225	-	3
	Homogenized (450°C – 24Hrs)	220	-	13.5
Zhao et. al. [19]	As-Manufactured	245	228	2
	Homogenized (400°C – 5Hrs)	241	136	14

Table 2.4 Mechanical properties of AZ31 & AZ91 at elevated temperatures [18-20]

Typical properties of AZ31 and AZ91 at various temperatures						
Temperature (°C)	AZ31 (horizontal [18] & asymmetric [19] twin roll casting)				AZ91C (T6) by ASM	
	Nakaura et. al. [18]		Zhao et. al. [19]		Yield Strength (MPa)	UTS (MPa)
	Elongation (%)	UTS (MPa)	Elongation (%)	UTS (MPa)		
21	3	225	2	245	160	250
150	4.5	170	-	-	97	185
200	6.5	165	-	-	83	115
300	24	110	-	-	-	-

2.7 Material strengthening methods

There are several methods to modify the yield strength, ductility, and toughness of polycrystalline materials. Virtually all strengthening techniques rely on hindering dislocation motion. Some of the main techniques to enhance the mechanical properties of the metallic alloys are listed below [16]:

- Reduce grain size
- Solid-solution strengthening
- Precipitation strengthening (age hardening)
 - Creating non-stoichiometric intermetallic compounds
- Strain hardening (or cold working)

2.7.1 Age-hardening:

In most of the binary systems, alloying higher than a concentration given by the phase diagram will bring about the formation of second phase particles. The second phase particles can also be created by thermal or thermo-mechanical treatments. These second phase precipitates act as pinning points in a similar manner to solutes. The dislocations in a material can interact with the precipitate particles through one of two ways (see Figure 2.10). If the precipitate particles are small, the dislocations would cut through them. As a result, new surfaces (Figure 2.10b) of the particle would get exposed to the matrix and the particle/matrix interfacial energy would increase. For larger precipitates, looping or bowing of the dislocations would occur. In this case, the length of the dislocations increases. Hence, at a critical radius of about 5 nm, dislocations will preferably cut across the precipitate while for a radius of 30 nm and larger, the dislocations will readily bow or loop to overcome the precipitates [21].

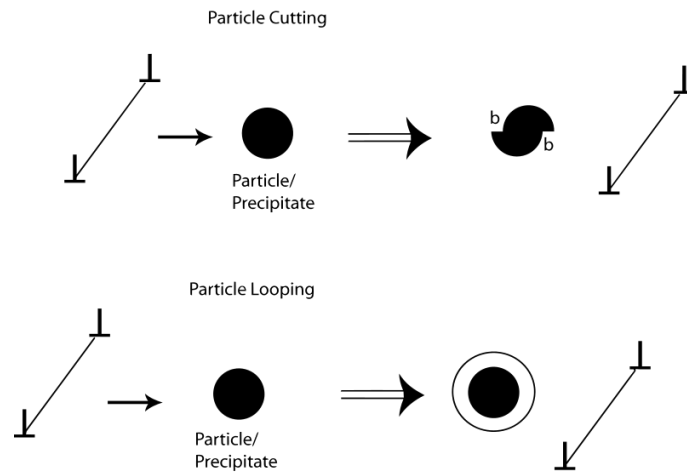


Figure 2.10 dislocations crossing the precipitates [21]

Intermetallics created during aging are often brittle and hard but have high melting temperature and good corrosion resistance and creep behavior. Precipitation strengthening is possible in a material when the solid solubility line inclines strongly toward the center of a phase diagram [22].

2.8 Deformation mechanisms in magnesium

2.8.1 Mg Crystal structure

The crystal structure for magnesium is hexagonal closed packed (hcp), with a c/a ratio of the unit cell of 1.623. The ideal ratio of "hcp" lattice is 1.633 which is very close to that of magnesium [13, 22]. The important planes and directions for deformation mechanisms in "hcp" metals are shown in Table 2.5. Figure 2.11 illustrates the planes in the hcp materials. The plane (0001) is the basal plane and (hki0) are called prism planes which are perpendicular to basal planes [22].

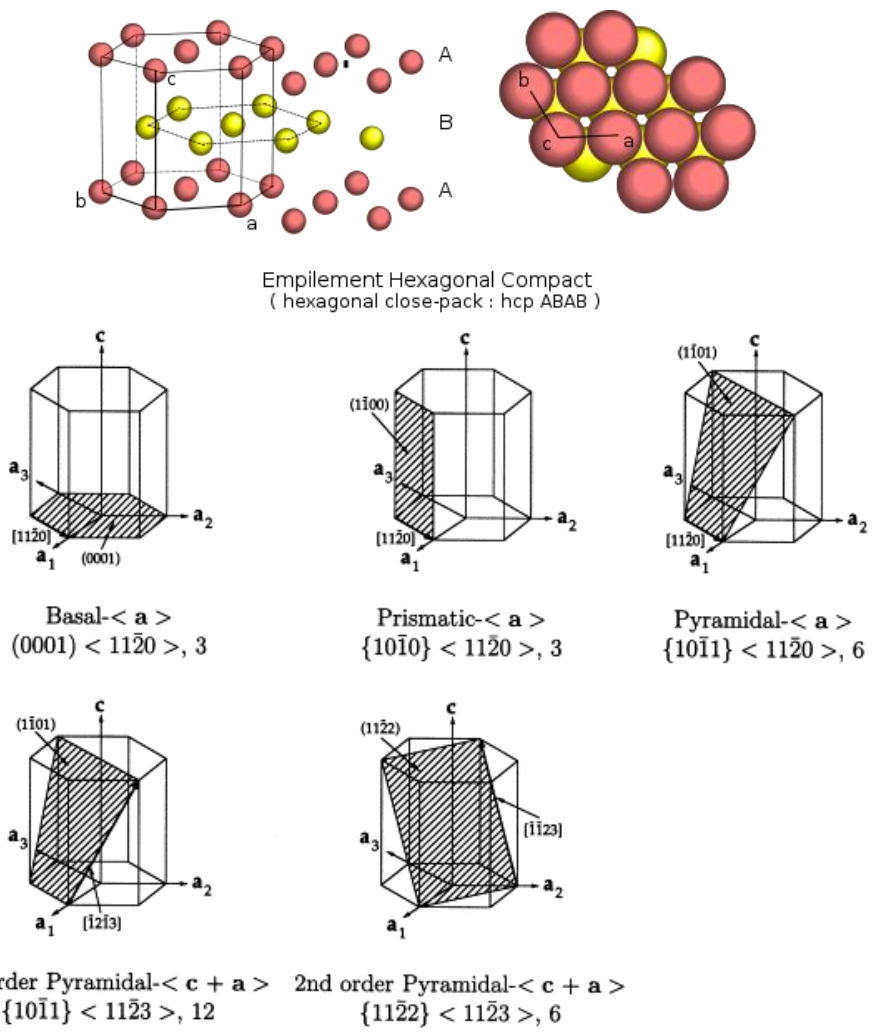


Figure 2.11 Atoms, planes and directions in hcp metals [23]

2.8.2 Slip systems in Magnesium

Slip systems in “hcp” metals are listed in Table 2.5. The critical resolved shear stress for basal slip systems and non-basal slip systems is displayed in Figure 2.12.

The critical resolved shear stress for non-basal slip systems is much greater than that of basal slip systems at room temperature, so magnesium can be deformed easily only within their basal plane at room temperature [24-26]. From Table 2.5, only two independent slip systems exist along slip direction $\langle 1120 \rangle$ in basal plane for “hcp” metals. This disobeys Taylor’s criteria that at least five independent slip systems are required to be activated for an arbitrary shape change. However, when the temperature increases, the critical resolved shear stress for non-basal slip systems will decrease rapidly, thus non-basal slip systems will be activated at

elevated temperature. Therefore, Taylor's criteria will be satisfied for plastic deformation [27, 28].

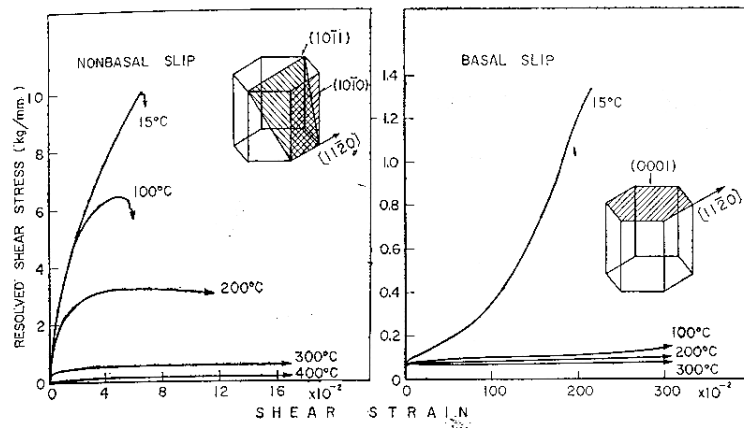


Figure 2.12 CRSS for basal and non-basal slip at room and elevated temperatures [26]

Table 2.5 Slip systems in hcp metals [8]

Slip System	Burgers Vector type	Slip Direction	Slip Plane	No. Of Slip Systems	
				Total	Independent
1	a	$\langle 1120 \rangle$	Basal Plane (0001)	3	2
2	a	$\langle 1120 \rangle$	1 st order Prism Plane $\langle 1010 \rangle$	3	2
3	a	$\langle 1120 \rangle$	1 st order Pyramidal Plane $\langle 1011 \rangle$	6	4
4	c + a	$\langle 1123 \rangle$	2 nd order Pyramidal Plane $\langle 1122 \rangle$	3	2
5	C	$\langle 0001 \rangle$	1 st order Prism Plane $\langle 1010 \rangle$	3	2
6	c	$\langle 0001 \rangle$	2 nd order Prism Plane $\langle 1120 \rangle$	3	2

2.8.3 Twining mechanism in Magnesium

Once the yield or flow stress has been exceeded plastic or permanent deformation starts and proceeds. Plastic deformation can take place by two simple processes, slip and twinning. During slip, which is shown in Figure 2.13.a, the top half of the crystal moves over the bottom half along certain crystallographic planes, known as slip planes. The atoms move forward by numbers of lattice vectors; as a result the continuity of the lattice is maintained. During twinning (Figure 2.13.b) the atomic movements are not whole lattice vectors. The lattice generated in the deformed region, is oriented in a twin relationship to the parent phase. It will also be observed that in contrast to slip, the sheared region in twinning may occur over many planes. The atoms in each plane move forward by the same amount relative to those on the plane below them [21].

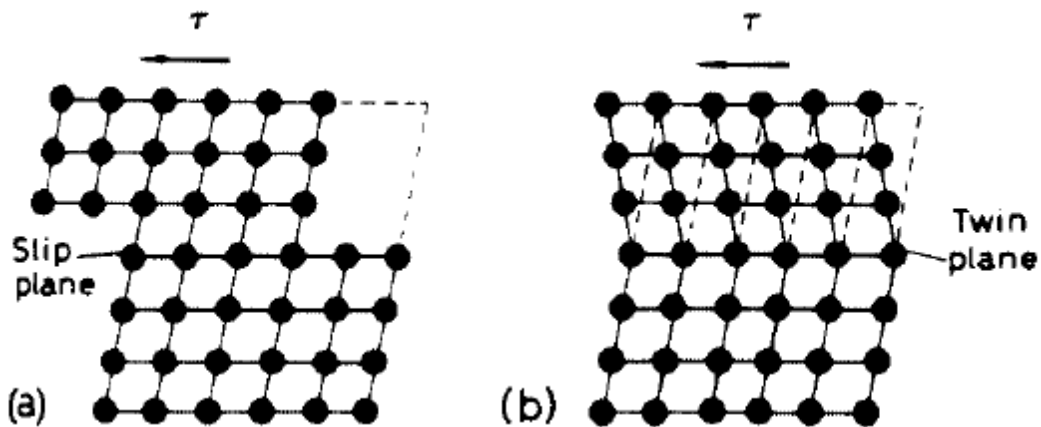


Figure 2.13 Slip and twinning in a crystal [21]

Due to the lack of independent slip systems for magnesium at room temperature deformation, mechanical twinning becomes an important deformation mechanism. The dominant twinning mode observed in magnesium is $(10\bar{1}2) \langle 10\ 1\ 1 \rangle$ [22, 27]. The formation and growth of the mechanical twinning are also related to the grain size and the texture of polycrystalline materials. The average stress of mechanical twinning for a fine grain size material is higher than the stress for a coarse grain material because of the higher interaction between the crystals in a fine grain size case [29].

Although mechanical twinning can be activated during the room temperature deformation of magnesium alloys, this will result in large internal stress. Thus, this

leads to reduced ductility of the alloy [27]. At elevated temperatures, mechanical twinning becomes less important due to the activation of non-basal slip systems as discussed in the previous section.

2.9 Strengthening mechanisms for Mg alloys

It was mentioned before that plastic deformation in Mg alloys happens in various conditions such as dislocation motion and mechanical twinning. The plastic deformation begins when the resolved shear stress reaches a critical value (yield stress). Polycrystalline materials contain crystal defects such as vacancies, foreign atoms and dislocations etc. The crystal defects restrict the dislocation movement. Therefore, the deformation behavior of polycrystals is influenced by the presence of crystal defects [16].

Most commercial wrought Mg alloys are the alloys which have the potential for precipitation hardening. However, strengthening after precipitation hardening is not high enough due to coarse dispersions of precipitates [30]. For effective precipitation hardening of Mg alloys, finely dispersed precipitates with various habit planes are required [17]. However, the promotion of such precipitates is difficult and most of the precipitates in Mg alloys form with the habit planes on the basal plane.

2.9.1 Dislocation Strengthening

Plastic deformation starts and proceeds by the movement and introduction of dislocations. The yield strength of Mg polycrystals depends on dislocation density in the microstructure as described by the following relationship:

$$\sigma_{yD} = M\alpha Gb\rho^{1/2} \quad (2.1)$$

In this equation, G is the shear modulus, b is the magnitude of the Burgers vector, ρ is the dislocation density, M is the Taylor factor and “ α ” is a constant in the range 0.1 to 0.5. The constant “ α ” = 0.2 has been estimated for the interaction between the dislocation forest and basal dislocations in magnesium single crystals at 300 K [16].

2.9.2 Solid Solution Hardening

Solute atoms are also responsible for the strengthening of materials. Solute atoms in Mg or in Mg alloys change the lattice constants (both the “a” and “c” parameter) and modify the binding forces. In a very dilute solid solution, the mobile dislocation interacts with a solute atom. The interaction intensity can be described by the relative change in the lattice parameter (the size misfit parameter) $\delta=(da/dc)/a$ and the relative change in the modulus (modulus misfit parameter) $h=(dG/dc)/G$. In both expressions C is the atomic solute concentration. The mobile dislocations may interact with many solute atoms. The interaction force between a dislocation and solute atom depends on the distance between the dislocation and the atom. The minimum force is given by a statistical sum of the interactions of many solute atoms. The yield strength of dilute Mg based alloys can be expressed as described by Fleischer [31].

$$\sigma_{ys} = \sigma_{y0} + Z_F G (|\delta| + \beta |h|)^{3/2} C^{1/2} \quad (2.2)$$

Or according to Labusch [48]

$$\sigma_{ys} = \sigma_{y0} + Z_L G (\delta^2 + \beta^2 h^2)^{2/3} C^{2/3} \quad (2.3)$$

In both equations σ_{y0} is the yield strength of pure magnesium, Z_L and Z_F are constants and “ β ” is between 1/20 and 1/16. It can be obtained from the published experimental results [16, 29] that the value of the solution hardening rate increases in Mg-Li, Mg-Al alloys as well as in Mg-Zn. The strengthening effect of the various solutes arises from the concentration dependence of both lattice parameter and elastic constants. The concentration dependence of the lattice parameter for some Mg base alloys has been determined or the size factor may be estimated as computed by King. On the other hand, the concentration dependence of elastic constants has been measured only for a few Mg alloy systems. In the case where the concentration dependence of the shear modulus G is not known, an approximate value of h can be calculated using the equation 2.4.

$$h = 2(G_1 - G)/(G_1 + G) \quad (2.4)$$

Where G_1 is the shear modulus of the alloying metal. In commercial alloys many different solute atoms are present like in ternary or quaternary alloys. The solute atoms then cause different interactions because the strength of the solute atoms is

not always same. Various relationships for the superposition of two kinds of obstacles have been discussed in the literature [32].

2.9.3 Precipitation Strengthening

The strength of precipitate strengthened polycrystalline magnesium alloys depends on the size, distribution and volume fraction of the precipitates and on the nature of the interface between the precipitates and the matrix (coherent or incoherent). Dislocations may be able to cut fine precipitates but cannot shear through larger incoherent precipitates. The dislocations then bow out between precipitates. The value of the stress that the precipitate particles should overcome can be expressed by a more general formula [54, 55]:

$$\sigma_{yp} = MF/bL \quad (2.5)$$

Where L is the average particle spacing along the dislocation line and F is the mean obstacle strength [54, 55]. In the case of particle shearing, the obstacle strength depends on the main interaction mechanism between precipitates and the mobile dislocations (for instance the creation of new interfaces or a difference in the stacking fault energy between the precipitates and the matrix) and it can be written in the following form:

$$F_o = K_p G b R \quad (2.6)$$

Where K_p is the parameter depending on the mechanism considered and R is the average radius of precipitates. However, the mean obstacle strength F depends on the precipitate size distribution. The average particle spacing depends on the particle volume fraction f and on R. The yield stress for the case that all precipitates are sheared is given by [16]:

$$\sigma_{yP} = Z_p M G K_p^{3/2} (fR/b)^{1/2} \quad (2.7)$$

Where Z_p is a constant. In the case of bowing dislocations between precipitate particles (incoherent precipitates), the obstacle strength is constant [16].

$$F_o = G b^2 \quad (2.8)$$

The yield stress needed to by-pass precipitates is given as [16]:

$$\sigma_{y0} = 2M G b / L_p \quad (2.9)$$

Where L_p is the average interparticle spacing in the glide plane. This stress is called the “Orowan stress”. The average particle spacing along the dislocation line is larger than the average interparticle spacing in the glide plane and then the yield stress is expressed as[16]:

$$\sigma_{yo} = Z_o M G b f^{1/2} R \quad (2.10)$$

Where Z_o is a constant which is about 0.6. The critical radius of the precipitates for the transition between the shearing and by-pass modes is the radius at which the obstacles strengths are identical for both mechanism, i.e. [16],

$$R_c = \frac{b}{K_p} \cdot \left(\frac{Z_o}{Z_p}\right)^{2/3} \quad (2.11)$$

Where $\frac{Z_o}{Z_p}$ is almost one. This radius controls the peak strength of the material.

Usually in practice, the strength of an alloy is the result of the superposition of all hardening mechanisms such as dislocation hardening; solid solution hardening and precipitation hardening. Then the yield strength of the alloys can be calculated as the equation 2.12 [16] :

$$\sigma_{ya} = \sigma_{ys} + \left[(\sigma_{yD})^2 + (\sigma_{yP})^2 \right]^{1/2} \quad (2.12)$$

2.10 Latest related research

Previous studies have shown that in Mg-Al-Zn alloys, an increase in the amount of the “Al” content gains to large amount of β -Mg₁₇Al₁₂ precipitates inside the “ α ” matrix [17, 33-35]. There are two types of precipitation morphologies which are named as continuous and discontinuous precipitates in these alloys. The morphologies and amount of this “ β ” precipitates are in direct relation with the mechanical properties of these alloys and these might either increase or decrease the mechanical properties of Mg alloys [35]. Yakubtsov et. al. [36] analyzed the effects of various heat treatments on the microstructure and tensile properties of AZ80 and they discovered that the yield strength was in direct relation with the volume fraction of the coarse “ β ” phases and also grain sizes.

There are numbers of disadvantages in commercial magnesium alloys which are preventing widely usage of these alloys [17]. These disadvantages are listed below:

1. Magnesium alloys have lower yield strength in comparison with the aluminum alloys. The highest achieved yield strength in wrought Mg alloys is 240MPa. In order to compete with Al alloys, the yield strength should be improved to more than 300MPa. Tensile and yield strength of some commercial Mg alloys were given in Figure 2.5.
2. There is a high tension-compression asymmetry in Magnesium alloys. Yield strength anisotropy ratio is 0.3 and 0.6 for compressive and tensile strengths respectively for the extruded products. The lower ratio in compression strength is because of the twinning mechanism activation during compressive loadings. Many of these twinning systems are not activated under tensile loads [17, 37].
3. The other important problem is the forming of the Mg alloys at high temperatures [14, 17]. This leads to strength reduction due to considerable grain growth and dynamic recrystallization [38, 39].

As mentioned in previous sections, there is a couple of strengthening methods for Magnesium alloys, each seeking to make these alloys more strong. All of these methods are known and tried for years on different metallic materials and also on Magnesium alloys, however these methods have their own limits and they are only capable of increasing the yield strength of the Mg alloys to a limited value. Recently, different advanced methods have started to be investigated in magnesium alloys like severe plastic deformation methods via equal-channel extrusion or high pressure torsion. These advanced methods have a very good influence on the strength of the magnesium alloys. It is believed that these methods are precious for commercial alloys, but on the other hand, they are very complicated to be used widely in the Magnesium industry.

In this study, a new mixed method of strengthening is employed on magnesium alloys to see the effect of thermal and mechanical deformation at the same time. As far as we know, literature doesn't show any similar research to this work. The used method is based on the precipitation hardening and orientation of these

precipitations as well as expected grain size reduction. During aging process, a constant stress value in the elastic range of the material at room temperature is applied to the specimen to reinforce the dislocations and precipitates and enhance precipitation-dislocation interaction to increase the yield strength [17]. Also another main purpose of this type of thermo-mechanical treatment is to create equiaxed grains during aging to increase the compatibility of the growing intermetallics inside the matrix with the grains by applying constant stress. The constant stress may change the shape or orientation of the precipitates during aging heat treatments.

3 EXPERIMENTAL PROCEDURE

3.1 Materials

Nominal compositions of the as-received AZ31 and AZ91 plate, as provided by the suppliers, were given in Table 3.1.

AZ31 plates were produced using a relatively new technique which is called as twin-roll casting method. On the other hand, AZ91 series plates were produced using conventional casting and then hot rolling process. The as-received AZ31 plates were then tempered according to ASTM B90/B90M-07 standard [40] with the H24 condition and AZ91 plates were tempered with the H5 condition by the suppliers. Both of the as-received alloy plates were cut into rectangular coupons for aging and further microstructural characterization.

Table 3.1 Chemical compositional of the alloys

Material	Elemental Composition (Atomic %)					
	Al (%)	Zn (%)	Mn (%)	Si (%)	Fe (%)	Mg (%)
AZ31B	2.5-3.5	0.6-1.4	Min 0.2	Max 0.10	Max 0.005	The rest
AZ91D	8.3-9.7	0.35-1	Min 0.15	Max 0.10	Max 0.005	The rest

The rectangular coupons from both of the alloys were homogenized according to the binary phase diagram of Mg-Al alloy system which is shown in Figure 3.1 and also according to what has been suggested in the literature [41]. AZ31 was homogenized at 400°C for 2 hours and AZ91 was homogenized at 425°C for 15 minute.

3.2 Heat treatment

All the metallography samples and the tensile coupons were homogenized after the samples were cut from the plate. In order to eliminate the cast structure in AZ31 and to homogenize AZ31 and AZ91 alloys, the samples were homogenized. Some preliminary experiments were performed to achieve the optimum homogenization condition for both alloys and different homogenization parameters

were applied. The AZ31 coupons were homogenized at 400°C for 2 and 24 hours and the AZ91 coupons were homogenized at 400°C, 425°C and 450°C for 15 minute, 2 hour and 24 hour respectively.

Aging heat treatments were carried out at three different temperatures and for five different time durations. The selected aging temperatures for the alloys are presented in Figure 3.2. The samples were heat treated using a tabletop furnace which is shown in Figure 3.3 and quenched in water immediately right after the aging treatment was ended. Figure 3.3 shows the typical procedure for the aging heat treatments.

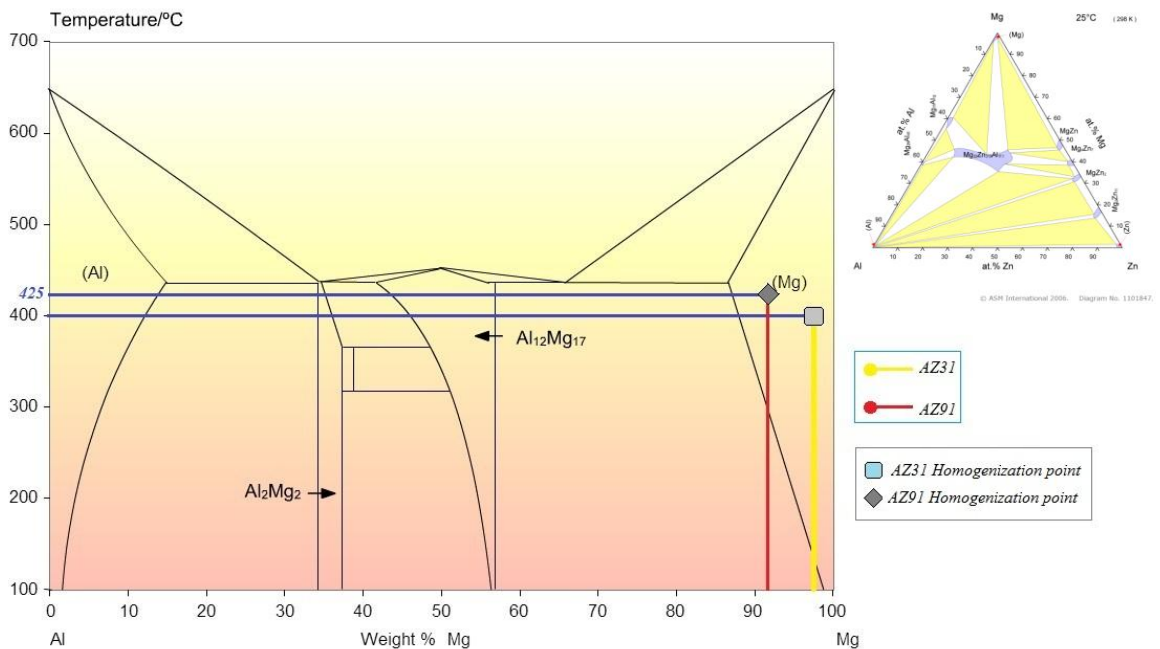


Figure 3.1 Binary phase diagram of Mg-Al alloy system, showing homogenization points for AZ31 and AZ91 alloys [13]

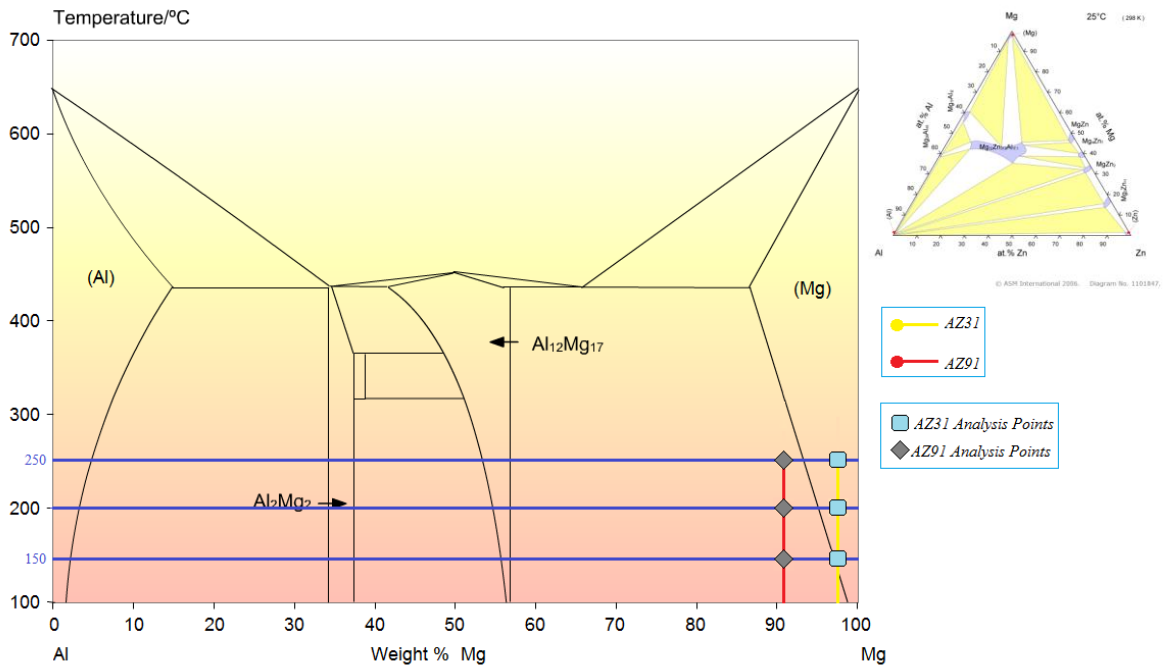


Figure 3.2 Binary phase diagram of Mg-Al alloy system, showing aging points for AZ31 and AZ91 alloys [13]

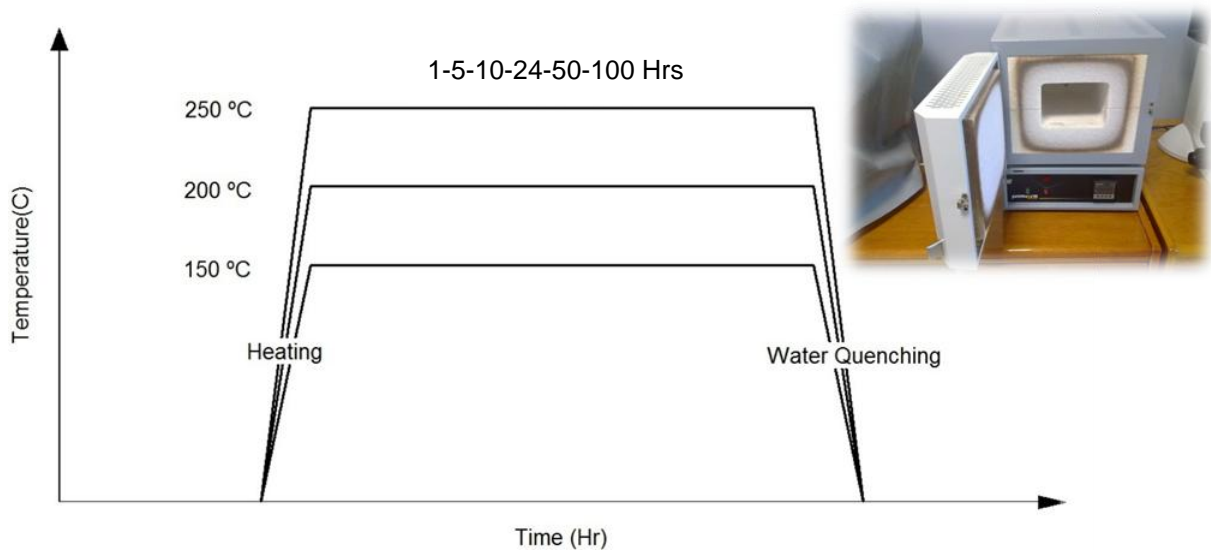


Figure 3.3 Temperature vs. Time schematic for aging heat treatments and the digital image of tabletop furnace

3.3 Thermo-mechanical Procedure

3.3.1 Thermo-mechanical experiment set-up

Thermo-mechanical experiments were performed using a special environmental chamber which was designed especially for this study. It was manufactured by a local furnace manufacturer and mounted on our universal tensile test machine. The chamber specifications and CAD models are tabulated in Table 3.2 and Figure 3.4 respectively.

In order to control and measure the temperature, there were four thermocouples. Three of them were built-in furnace thermocouples and one of them is external thermocouple to check the sample temperature which could be inserted inside the chamber through a front-side hole to measure the temperature right next to specimen (Figure 3.5). Each zone had the ability to be programed separately through 3 different PID controllers. The PID controllers were connected though a serial port to the environmental chamber and two data acquisition device, one for internal thermocouples and one for external sample thermocouple was connected through USB port to the PC in order to record the temperature. Figure 3.6 shows the typical 3D computer aided model of the chamber and grips and also the final manufactured chamber and grips as well.

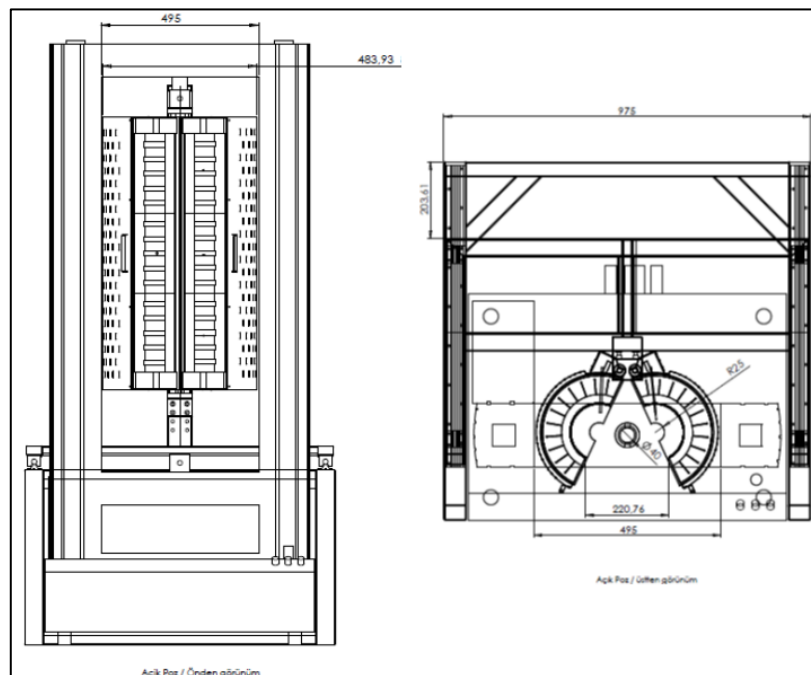


Figure 3.4 Mounting plots of environmental chambers on the UTM

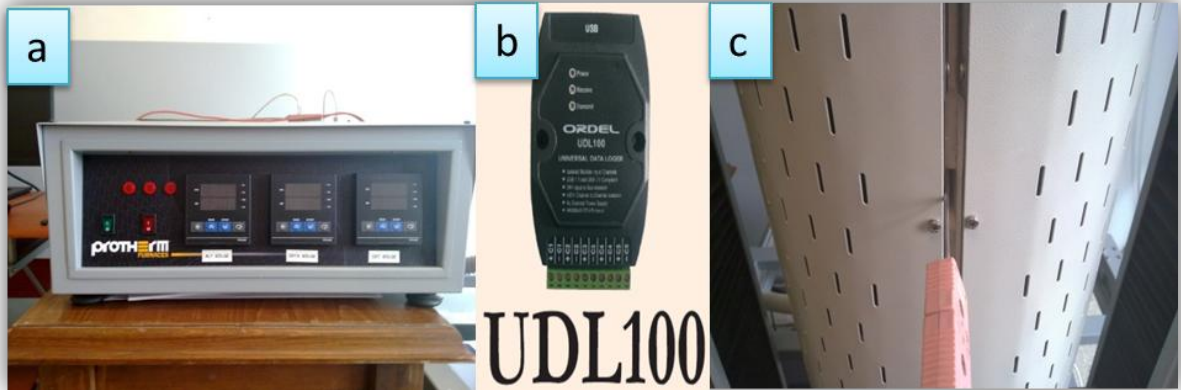


Figure 3.5 a) PID controllers for 3 zones separately b) the data acquisition device connected through USB to PC c) external controller thermocouple and the hole in front of the chamber

Table 3.2 Protherm Environmental chamber specifications

Chamber Specifications	
Max. working temperature	1100°C
Continuous working temperature	1050°C
Chamber Type	Vertical, 3 independent zones
Dimensions	Max. ID 150mm Total height 800mm Total distance of modules in open condition : 180 mm
heating controller system	3 x PC442/6 , 6 step programing capacity Delay Timer PID control Dual Display
Heating elements	Kanthal HAS Modules , # 6
Heating zone dimensions	3x250mm
Safety Instruments	Electric safe switch when the modules are open
Input power	220 Volt, 2.0 kW

To be able to do the thermo-mechanical and mechanical fracture experiments, the standard grips and columns should be changed and replaced with the other grips and columns which are compatible with the dimensions of the chamber. These grips and columns were designed and manufactured with proper materials, which do not creep at high temperatures and with low expansion ratio. The CAD model

of the grips and their columns which designed and manufactured are represented in Figure 3.6.

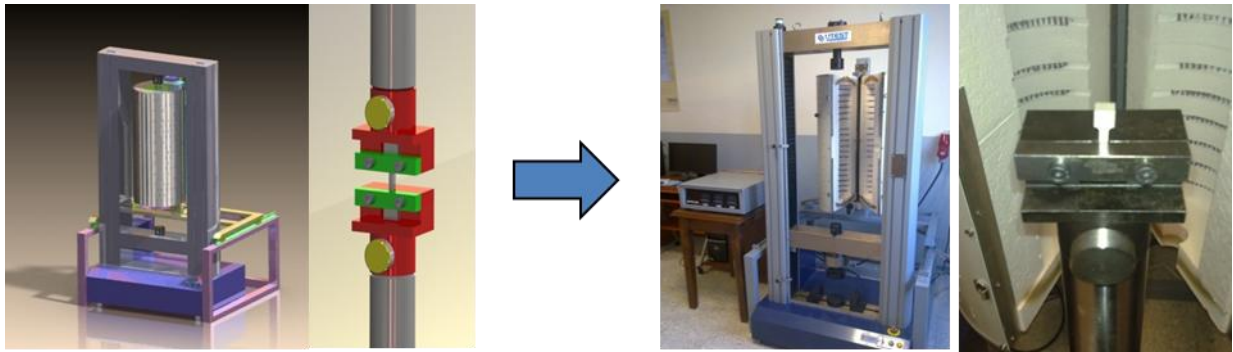


Figure 3.6 Designed chamber and grips and the final assembly

3.3.2 Thermo-mechanical Treatments

The main purpose of thermo-mechanical treatments was the investigation of the effect of applied constant stresses to the secondary phases. These 2nd phase particles appear during aging heat treatments. In addition, the effect of microstructural evolution to the mechanical properties of AZ31 and AZ91 alloy were investigated. The constant stresses were applied to tension coupons.

All AZ31 and AZ91 specimens were tensioned under specified constant stresses in the elastic range. After performing the aging tests and understanding the aging effect on the microstructure of the aged samples, the thermo-mechanical experiments were performed. The age-tensioned samples were heat treated according to the procedure which is shown in Figure 3.7. The applied stresses are presented in the Table 3.3.

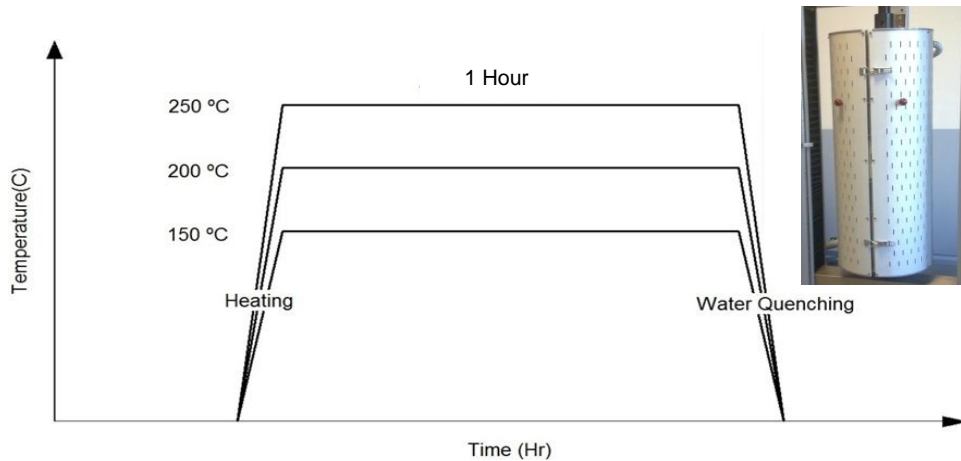


Figure 3.7 Heat treatment procedure for aging under stress experiments

Table 3.3 Thermo-mechanical experiments procedure

Aging Under Stress experiment plan		
Aging Condition	Applied stress (MPa)	Cooling method
150°C – 1H	20	Water Quenched (5-10s)
	40	
	60	
	80	
200°C – 1H	20	
	40	
	60	
	80	
250°C – 1H	20	
	40	
	60	
	80	

To perform the thermo-mechanical experiments, the samples were placed between the grips and the high temperature extensometer was mounted on the sample and then the chamber was closed. The heating process was started according to the experiments by programming the PID controllers. Each experiment consists of 4 steps:

1. Applying the required stress
2. Heating sample till the experiment temperature was achieved
3. Waiting at the required temperature for the specified time
4. Unloading the sample and quenching it immediately

All the specimens were kept for further analysis. The microstructures of the thermo-mechanically treated samples were analyzed by optical microscope and scanning electron microscope and then fracture experiments were performed to analyze the mechanical properties.

3.4 Microstructural Characterization

Microstructures of both alloys were characterized by optical microscope (OM) and scanning electron microscope (SEM). Image processing tools were utilized to process the microstructure of the alloys.

To reveal the desired microstructure, different metallographic preparation methods and polishing lubricants were tried. BUEHLER's⁵ oil based diamond polishers were used as the recommended polishing agents in the literature[42]. Due to the fact that Mg alloys are very sensitive to water and react with oxygen very quickly, so much effort was spent to reach the required polished surface. After O.M. and SEM analysis, Mechanical tests were performed.

3.4.1 Surface Microscopy and characterization

In order to perform optical microcopy analysis, first of all, the sample surfaces should be prepared using metallographical preparation methods. Due to the high reactivity of Magnesium alloys with oxygen, preparation of these alloys was very difficult and very time consuming.

Optical microscopy was performed using Nikon scientific microscope and scanning electron microscope (QUANTA 400F Field Emission SEM) was utilized to observe the microstructure of the aged and thermo-mechanically treated samples. These samples were cut by a low speed precision cutter machine and then homogenization heat treatment was applied to all of the samples to eliminate twinning deformation which might occur during cutting procedure and to get rid of the cast dendritic structure. After all, samples were cold mounted using epoxy resin mixed with epoxy hardener (see Figure 3.8). Hot mounting was not used

⁵ A Germany based metallography tools and chemicals manufacturer

because high temperature and high pressure during this process might drastically affect the microstructure of the thermo-mechanically treated or aged samples.



Figure 3.8 Cold mounting mold and sample

The Nikon L150A optic microscope (see Figure 3.9) utilized with a 3.2 MP digital camera was enabled to take images of the microstructures. Bright field examination mode was used to capture images of the samples, but also dark field examinations show good results of precipitate distribution in AZ91 alloys. Microstructures of AZ91 alloys were revealed easier than that of AZ31. The recommended and used procedure to reveal the final polished surface of both alloys is tabulated in Table 3.4.



Figure 3.9 Nikon optical microscope

Table 3.4 Six-step grinding polishing procedure

<i>Grinding/Polishing Steps</i>				
<i>Surface</i>	<i>Abrasive/Size</i>	<i>Load Lb. (N)</i>	<i>Speed (rpm/Direction)</i>	<i>Time (minutes)</i>
Waterproof Paper	SiC Paper 320 Grit	With hand	250	Until Plane
Waterproof Paper	SiC Paper 800 Grit	With hand	250	Until Plane
Waterproof Paper	SiC Paper 2000 Grit	With hand	250	Until Plane
Flocked cloth	9 Micron Monocrystalline Oil based Diamond Suspension	With hand	150	6
Flocked cloth	3 Micron Monocrystalline Oil based Diamond Suspension	With hand	120	5
Flocked cloth	1 Micron Monocrystalline Oil based Diamond Suspension	With hand	120	4
Flocked cloth	0.05 Micron Colloidal silica	With hand	120	1.5 - 3

At the end of each step the surface of the sample was washed with Ethanol and dried with stream of hot air. At the last step, due to the nature of colloidal silica suspension, removing this suspension from surface was very difficult. To prevent any further scratch formation at the surface and remove the suspension fully from surface, a 5 second polishing step with water based Al_2O_3 was performed on every sample.

There are different types of etchants in the literature [13] which are recommended for Mg alloys and those were useful in revealing the general microstructure and grain boundaries. In order to reveal the general microstructure of AZ91, acetic-picral with different compositions was used and for AZ31 both acetic-picral and acetic-glycol were used for some samples. Revealing AZ31 microstructure was a little difficult and sometimes AZ31 alloy doesn't respond well to acetic picral. So, instead, acetic-glycol was used to reveal the microstructure of the AZ31 samples.

Table 3.5 The used etchants for microstructure revealing[13]

Etchants		
Name	<i>Composition</i>	<i>Characteristics and use</i>
Acetic-Picral 1	5 mL Acetic Acid 6 g Picric Acid 10 mL Water 100 mL Ethanol	A universal etchant. Defines grain boundaries in most alloys and tempers by etch rate and color of stain. Reveals cold work and twinning readily.
Acetic-Picral 2	20 mL acetic acid 3 g picric acid, 20 mL Water 50 mL ethanol	Orientation of crackled film is parallel to trace of basal plane. Film crackles in high-alloy areas. Distinguishes between fusion voids surrounded by normal level of alloy and micro-shrinkage with low alloy content.
Acetic-glycol	20 mL acetic acid 1 ml HNO ₃ 60 mL ethylene glycol 20 mL water	General purpose etchant

After metallographic preparation, images of the microstructure with different scales were captured and analyzed using the optical microscope. The etchants which were tabulated above produce somewhat different features of the microstructure. Therefore, using only the general-purpose etchants (glycol, acetic-glycol or acetic-picral) was insufficient [13].

The microstructures of AZ31 and AZ91 samples were further studied by Scanning Electron Microscopy (SEM) using Secondary Electron (SE) imaging technique. Energy Dispersive Spectrometer (EDS) analysis was used to investigate the chemical composition of second phase particles. The energy of the peak position in a spectrum is the critical information used to identify the elements, which is formed by characteristic X-rays. In this research, accelerating voltage around 15-20 keV is optimum for AZ31 considering the critical ionization energy for Mg, Al, Mn, Zn elements. More accurate phase analysis was performed by Advanced X-ray diffractometer (XRD).

The average grain size measurements were done using the ASTM linear intercept method. Clemex image processing was used to obtain grain size distribution and volume fraction of fine grains.

3.4.2 Quantitative X-Ray Diffraction

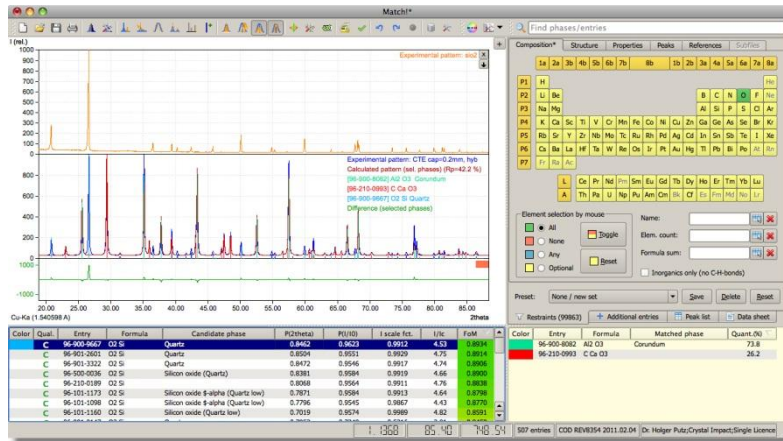
More accurate phase analyses were carried out using X-ray diffraction method. Qualitative analysis involved the identification of a phase or phases in the specimen by comparison with “standard” patterns. Relative estimation of proportions of different phases in multiphase specimens was done by comparing peak intensities which were attributed to the identified phases.

All aged samples were analyzed using Rigaku Ultima IV XRD device which is shown at Figure 3.10.b. All measurements were conducted between 20 and 120 degree by a scanning rate of 2°/min. The results were compared with the data provided by the International Centre for Diffraction Data. The used database version was old (PDF 2.0) but it was precise and accurate enough for Mg alloys and the precipitates which were observed in these alloys. There were approximately 1,570,048 entries in this database.

“Match!” is the software which was used to find out the ratio and quantity of Mg₁₇Al₁₂ intermetallic components in the heat treated samples using PDF-2.0 as a reference database (see Figure 3.10.a).

3.5 Mechanical Behavior Characterization

Mechanical tensile experiments were performed using UTEST servo-mechanic universal tensile test machine. Axial strain was measured using epsilon 3442 extensometer which is shown in Figure 3.11. Tension samples were cut to the dog-bone shape according to the ASTM B 557M – 02a standard using electron discharge machine to reduce the residual stresses on the surface of the samples to a minimum level. The schematic and the dimensions of the tensile samples are shown in the Figure 3.12. All of the samples were extracted from the rolling direction of the plates.



a)



b)

Figure 3.10 a) Match! Crystal Impact software b) Rigaku Ultima IV XRD device



Figure 3.11 The Epsilon 3448 high temperature extensometer

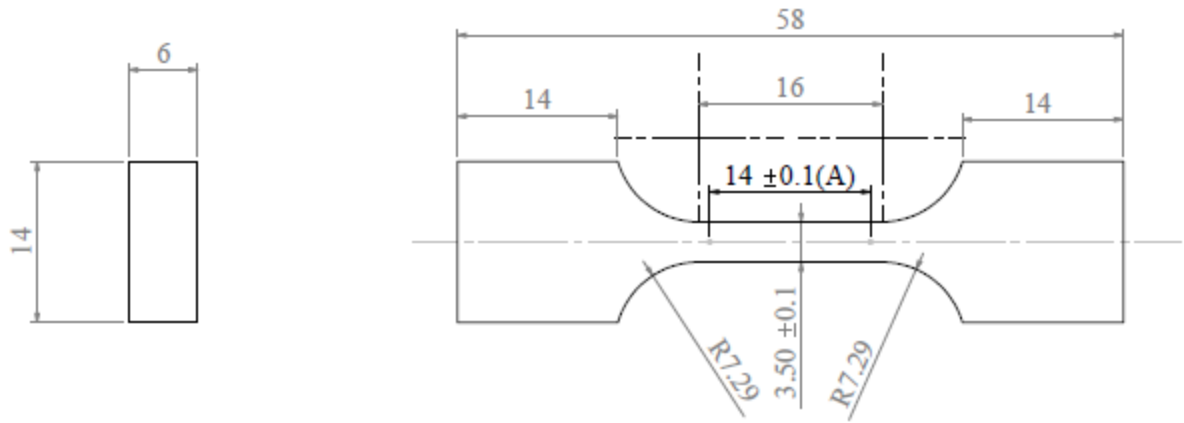


Figure 3.12 Tension sample and the related dimensions according to ASTM standard

4 RESULTS AND DISCUSSION

This chapter is divided into two sections. The results of aging heat treatments and thermo-mechanical treatments of AZ31 and AZ91 will be explained in section 4.1 and 4.2, respectively. Microstructures and the related analysis of AZ31 will be discussed in section 4.1.1 and of AZ91 in 4.2.1. The phase analysis of AZ31 and AZ91 using XRD analysis will be discussed in section 4.1.2 and 4.2.2, respectively. Aging under stress heat treatment processes will be discussed in section 4.1.3 for AZ31 and in section 4.2.3 for AZ91. At the end, the results of mechanical testing at room temperature with a constant strain rate for will be discussed in sections 4.1.4 for AZ31 and 4.2.4 for AZ91.

4.1 Enhancement of AZ31

It was mentioned in the previous chapter that aging experiments were carried out at 150-200-250°C where AZ31 samples were quenched in water immediately right after aging. The aging microstructures, phases and aging under stress results of AZ31 alloys will be discussed through the following sections. Additionally, tensile test results at room temperature after aging and thermo-mechanical treatments will be discussed at the end.

4.1.1 Aging heat treatment

The aging heat treatments without application of stress were tabulated in Table 4.1. Before performing any aging heat treatment, as-received AZ31 was investigated by using optical microscopy. The investigations showed a lot of dendritic cast features in the microstructure. Figure 4.1 illustrates the as-received AZ31 microstructure. This microstructure is a usual cast microstructure which can be seen for all types of cast metal alloys. Although this method has been used for more than 40 years it was recently utilized for Mg alloys productions [43]. According to ASTM standards in Table 2.3, the tensile experiment of the as-received material was in a good range.

The as-received materials were solutionized using different homogenization parameters according to the Mg-Al binary phase diagram as it was shown in Figure 3.1. The homogenization heat treatments were done under open atmosphere at 400°C for different durations (1, 2, 5 and 24 Hours). As a result, 2 hours of solutionizing treatment was chosen to be applied to all other samples due to the elimination of the dendrites and crystallized grains as a homogenization heat treatment on AZ31 samples. Figure 4.2 demonstrates the homogenized microstructure of the AZ31. Another important reason to select a low duration homogenization heat treatment was to protect the matrix from further oxidation.

Table 4.1 Aging conditions for AZ31 alloy

AZ31 Aging Heat treatment workplan	
Time (Hour)	Temperature (°C)
1	150
	200
	250
10	150
	200
	250
24	150
	200
	250
50	150
	200
	250
100	150
	200
	250

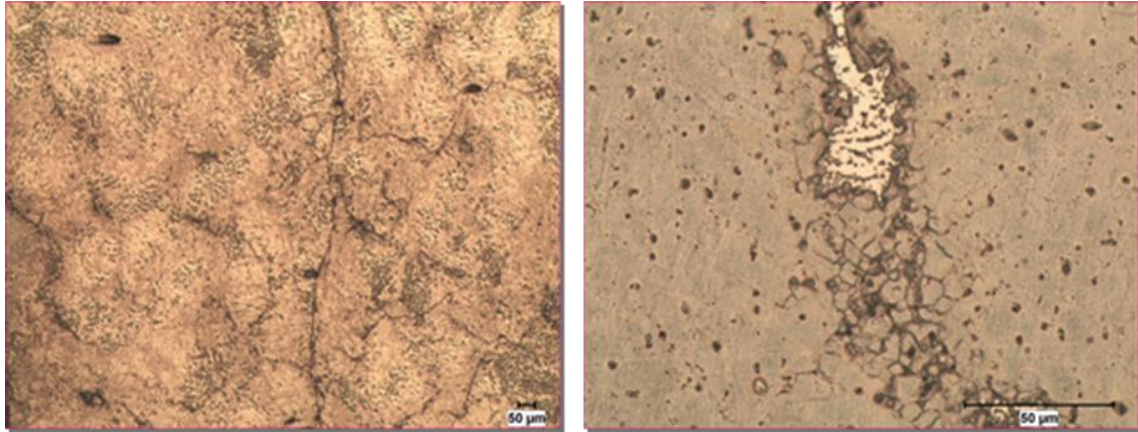


Figure 4.1 Microstructure of as-received twin-rolled AZ31 (left) 50X (right) 500X

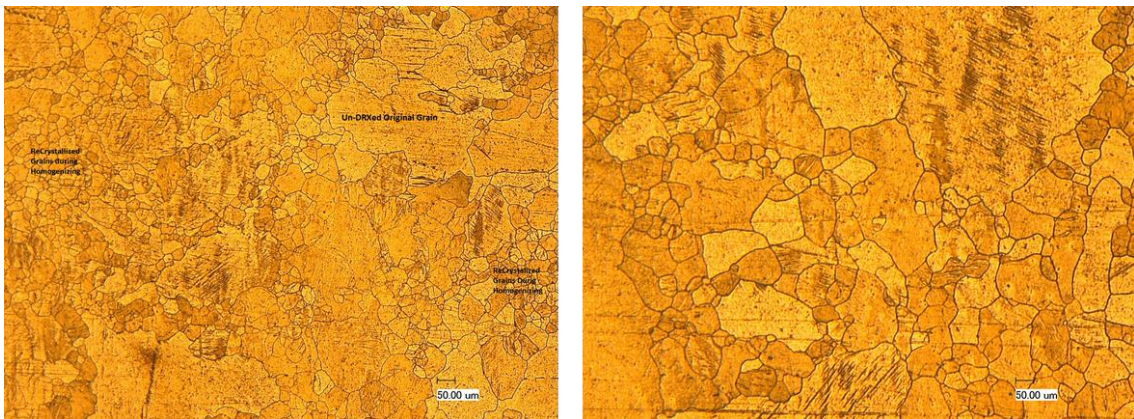


Figure 4.2 Microstructure of the homogenized AZ31 (right) 500X (left) 1000X

Figure 4.3 shows the microstructures of samples which were aged at 150°C, 200°C and 250°C for 1hr and 10hrs. β type $Mg_{17}Al_{12}$ precipitates were not observed in these samples. Some dark particles were revealed mostly inside the grains after etching. It is believed that these might be the precipitates which contain manganese (Mn). Mn is not a standard element which is added to AZ alloys. However, the use of this element has been increased significantly since the addition of Mn to Mg-Al-Zn ternary system causes notable grain refinement [44]. Figure 4.4 shows the microstructures of samples which were aged at 150°C, 200°C and 250°C for 24hrs and 50hrs. Numerous amount of precipitates inside the grains were observed in the sample which was aged at 250°C for 24 hrs. These precipitates were also visible in the in the sample which was aged at 200°C for 24 hrs, however the amount of these precipitates was less than that of the aged sample at 250°C for 24 hrs. The amount of these precipitates was increased significantly via aging for 50 hours. The maximum magnification capability of optical microscopy is around 1,000X. In order to observe the microstructure of the

aged samples with higher magnification and resolution than that of optical microscopy, scanning electron microscopy with an EDS⁶ attachment was used. The chemical composition of the secondary phases was determined using EDS.

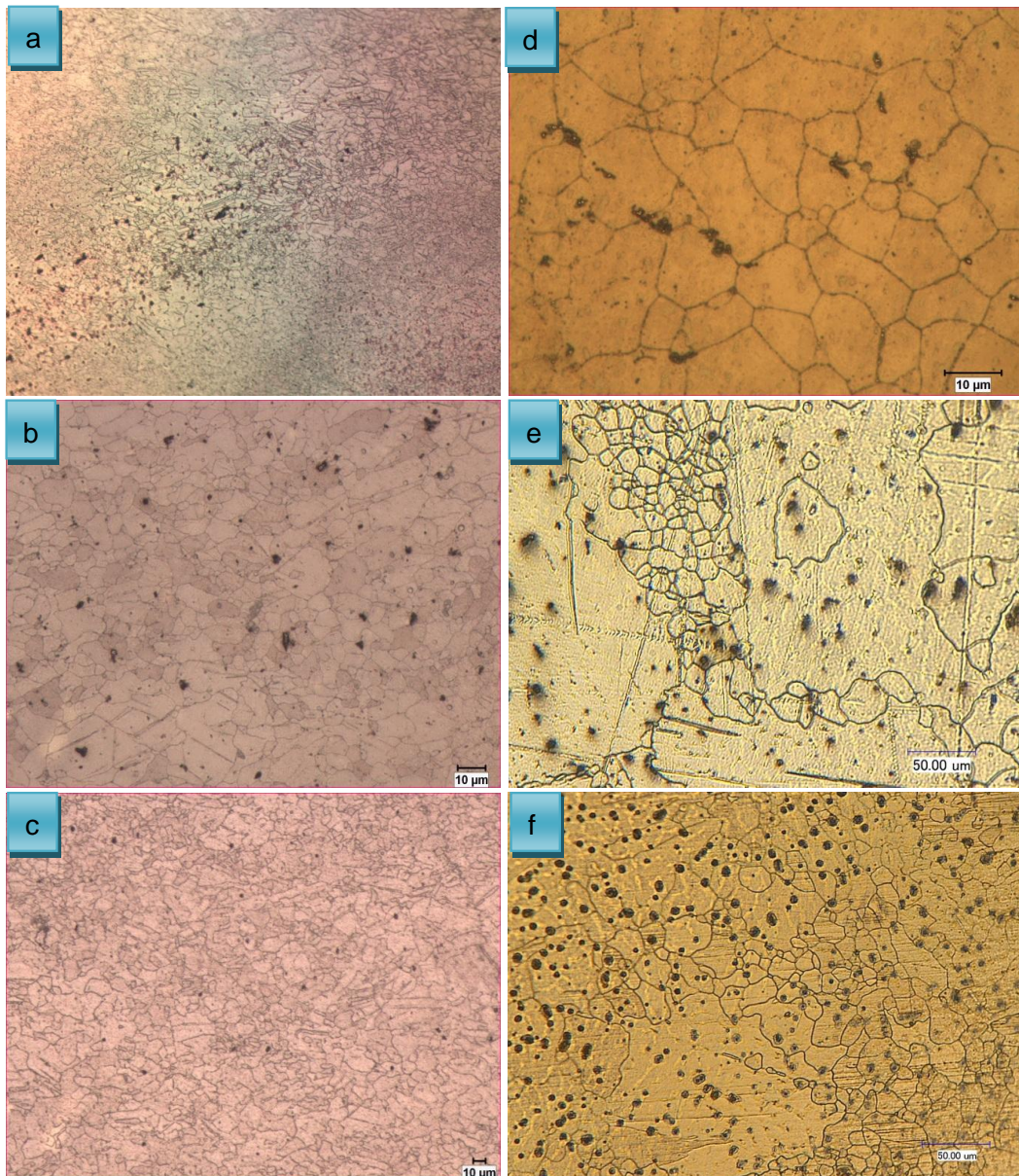


Figure 4.3 Microstructure of aged AZ31 for 1hr at a) 150°C b) 200°C c) 250°C and for 10hrs at d) 150°C e) 200°C f) 250°C

⁶ Electron Dispersive Spectroscopy

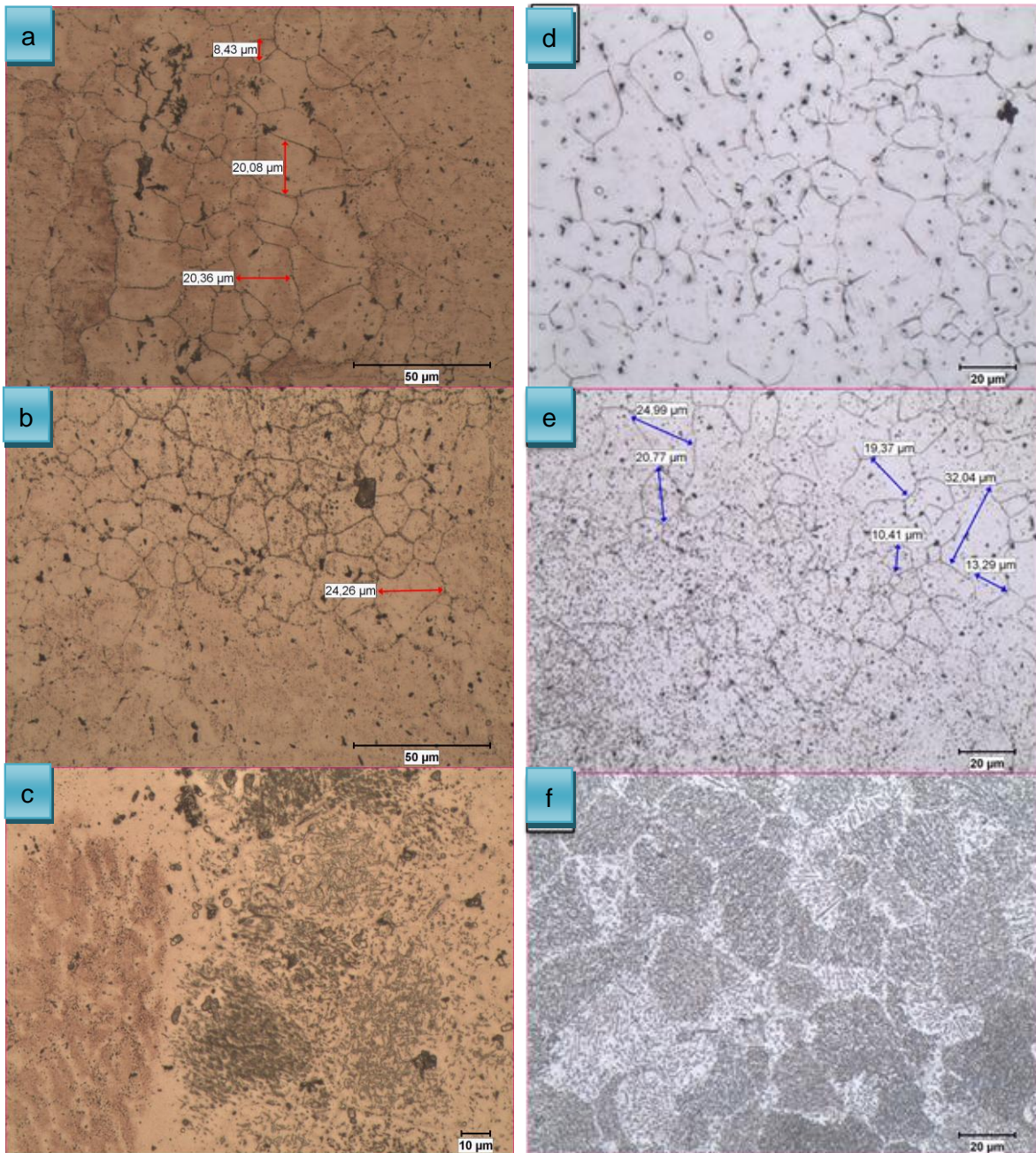


Figure 4.4 Microstructure of aged AZ31 for 24hrs at a) 150°C b) 200°C c) 250°C and for 50hrs at d) 150°C e) 200°C f) 250°C

Figure 4.5 shows SEM image and EDS analysis of the AZ31 sample for 1hr-250°C aged sample from the illustrated region. The normalized element weight percent shown in this figure was around 96.13 wt. % for “Mg”, 2.21 wt. % for “Al”, 0.47 wt. % for “Mn” and 1.19 wt. % for “Zn”. The values were in the specified range of ASTM standards (see Table 3.1) for the elemental compositions of AZ31D.

Further EDS examinations in the aged samples, revealed presence of calcium, silicon and carbon elements in the AZ31 from different regions as in the Figure 4.6. Literature investigations [45, 46] reported the presence and origin of these elements in magnesium alloys. Conventional AZ alloys normally are melted in an electrical resistance furnace using a mild steel crucible. This process is conducted under the protection of mixed gas of CO₂ and SF₆, and during casting procedure C₂Cl₆ or Al₄C₃ powders are plunged into the melt at 740°C. Carbon as well as Manganese are advised as grain refiner elements which can be used in AZ alloys [47].

As mentioned before, aging AZ31 alloy for longer times caused significant increase in precipitation amount and this was observed in optical and SEM analysis clearly. In addition, increasing the aging temperature from 150°C to 200°C and then to 250°C for the same aging time periods, caused meaningful growth in the amount of the precipitates. This high amount of the precipitation growth might be the reason for a notable change in mechanical properties of the samples.

Figure 4.7 and Figure 4.8 depict the distribution of the β -Mg₁₇Al₁₂ precipitates in the matrix of aged samples at 200°C for 10 and 24 hours respectively. It was shown that the precipitates were randomly distributed inside the grains of the sample which was aged for 24 hours, however there were almost no precipitates in the microstructure of the 10 hour aged sample.

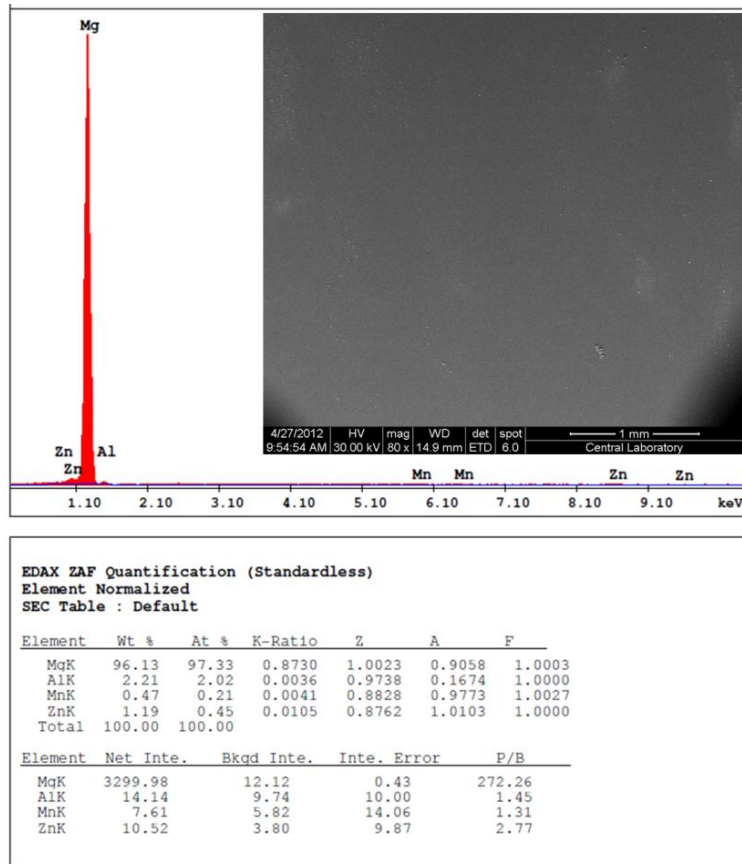


Figure 4.5 Investigation of the chemical composition of AZ31 sample aged at 250°C for 1 hour using EDS.

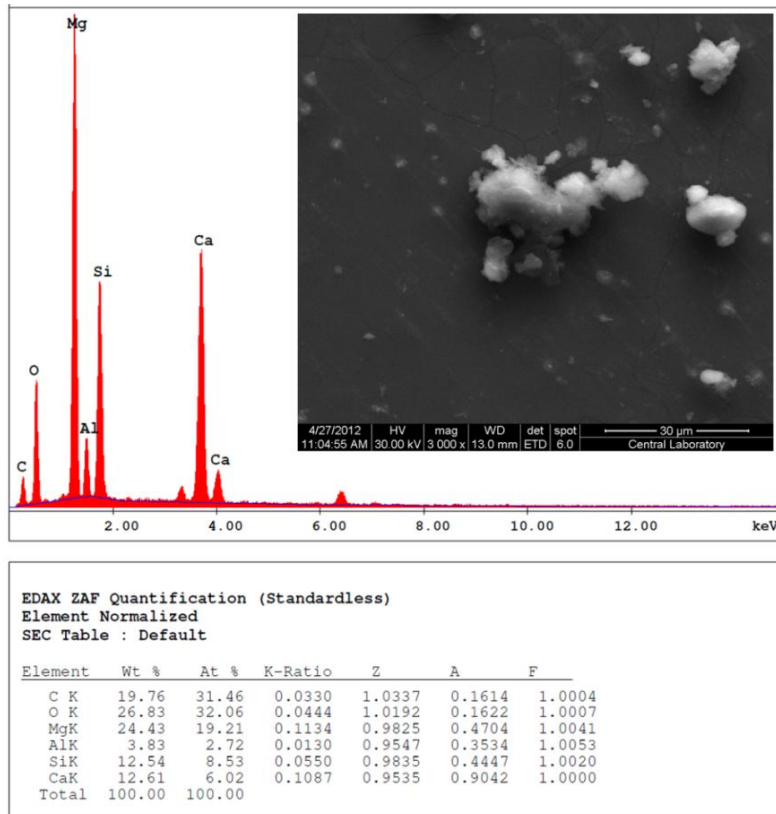


Figure 4.6 Detailed investigation of chemical composition and microstructure of AZ31 which was aged at 250°C for 10hrs

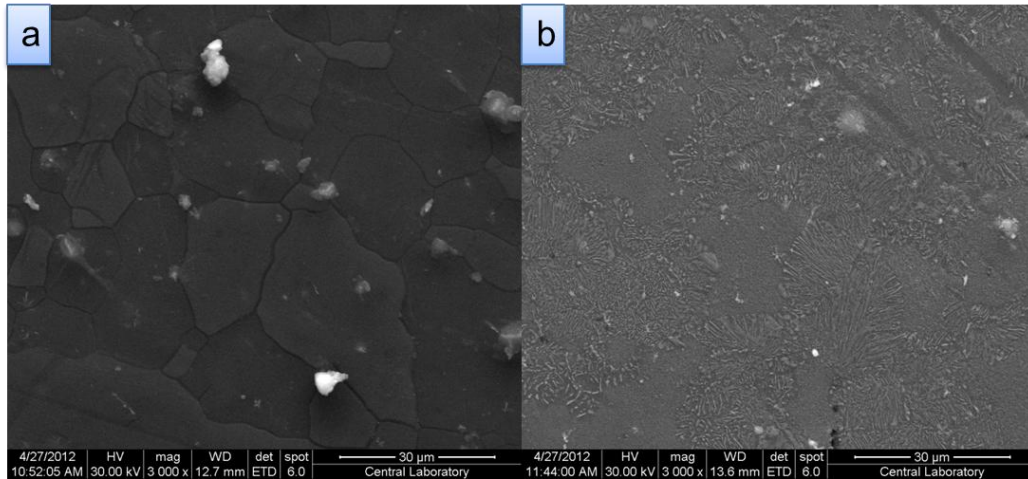


Figure 4.7 Microstructural and precipitate evolution after a) 10hrs and b) 24hrs of aging heat treatments at 200C

The AZ31 samples which were aged at 200°C and 250°C for 24 hrs were also investigated using SEM for revealing the shape and orientation of the precipitates inside the grains at higher magnifications (see Figure 4.8 and Figure 4.9). The precipitate formation is one of the methods to increase the strength of the metallic alloys [17]. However the precipitates which were grown along the grain boundaries of the AZ31 sample which was aged at 250°C for 24 hrs might be the reason of the decrease in mechanical properties. Comparing the amount of the precipitates inside and along the boundaries of grains demonstrate that the amount of the precipitates inside grains is much higher than that of along the boundaries.

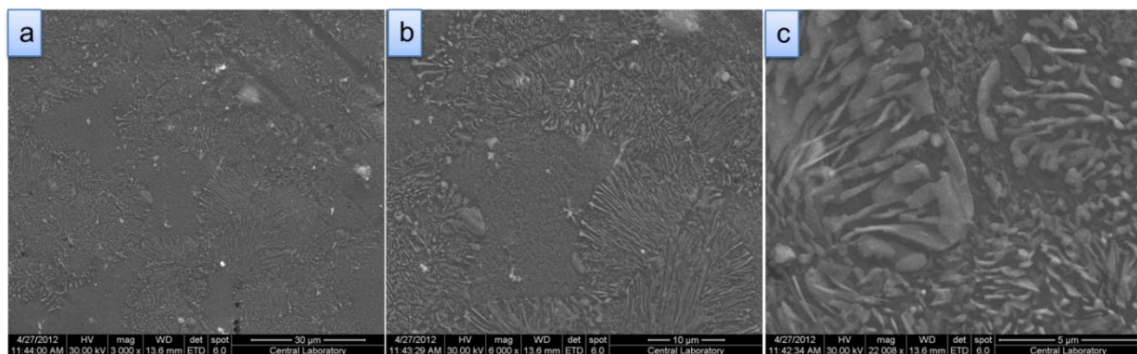


Figure 4.8 Precipitate distribution and shapes at 24H-200°C aging heat treatment a)3000x b)6000x c)22000x

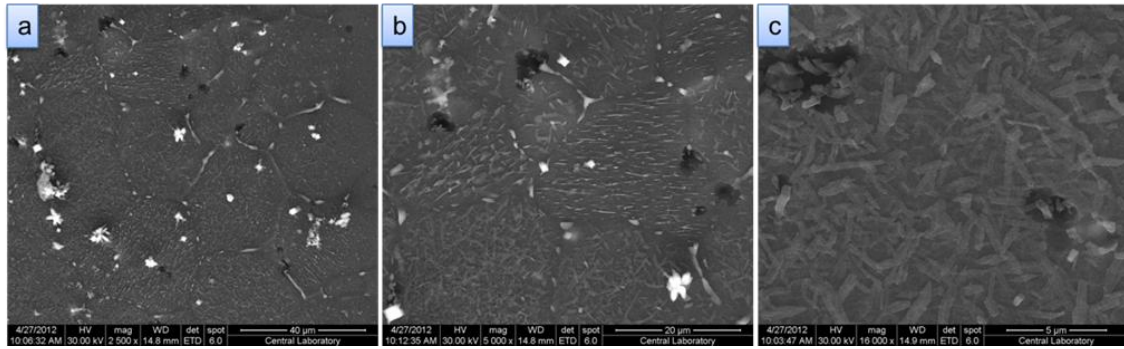


Figure 4.9 Precipitate distribution and shapes in the AZ31 sample aged at 250°C for 24 hrs a)2500x b)5000x c)16000x

4.1.2 Phase study in AZ31

Mg-Al-Zn(Mn) alloys were known to be a highly precipitation hardenable alloys. Recent studies on the ternary Mg-Al-Zn system using XRD, WDX/EDX kind of phase characterization techniques have distinguished around 10 different types of phases which are represented in the Table 4.2 [48].

Table 4.2 Crystal structures and phase descriptions

System	Phase	Prototype	Pearson symbol	Space group	Comments
Al	(Al)	Cu	cF4	$Fm\bar{3}m$	
Mg	(Mg)	Mg	hP2	$P6_3/mmc$	
Zn	(Zn)	Mg	hP2	$P6_3/mmc$	
Al-Mg	Al_3Mg_2	Al_3Mg_2	cF1832	$Fd\bar{3}$	β
	$Al_{30}Mg_{23}$	$Co_5Cr_2Mo_3$	hR53	$R\bar{3}$	ϵ
	$Al_{12}Mg_{17}$	αMn	cI58	$I\bar{4}3m$	γ
Mg-Zn	Mg_7Zn_3		oI142	$Immm$	$Mg_{51}Zn_{20}$
	MgZn				$Mg_{12}Zn_{13}$
	Mg_2Zn_3		mC110	$B2/m$	
	$MgZn_2$	$MgZn_2$	hP12	$P6_3/mmc$	Laves-C14
	Mg_2Zn_{11}	Mg_2Zn_{11}	cP39	$Pm\bar{3}$	
Al-Mg-Zn	Φ		orthorh.		
	τ	$Mg_{32}(Al,Zn)_{49}$	cI162	$Im\bar{3}$	

The main intermetallic component β - $Mg_{17}Al_{12}$ which grows generously in AZ alloys was our main concern. The evolution of this intermetallic with the application of different aging procedure was investigated using X-Ray diffraction method. The X-Ray investigations were performed between 20-120 degree with the scanning speed of 2°/min and using the Cu-K α source for the radiation.

Figure 4.10 and Figure 4.11 shows the comparison of the XRD patterns for the samples aged at 150°C, 200°C and 250°C for 1 and 5 hours, respectively. Figure 4.12 shows the XRD pattern for the homogenized AZ31 sample in comparison with the aged samples at 250°C. It was shown that due to effect of homogenization heat treatment, most of the precipitates were dissolved in the matrix and there was no obvious trend in quantitative and optical analysis either. Normally, β -Mg₁₇Al₁₂ peaks appear between 38 and 45 degrees with very small intensities. No peaks for β -Mg₁₇Al₁₂ have been observed for the samples aged for short period of times.

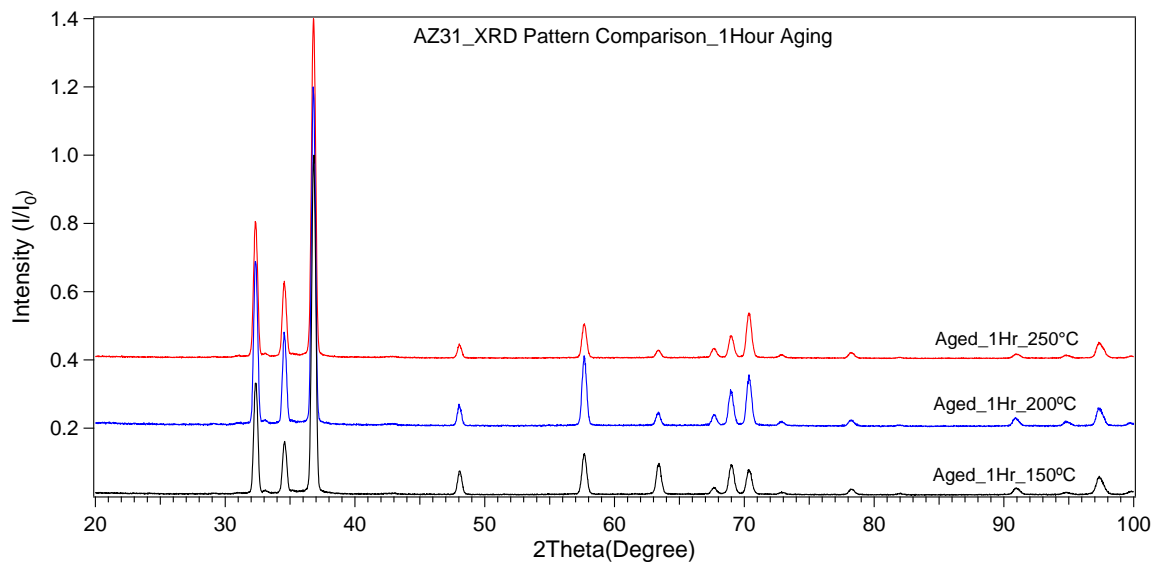


Figure 4.10 Comparison of the XRD patterns of the samples aged at different temperatures for 1Hour.

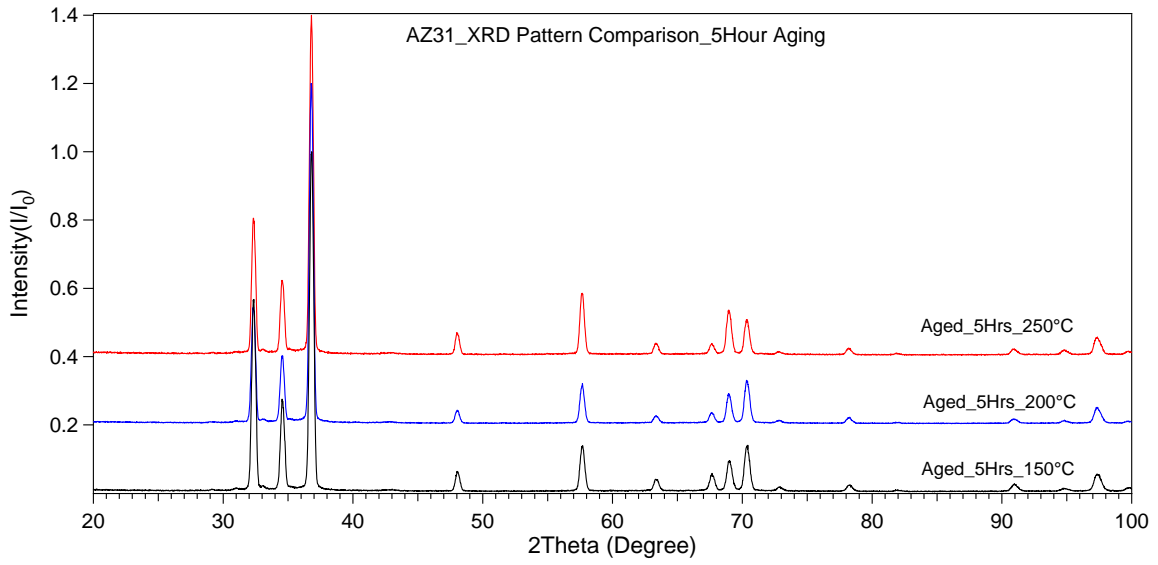


Figure 4.11 Comparison of the XRD patterns of the samples aged at different temperatures for 5 Hours.

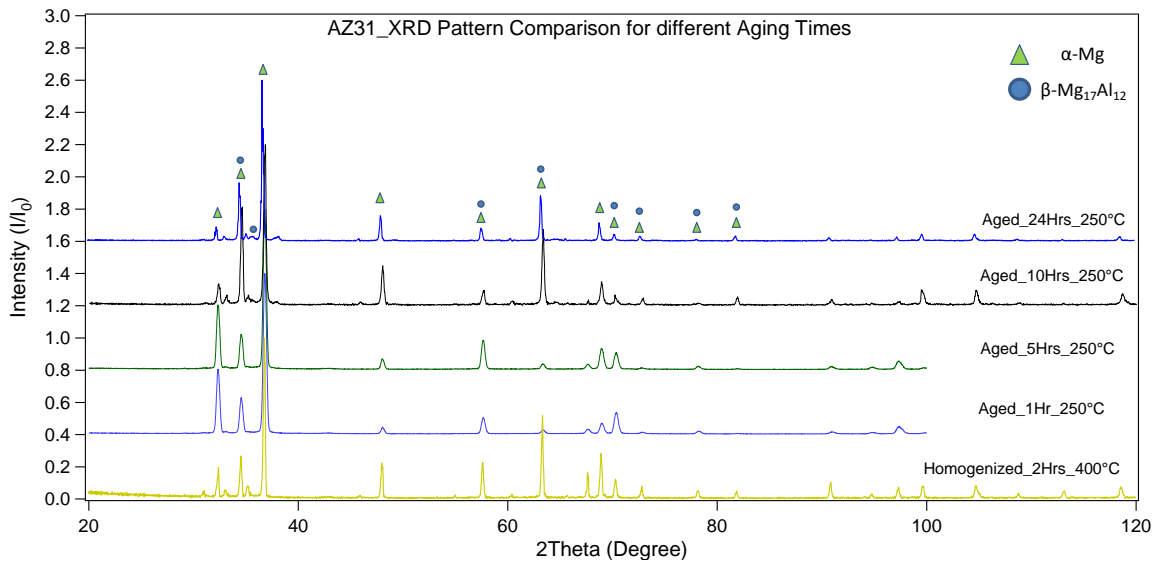


Figure 4.12 Comparison of the XRD patterns of the samples aged at 250°C for different aging periods.

Figure 4.13 compares the XRD patterns of the samples at different temperatures for 24 hours. According to the phase diagram of the AZ31, theoretically it is accepted that aging at 250°C is a way to increase the amount of $Mg_{17}Al_{12}$ precipitates. Investigation of the XRD patterns (Figure 4.10 to Figure 4.13) using the “Match!” software, the amount of the precipitates in the aged samples is found.

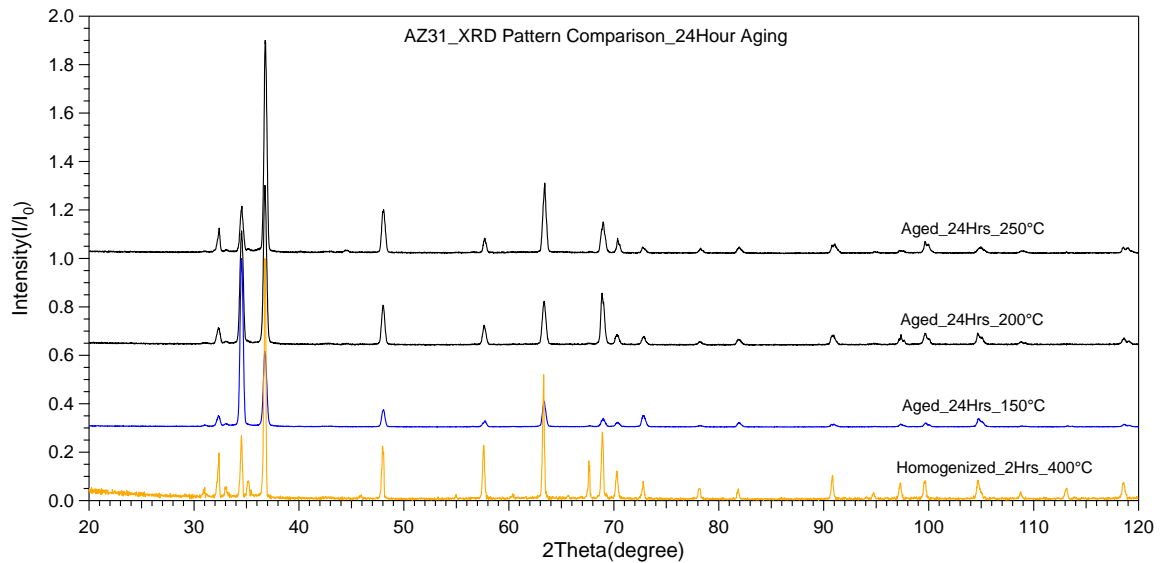


Figure 4.13 Comparison of the XRD pattern of the samples aged at different temperatures for 24 Hours

Using the International diffraction database version 2.0 in this work, the amount of β - $Mg_{17}Al_{12}$ precipitate was estimated. It was found that the amount of β - $Mg_{17}Al_{12}$ precipitate of the sample aged at 250°C for 24 hrs was around 2.2 weight percent. Aging at 250°C for 24hrs increases the amount of precipitates comparing with the aged samples for shorter time periods.

Table 4.3 shows the most important results which were determined by comparing the patterns of different samples using the PDF databases. P(I/I₀) is the probability of which the intensities of the entry's correlated peaks match the intensities of the peaks in the experimental pattern and P(Peak positions) is the probability of which the entry's peak positions match the 2 theta values of the peaks in the experimental pattern.

Table 4.3 Results which are obtained from the XRD patterns of AZ31 samples which are aged at 250°C

AZ31 XRD results comparison for different aging duration at 250°C			
Aging duration	P (Peak positions)	P (I/I0)	Mg ₁₇ Al ₁₂ (wt. %)
1	0.22	0.54	~ 0
5	0.27	0.21	~ 0
10	0.47	0.02	~ 0
24	0.74	0.75	2.2

In the XRD pattern of the sample aged at 250°C for 1hr, only 0.2265 of the peak positions were matched with the peaks in the standard pattern of β -Mg₁₇Al₁₂. In the pattern of the sample aged for 5hrs, only 0.2725 of the peak positions were matched with the peaks in the standard pattern of β -Mg₁₇Al₁₂ and for 10 hours aged sample, 0.4740 of the peak positions were matched with the peaks in the standard pattern of β -Mg₁₇Al₁₂. These results were just the approximate amount of the β -Mg₁₇Al₁₂ precipitates in the AZ31 samples after aging. It is possible to obtain near exact amounts of the precipitates by increasing the XRD scanning duration or decreasing the scanning speed. The XRD investigation proved that the amount of the β precipitates was increased by increasing aging duration at 250°C. As the aging time was increased to 24 hours, the peak positions and also the peak intensity factors were matched more than 0.75 with the standard peaks of β -Mg₁₇Al₁₂. Quantitative XRD analyses proved that 2.2 wt% of the aged sample at 250°C for 24 hours consists of the β precipitates. This result shows that almost all of the aluminum was converted to the β precipitates when aging the AZ31 alloys for longer than 24 hours. It should be noted that the amount of aluminum inside the AZ31 is around 3%.

Table 4.4 Calculated parameters for the AZ31-24Hour-250°C aged sample

Matched Phases for AZ31 24Hour 250°C Aged Sample			
Formula	Mg	Mg _{0.97} Zn _{0.03}	Mg ₁₇ Al ₁₂
Peaks matched	0.96	0.77	0.74
Intensity scale factor	0.79	0.98	0.75
Quant. (weight %)	94.1	3.7	2.2

4.1.3 Aging under stress

Aging under stress experiments were performed after all the free aging treatments were finished and the effect of aging temperatures and durations on the microstructure of the samples was investigated. Then, the samples were age-tensioned according to the tabulated parameters in Table 4.5.

Table 4.5 AZ31 aging under stress experiments

Aging under stress experiments			
Duration (Hour)	Temperature (°C)	Stress (MPa)	Load type
1	150	20	Tension
1	200	20	Tension
1	250	20	Tension
1	150	40	Tension
1	200	40	Tension
1	250	40	Tension
1	150	60	Tension
1	200	60	Tension
1	250	60	Tension
1	250	80	Tension

Figure 4.14 depicts the stress vs time curves for different age-tensioned experiments (aging under tensile type of stress) at 250°C. The oscillations at the beginning of some of the curves came from the high creep behavior of the AZ31 alloys which causes instabilities at the constant stress values. The used universal tensile machine was a servo-mechanic type and the employed AC motor in this device was not capable to respond to the rapid load changes. There was no oscillation during the experiments conducted at 150°C and under 20MPa constant stress experiments. As it was shown in Figure 4.14, 4.15 and 4.16, the creep and instability of stress values were increased as the stress or temperature were increased.

The amount of creep strain can be measured during these experiments, however due to the difficulty in the mounting of the extensometer and its low accuracy at low strain values, the creep strain measurements were not performed in detail.

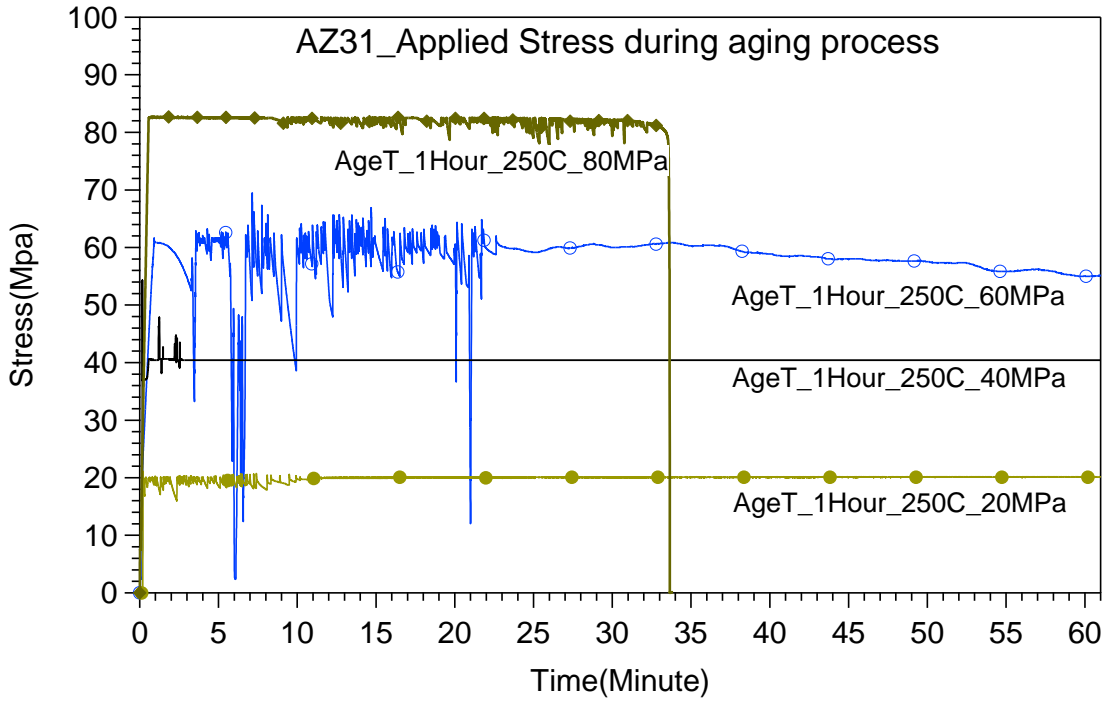


Figure 4.14 Applied stress vs Time curves for the samples aged at 250°C under 20, 40, 60 and 80MPa for 1hr.

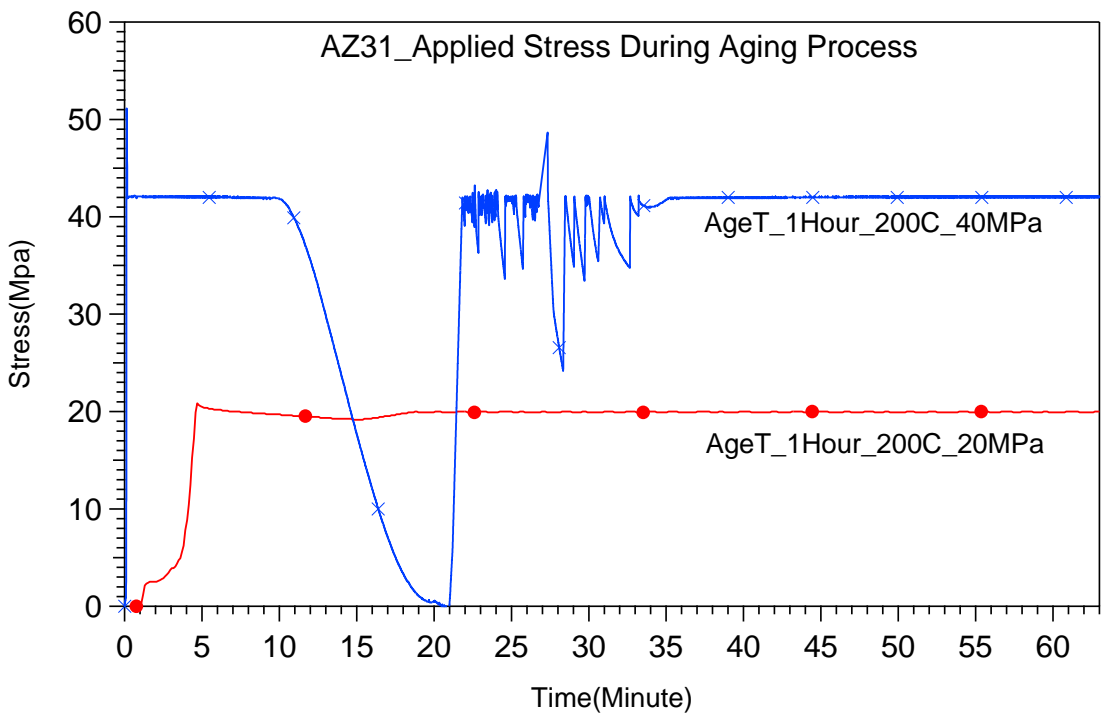


Figure 4.15 Applied stress vs Time curves for the samples aged at 200°C under 20 and 40MPa for 1hr.

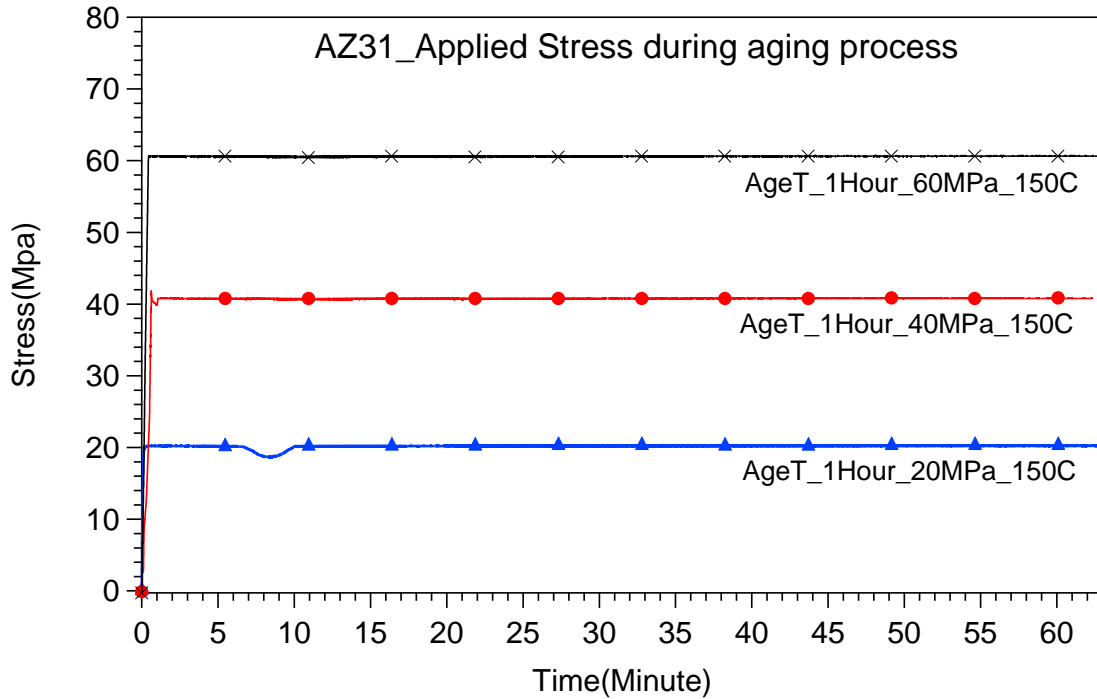


Figure 4.16 Applied stress vs Time curves for the samples aged at 150°C under 20, 40 and 60MPa for 1hr.

The heating setup for aging under stress experiments by using the environmental chamber was shown in Figure 3.7. This process was explained in the previous chapter. The heating time took around 15 minutes to reach to the desired temperature and stabilize there. There was a waiting moment in the chamber to reach the required temperature however, during this waiting period the samples were still under constant stress. Figure 4.17 shows the heating procedure of the age-tensioned samples inside the environmental chamber.

The age-tensioning experiment at 250°C under 80 MPa constant stress could not be successfully performed till the end due to the creep failure of the sample. Figure 4.18 illustrates the stress versus the measured strain by using the high temperature extensometer. As it is mentioned before, our extensometer was not precise enough to measure the amount of strains at these low loads. However, the amount of elongation in this specimen was high enough to be measured by the extensometer due to its creep behavior. This sample showed around 21% creep strain until necking point and then quickly fractured.

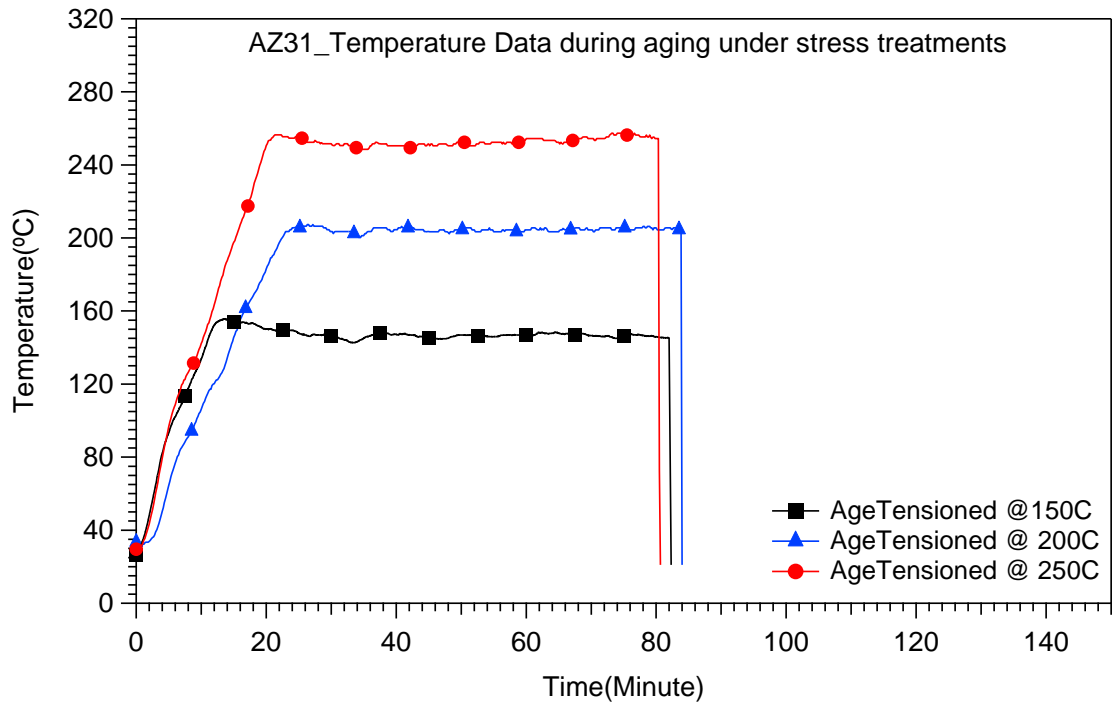


Figure 4.17 Temperature vs Time curves for the samples age-tensioned at 150, 200 and 250°C samples.

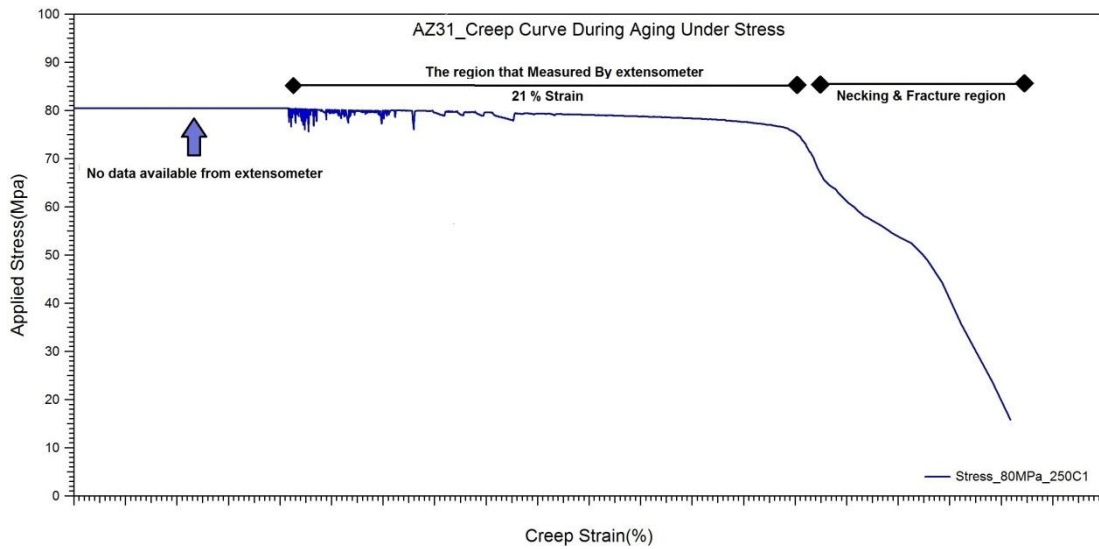


Figure 4.18 Creep behavior and fracture of AZ31 under 80MPa loading

4.1.4 Tensile testing of AZ31

After all the aging and aging under stress experiments were performed and their microstructures were revealed, tensile tests were performed at room temperature to characterize the mechanical properties of heat treated samples.

Figure 4.19 shows the stress-strain curves of the samples aged at 150, 200 and 250°C for 1hr in comparison with the as-received and the homogenized samples. A quick look at this curve shows that the aged samples have better ductility and strength than that of the as-received and homogenized samples. The as-received sample showed similar ultimate tensile strength (UTS) as the aged samples showed however due to the heterogenous microstructure; it was fractured via showing less elongation (8% of strain). On the other hand, the homogenized sample showed both better ductility and ultimate tensile strength than that of the aged and as-received samples. However, its yield strength was much lower than that of the aged samples. This result was the proof of precipitation hardening capacity of the AZ31 alloy.

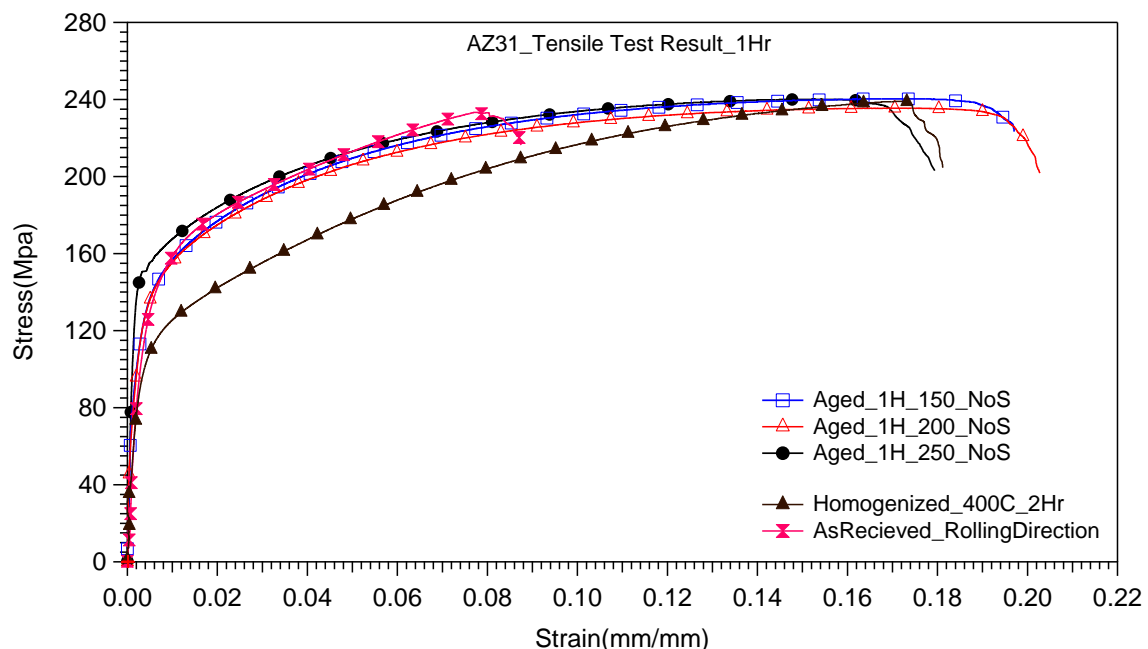


Figure 4.19 Tensile test results of the samples aged at 150, 200, 250°C for 1 hr, as-received and homogenized samples.

Figure 4.20 shows that there was no need to age the samples for longer times at 150°C. Even though the highest strain value (22.71%) was achieved from the sample aged at 150°C for 100 hours, the yield and tensile strength of this aged samples were lower than that of the sample aged at the same temperature for 1hr. The elongations of the samples aged for 5hrs and for 1hr under 40MPa were 20.5% and 18.72%, respectively. These values are close to the elongation values of the sample aged for 100hrs. The sample aged for 1hr under 40MPa showed the highest ultimate tensile strength value which was 241.4MPa.

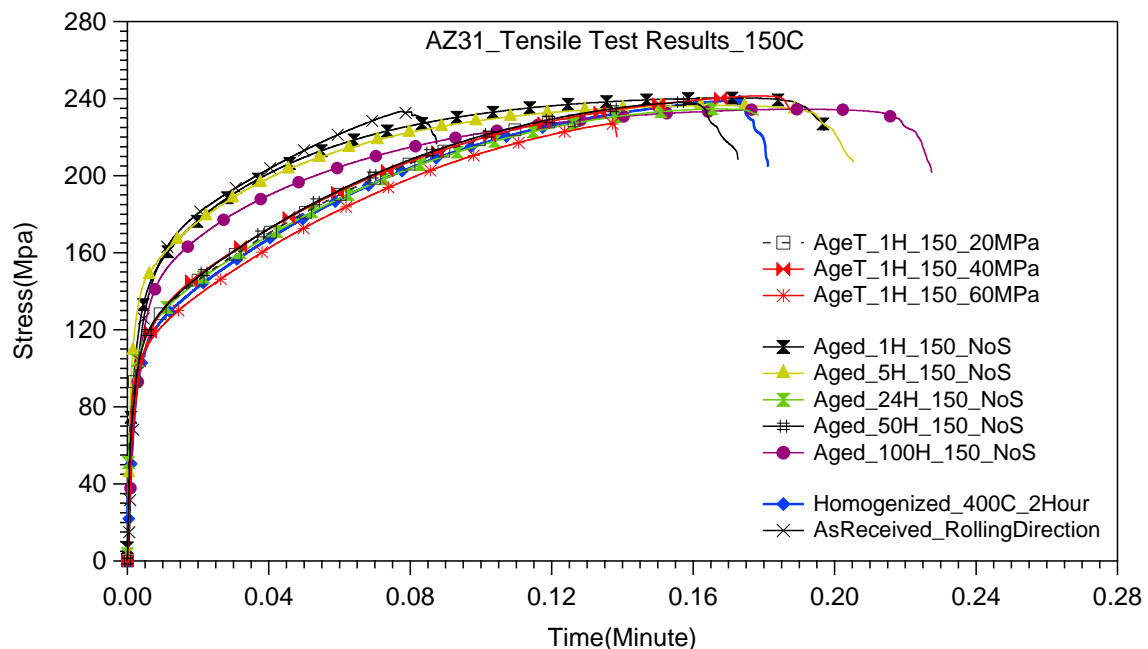


Figure 4.20 Tensile test results of the samples aged at 150°C for 1, 5, 24, 50 and 100hrs under no stress and for 1hr under 20, 40 and 60MPa constant stress levels.

Figure 4.21 demonstrates the tensile results of the samples aged at 200°C. The sample aged at 200°C for 1hr under 20MPa shows the highest yield and fracture strength and also the highest elongation in comparison with the other samples aged at this temperature. Additionally, the UTS of this sample was 255.7MPa and its yield strength was 147MPa which were the highest values comparing with all of the other samples aged at the other temperatures.

Figure 4.22 compares the tensile test results of all of the samples aged at 250°C. Similar to the results determined from the samples aged at 200°C, it was observed that the yield strength, tensile strength and ductility of the sample aged under 20MPa were notably higher than that of the other aged and age-tensioned samples at 250°C. This might be because of possible precipitate orientations inside the matrix causing the increase in the strength of the samples, however this needs more investigations using advanced microstructure characterization methods such as transmission electron microscope.

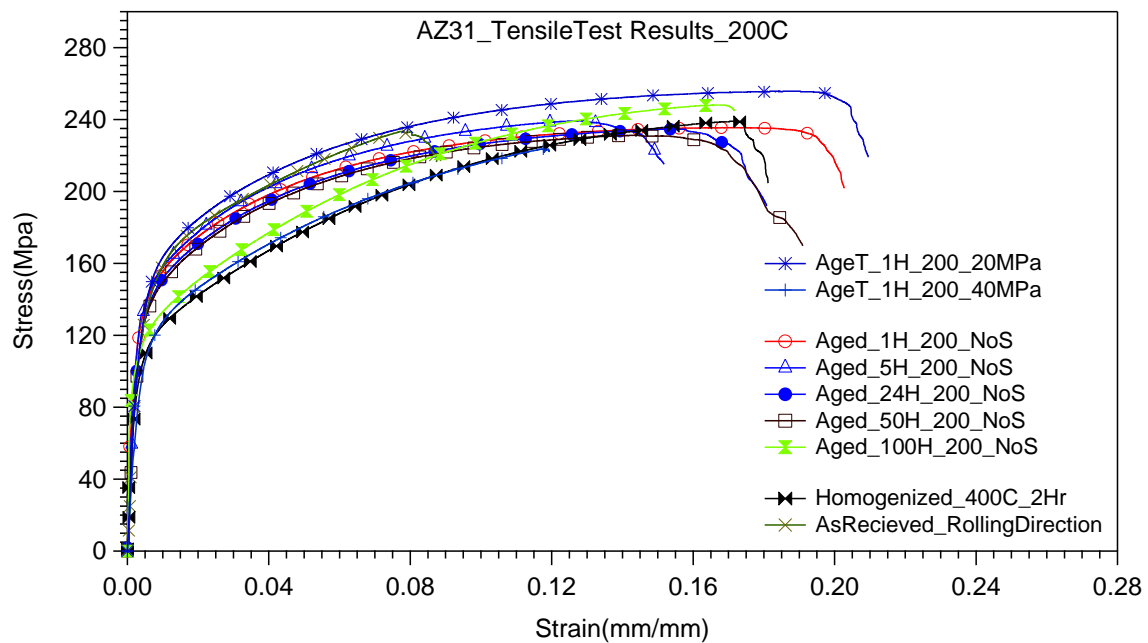


Figure 4.21 Tensile test results of the samples aged at 200°C for 1, 5, 24, 50,100 hrs under no stress and for 1 hr under 20 and 40MPa.

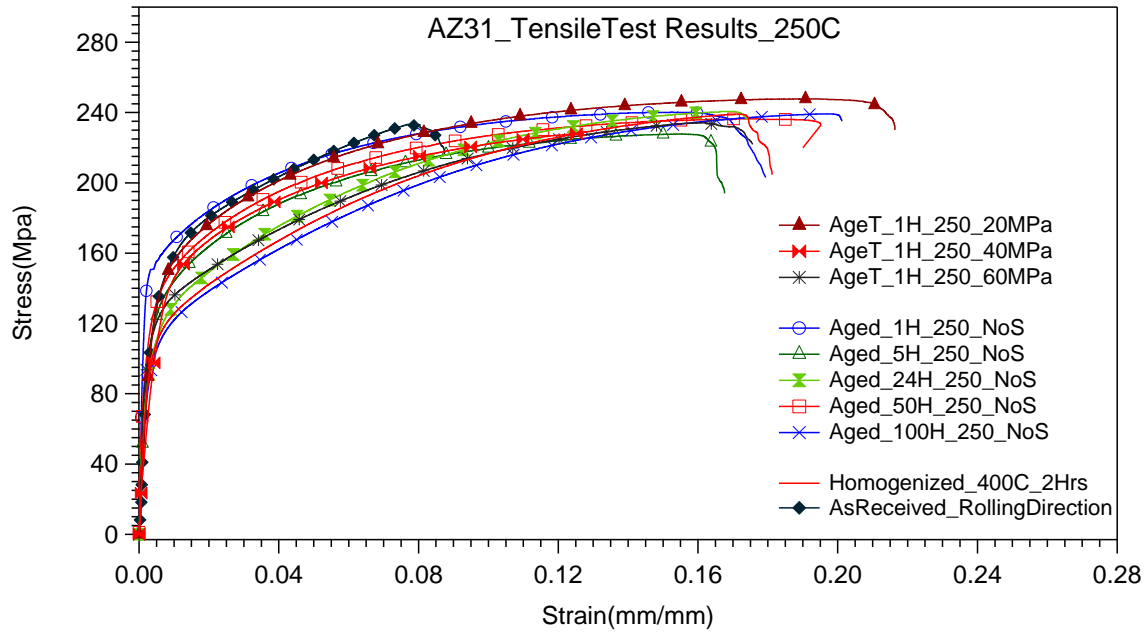


Figure 4.22 Tensile test results of the samples aged at 250°C for 1, 5, 24, 50,100 hrs under no stress and for 1 hr under 20, 40MPa and 60MPa.

The analyses of the tensile curves of the AZ31 samples aged at different conditions were tabulated in Table 4.6, 4.7 and 4.8. The yield strength values from the curves were obtained using 0.2% offset method.

Table 4.6 AZ31 Tensile Properties for 150°C Heat Treatments

AZ31 Tensile Properties for 150°C Heat Treatments			
Heat Treatments	Elongation @ Fracture (%)	Yield Stress (MPa)	UTS (MPa)
As-Received	8.7	112	233.31
Homogenized	18.1	111	239
1 Hour	19.7	129	240.3
5 Hours	20.5	137	236.5
24 Hours	17.85	105	234.7
50 Hours	17.27	111.65	238.13
100 Hours	22.71	141	234.47
1 H – 20 MPa	12.66	112.41	229.75
1 H – 40 MPa	18.72	116.31	241.39
1 H – 60 MPa	13.78	107	226.99

Zhao et. al. Results [19]
As-Received, UTS: 245MPa Elongation 2%
Homogenized, UTS: 241MPa Elongation 14%

Table 4.7 AZ31 Tensile Properties for 200°C Heat Treatments

AZ31 Tensile Properties for 200°C Heat Treatments				
Heat Treatments	Elongation @ Fracture (%)	Yield Stress (MPa)	UTS (MPa)	Zhao et. al. Results [19] As-Received, UTS: 245MPa Elongation 2% Homogenized, UTS: 241MPa Elongation 14%
As-Received	8.7	112	233.31	
Homogenized	18.1	111	239	
1 Hour	20.1	136.2	235.5	
5 Hours	15.8	137	239.17	
24 Hours	17.4	137	234.62	
50 Hours	16.9	138	231.3	
100 Hours	17	109	248.07	
1 H – 20 MPa	20.89	147	255.7	
1 H – 40 MPa	11.93	116	223.59	
1 H – 60 MPa	-	-	-	

Table 4.8 AZ31 Tensile Properties for 250°C Heat Treatments

AZ31 Tensile Properties for 250°C Heat Treatments				
Heat Treatments	Elongation @ Fracture (%)	Yield Stress (MPa)	UTS (MPa)	Zhao et. al. Results [19] As-Received, UTS: 245MPa Elongation 2% Homogenized, UTS: 241MPa Elongation 14%
As-Received	8.7	112	233.31	
Homogenized	18.1	111	239	
1 Hour	17.9	153	240.28	
5 Hours	16.5	121	227.7	
24 Hours	17.3	103.5	240.5	
50 Hours	19.5	136	236.3	
100 Hours	20	105	239.24	
1 H – 20 MPa	21.57	145	247.7	
1 H – 40 MPa	17.36	125.1	240.53	
1 H – 60 MPa	17.49	113	234.18	

4.2 Enhancement of AZ91

Aging, aging under stress heat treatments and characterization of the AZ91 samples will be discussed in this section. All types of heat treatments and characterizations which were conducted on AZ31 were also performed on AZ91 samples. The aging microstructures, phases and aging under stress results of AZ91 alloys will be discussed through the following sections. Furthermore, tensile test results at room temperature after aging and thermo-mechanical treatments will be discussed at the end.

4.2.1 Aging heat treatment

The aging heat treatments were carried out at 150-200-250°C without application of any stress. The samples were quenched in water right after aging. The investigations of the microstructure of the as-received, homogenized and aged AZ91 samples are presented correspondingly in this section. Table 4.9 shows the aging conditions. The influence of three different temperatures in different aging durations was analyzed. Before performing any aging heat treatment, as-received AZ91 was investigated by using optical microscopy. Figure 4.23.a illustrates the as-received AZ91 microstructure. The result of the tension experiment of the as-received material was consistent with the tensile test result which was found in ASTM standards. The data from these standards were previously shown in Table 2.3.

The as-received materials were solutionized using different homogenization parameters considering the Mg-Al binary phase diagram and the studies in the literature [49]. According to the previous reports, the “ β ” precipitates begin to dissolve in the “ α ” matrix at temperatures around 330°C [50]. First of all, homogenization heat treatment in open atmosphere at 450°C for 30 minutes was performed. Due to the fact that magnesium is very reactive at high temperatures under open atmospheric conditions, the sample was vaporized and there was almost nothing left inside the furnace. The vaporized sample is shown in the Figure 4.24. This high temperature was selected according to the binary phase diagram of Mg-Al alloy system in order to dissolve the “ β ” phases as quick as possible with minimum increase in grain size and minimum loss of mechanical

properties according to Hall-Patch equation [22]. However due to the problem observed in the previous homogenization treatment, the homogenization temperature and its duration were decreased to 425°C and 15 minutes respectively. The result of this heat treatment was acceptable from microstructural point of view and it was shown in Figure 4.23. There was a small amount of precipitates all around the structure and along the grain boundaries. The average grain size of the homogenized sample was around 230µm. All of the samples were homogenized at this condition before performing any type of aging and thermomechanical treatments.

Table 4.9 Aging conditions for AZ91 alloy

AZ91 Aging Heat treatment workplan	
Time (Hour)	Temperature (°C)
1	150
	200
	250
10	150
	200
	250
24	150
	200
	250
50	150
	200
	250
100	150
	200
	250

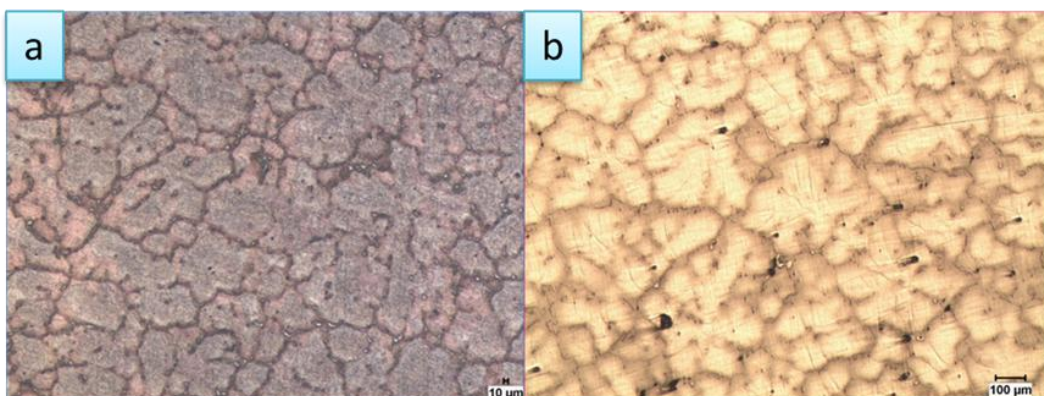


Figure 4.23 AZ91 samples a) before homogenization and b) after homogenization



Figure 4.24 Vaporized AZ91 sample which was tried to be homogenized at 450C for 30 Minutes

Figure 4.25, Figure 4.26 and Figure 4.27 present the aged microstructures of AZ91 at 150, 200 and 250°C for 1, 24 and 50hrs, respectively. There were many precipitates along the grain boundaries such that in some cases the width of the precipitates reached to 15 μm . Figure 4.28 shows the aforementioned large precipitates along the grain boundaries of the samples which were aged at 250°C for 50hrs and at 150°C for 24hrs, respectively. Under equilibrium solidification conditions, microstructure of the AZ91 contains “ α ” solid solution with “ $\beta\text{-Mg}_{17}\text{Al}_{12}$ ” precipitates in the matrix[41]. More investigations using scanning electron microscopy revealed more $\beta\text{-Mg}_{17}\text{Al}_{12}$ precipitates along the boundaries. These observations proved that unlike AZ31, the β precipitate gathers at grain boundaries in AZ91.

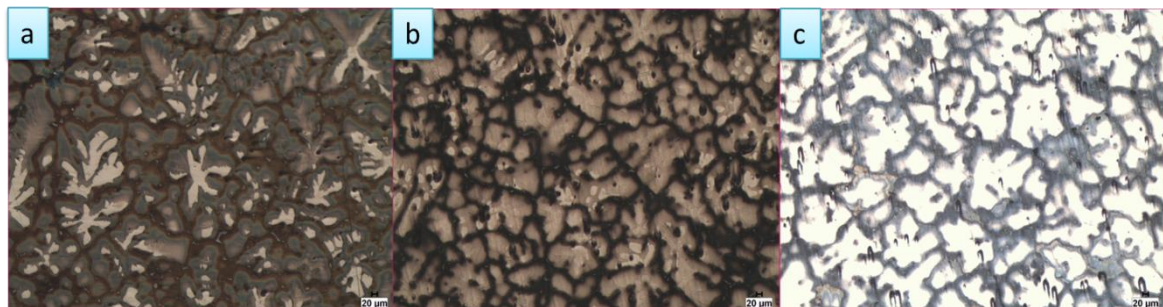


Figure 4.25 Microstructure of aged samples for 1 hour at a) 150°C b) 200°C c) 250°C

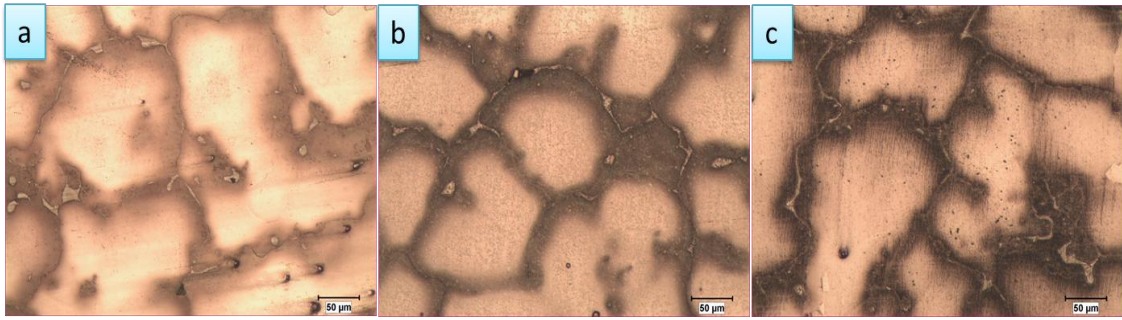


Figure 4.26 Microstructure of aged samples for 24 hours at a) 150°C b) 200°C c) 250°C

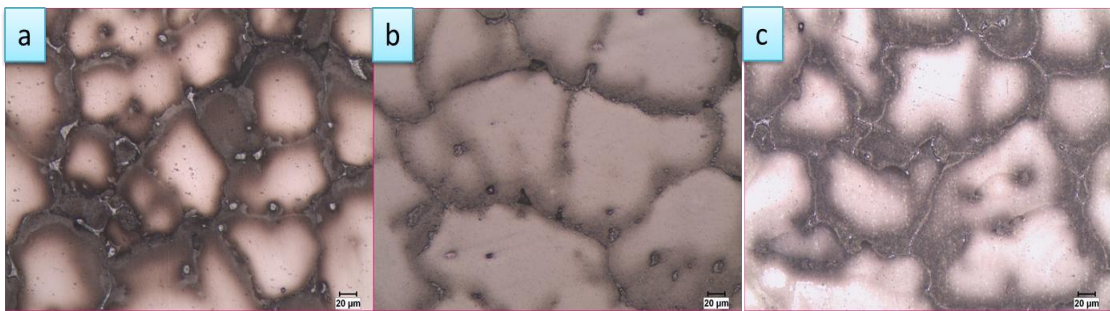


Figure 4.27 Microstructure of aged samples for 50 hours at a) 150°C b) 200°C c) 250°C

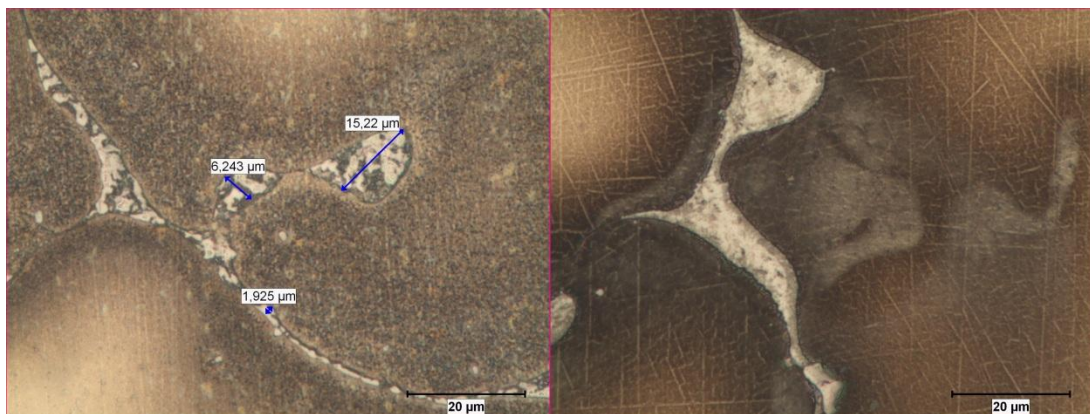


Figure 4.28 Precipitate distribution along the grain boundaries of AZ91 samples aged for left) 50hrs at 250°C and for right) 24hrs at 150°C

The accumulated “ β ” precipitates along the grain boundaries of AZ91 samples were in different shapes. Figure 4.29 and Figure 4.30 show the scanning electron microscopy images of the microstructures of the aged samples for 24hrs at 200°C and at 250°C respectively. These images show that the distribution of the precipitates was homogeneous all over the matrix. EDS analysis determined

calcium, Silicon and carbon elements numerous inside the AZ91 samples the same as AZ31. Figure 4.31 and Figure 4.32 show the estimated percentages of these elements which were determined from the shown regions. These elements were added during the process of melting to enhance the mechanical properties. Literature investigations show that carbon was plunged into the melt as C_2Cl_6 or Al_4C_3 powders and “manganese” was added due to its grain refining effects. [45-47].

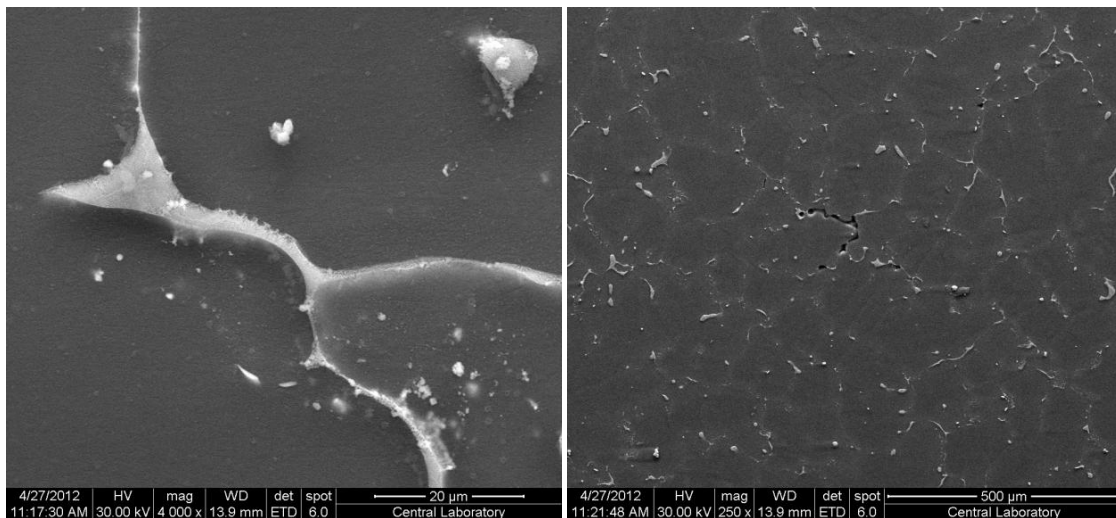


Figure 4.29 The precipitate distribution in the matrix and along the grain boundaries of the AZ91 sample which was aged at 200°C for 24 hrs

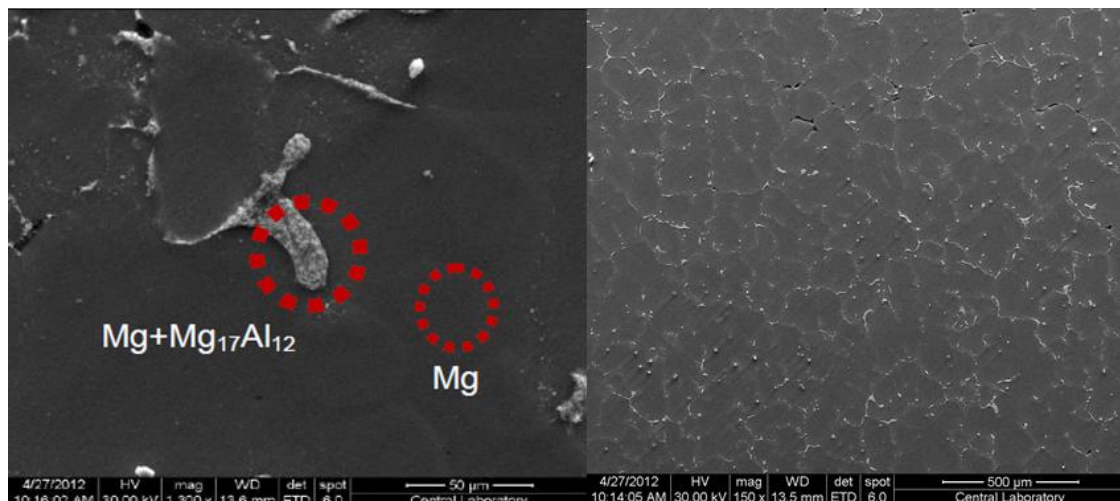


Figure 4.30 The precipitate distribution in the matrix and along the grain boundaries of the AZ91 sample which was aged at 250°C for 24 hrs.

The presence of Mn in AZ91 alloys was proved by EDS analysis which is shown in Figure 4.31, however due to low amount of Mn, these precipitates could not be observed easily. Eutectic “ $\alpha + \beta$ ” phases which normally are observed in cast AZ alloys [34] were not detected in the as-received AZ91 plates and in the homogenized samples due to the dissolution of this phase mixture during hot rolling and/or homogenization treatment (please refer to Figure 4.23).

Equiaxed grains and vast amount of “ β ” phases could be obviously seen in the microstructure of all aged and homogenized samples. According to the optic and SEM images of AZ91 samples, it could clearly be explained that the amount of “ β -Mg₁₇Al₁₂” precipitates and the aggregation of these intermetallics were increased significantly by increasing the aging duration. The average grain size was around 240 μm and there was not much change between the grain size values in the homogenized and the aged samples. More Investigations of these precipitates by utilizing XRD method will be discussed in the next section.

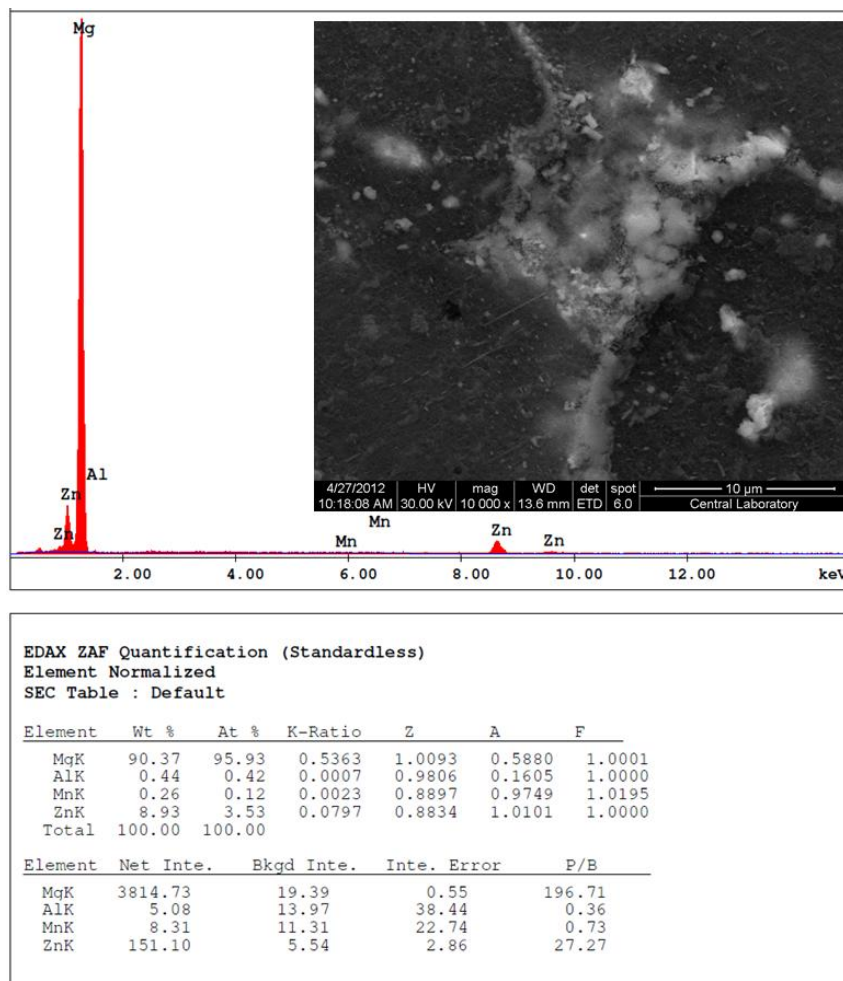


Figure 4.31 Energy Dispersive Spectroscopy of precipitates in AZ91 alloy

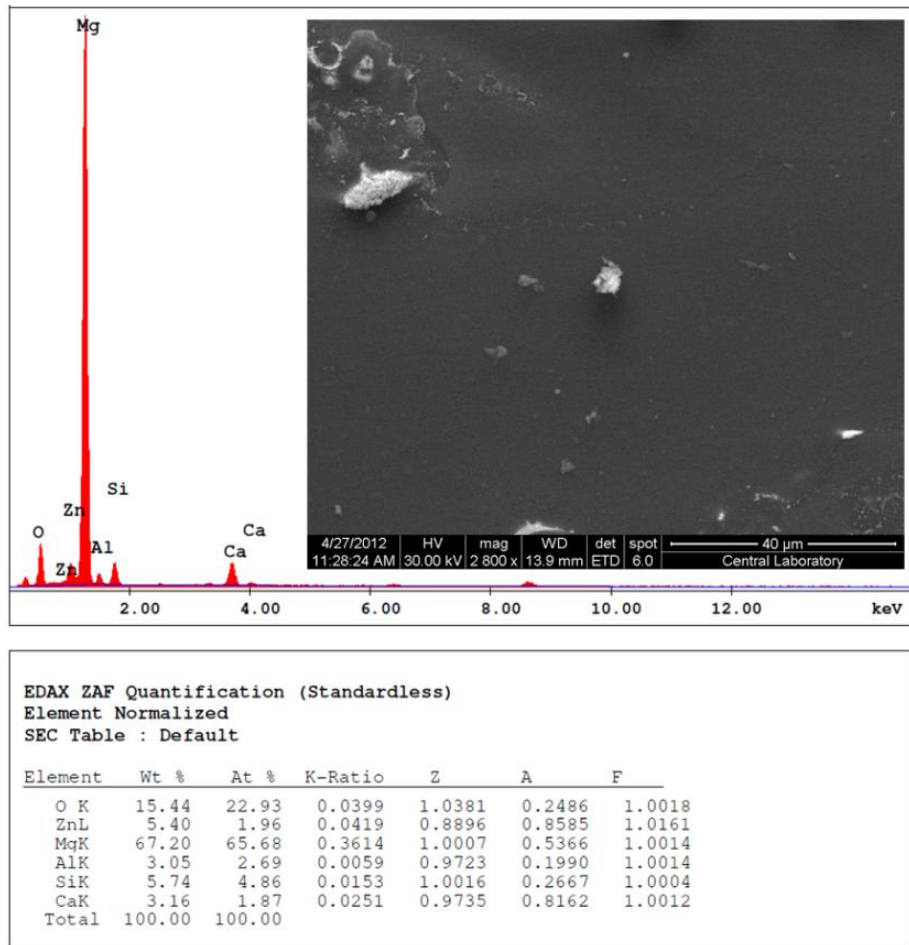


Figure 4.32 Energy Dispersive Spectroscopy of the shown region and presence of “Ca” and “Si” in AZ91 structure

4.2.2 Phase study in AZ91

As it is aforementioned before, X-ray analysis were performed to identify and estimate the amount of the phases in AZ91 samples as well. Figure 4.33 shows the XRD patterns of the aged samples at different temperatures for 24hrs in comparison with the XRD pattern of the homogenized sample.

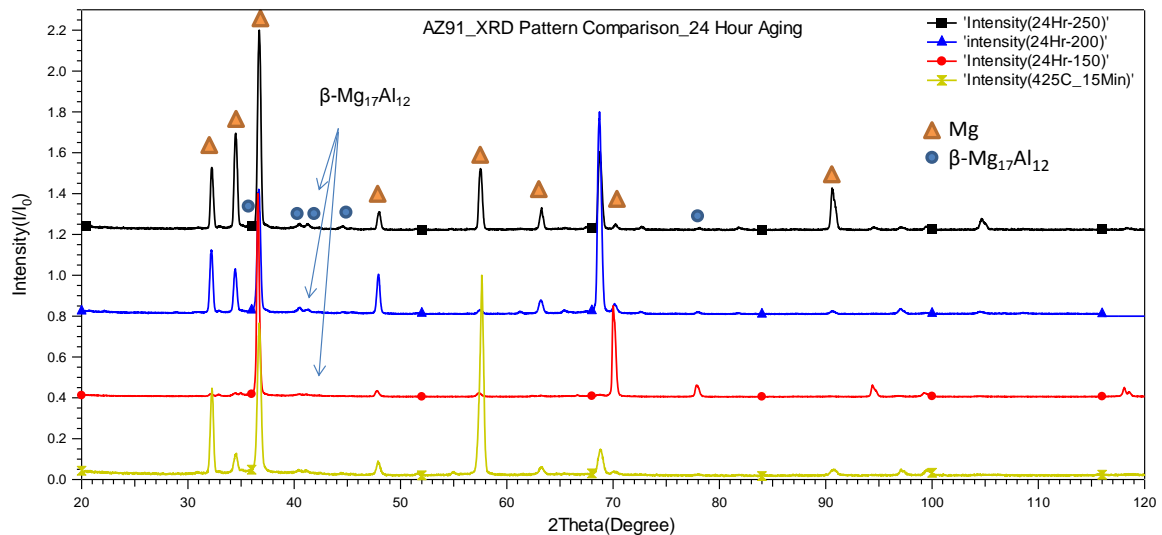


Figure 4.33 AZ91 XRD pattern comparison for 24 hours aging

Comparing the patterns of the 200°C and 250°C aged samples with the patterns in the literature, the presence of the “ β - $Mg_{17}Al_{12}$ ” precipitates in the matrix of our samples were proved as well. It is reported in the literature that there is a couple of low intensity peaks around $2\theta=40^\circ$ which are the identification peaks of the “ β - $Mg_{17}Al_{12}$ ” precipitates in AZ91 alloys[51]. Figure 4.33 shows the location of these peaks in the samples aged at 200°C and 250°C and in the homogenized sample. The specified triangles in this figure show the intensity of the matrix peaks of the AZ91 and the circles show the intensity of the β precipitate peaks.

The XRD investigations of the low duration aging heat treatments of AZ91 were performed on another AZ91 alloy bought from VIG-Metal industries in Turkey, This alloy was replaced later due to the micro-segregations and cast problems inside the alloy.

4.2.3 Aging under stress

Aging under stress experiments were performed after all the free aging treatments were finished and the effect of aging temperatures and durations on the microstructure of the samples was investigated. Aging under stress experiments were performed according to the parameters shown in Table 4.10.

Table 4.10 AZ91 aging under stress experiments

AZ91 Aging under stress experiments			
Duration (hour)	Temperature (°C)	Stress (MPa)	Load type
1	150	20	Tension
1	200	20	Tension
1	250	20	Tension
1	150	40	Tension
1	200	40	Tension
1	250	40	Tension
1	150	60	Tension
1	200	60	Tension
1	250	60	Tension
1	250	80	Tension

Figure 4.34 shows Figure 4.14 the stress vs time curves for the age-tensioned experiments at 250°C. The age-tensioning experiment at 250°C under 80 MPa constant stress could not be successfully performed till the end due to the creep failure of the sample. Furthermore, high temperature tensile test results from the ASM handbooks showed that 80MPa is a critical stress for AZ91 and this stress level is beyond the elastic range of the AZ91 at the elevated temperatures (please refer to Table 2.4).

Figure 4.35 demonstrates the stress vs time curves for age-tensioned experiments at 200°C. A closer look at the curves in this figure and Figure 4.34 show that there are stress drops under higher stress levels and also at higher temperatures. This was because of the high creep tendency of AZ alloy even at lower temperatures. We tried to avoid these drops by controlling the load rate of universal tensile test machine (UTM) manually during the experiments.

Figure 4.36 shows Figure 4.14 the stress vs time curves for age-tensioned experiments at 150°C. The amount of creep at 150°C was not so high and the machine held the samples under the required constant stress perfectly.

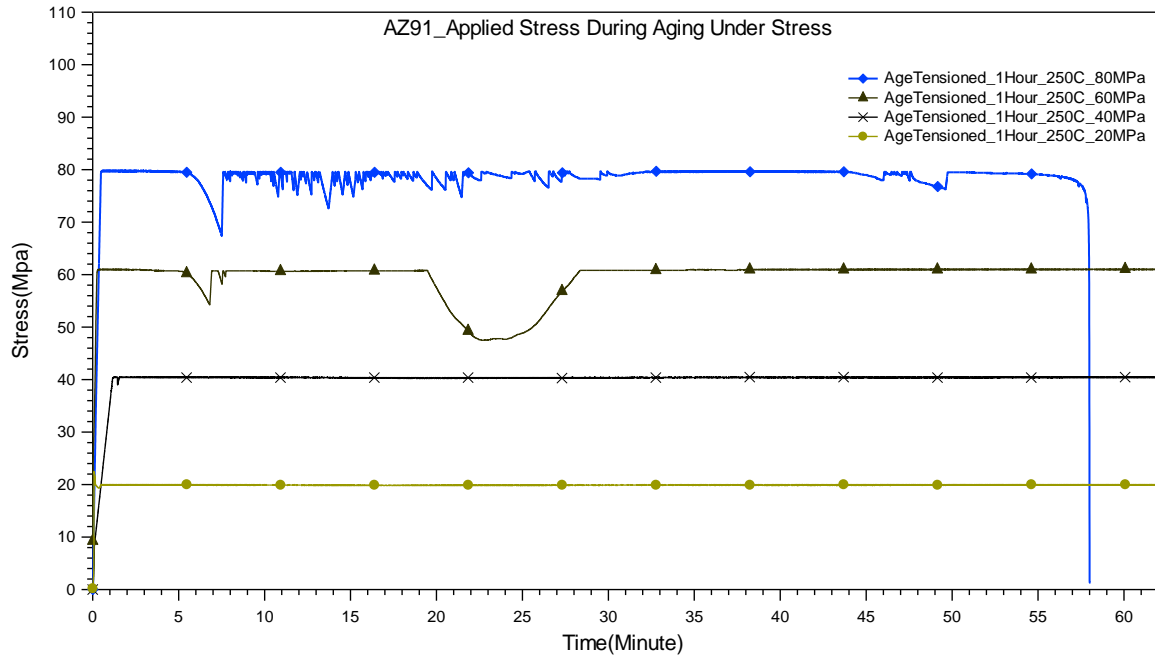


Figure 4.34 Applied stress vs Time curves for the samples aged at 250°C under 20, 40, 60 and 80MPa for 1hr.

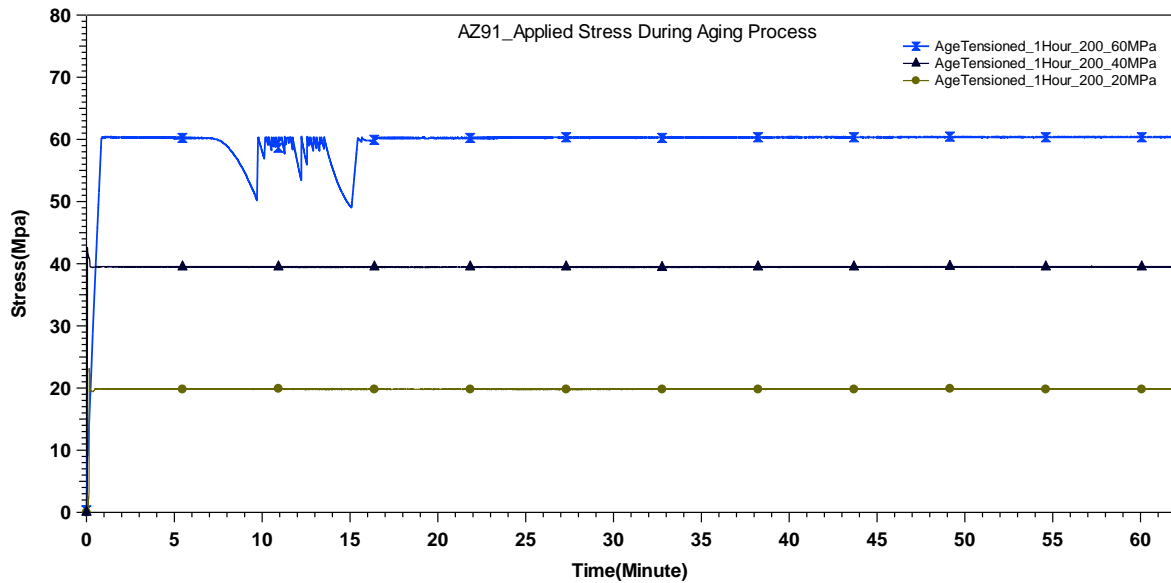


Figure 4.35 Applied stress vs Time curves for the samples aged at 200°C under 20, 40 and 60 MPa for 1hr.

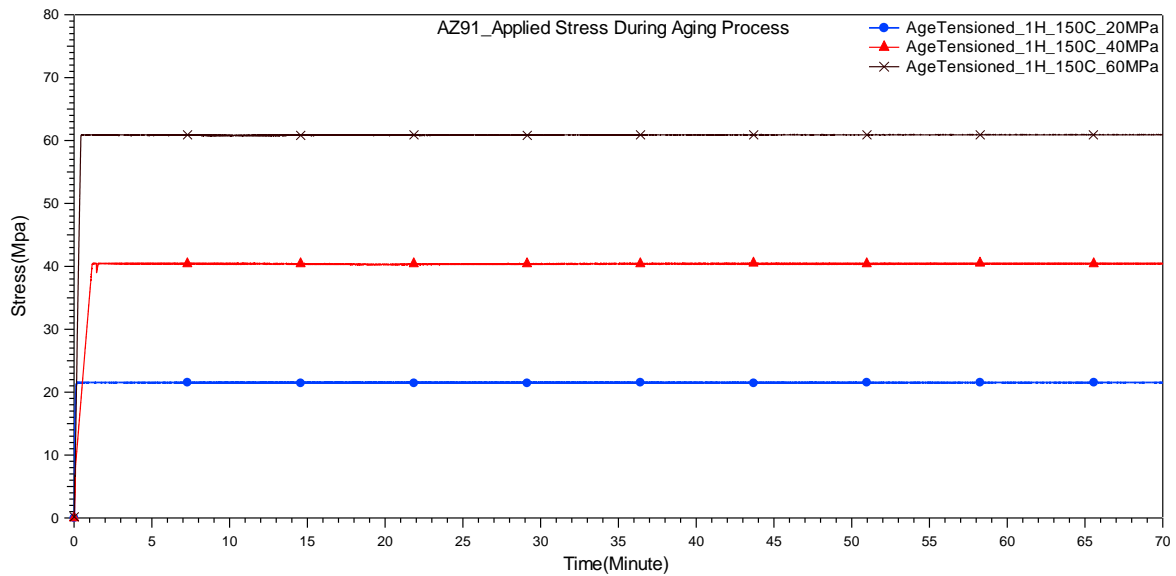


Figure 4.36 Applied stress vs Time curves for the samples aged at 150°C under 20, 40 and 60MPa for 1hr.

Figure 4.37 presents the microstructure of the thermo-mechanically heat treated samples at 250°C under 20MPa constant stress. The average grain size didn't change under the applied constant stress and it remained nearly the same in all aged and age-tensioned samples. There were some bright regions (Figure 4.37) which were revealed at grip section of the samples. These regions were not under the load like the gauge section of the sample. These bright regions were not present in any of the aged samples.

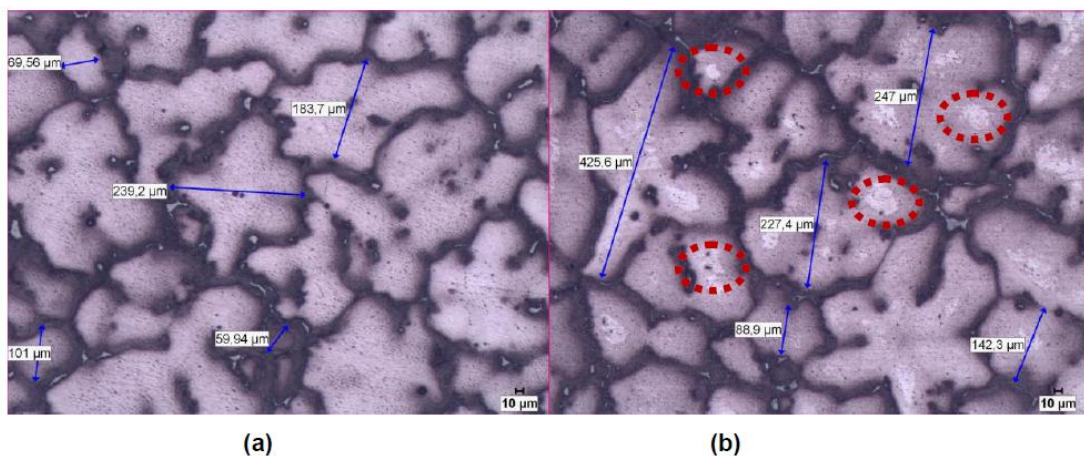


Figure 4.37 Microstructure of the aged-tensioned sample at 250°C for 1hr under 20MPa constant stress from the a) sample middle section b) grip section

Figure 4.38, Figure 4.39 and Figure 4.40 compare the microstructure of the age-tensioned samples at various temperatures under the 40MPa constant stress. These images were captured from the gauge section and the gripped section of the samples to compare the effect of the applied stress. The images show the possible grain directionalities in the direction of the applied stresses, however optical observations were not sufficient enough to prove this phenomenon and there is a need of further quantitative analysis.

Figure 4.41 shows a higher magnification of the grains and precipitates of the aged and age-tensioned samples at 250°C under 20 and 40MPa constant stresses. It seems that by increasing the applied stress value some of the precipitates were dissolved inside the matrix or forced to move inside the grains. Also some of the grains were forced to change their shape through the applied direction (Figure 4.41.a).

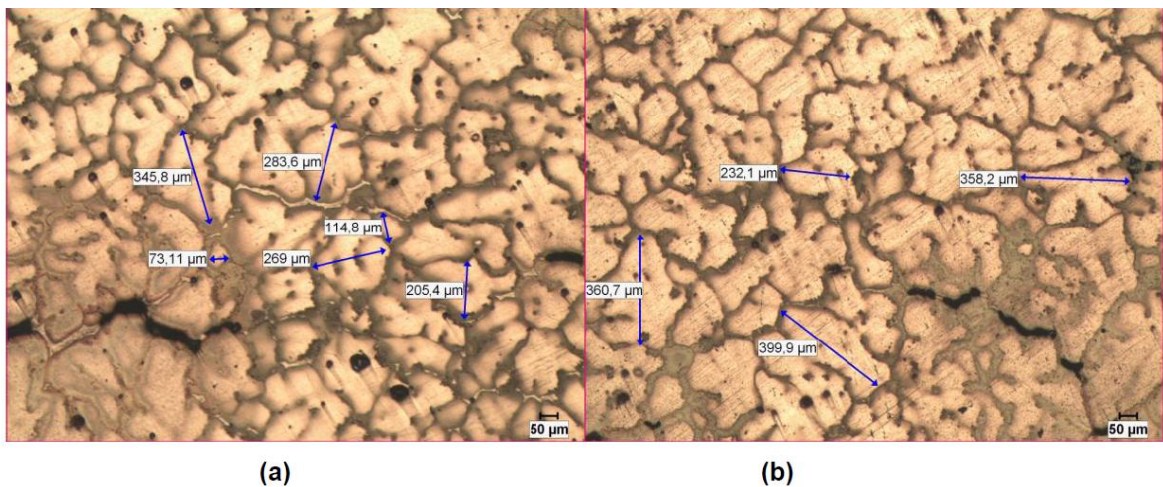
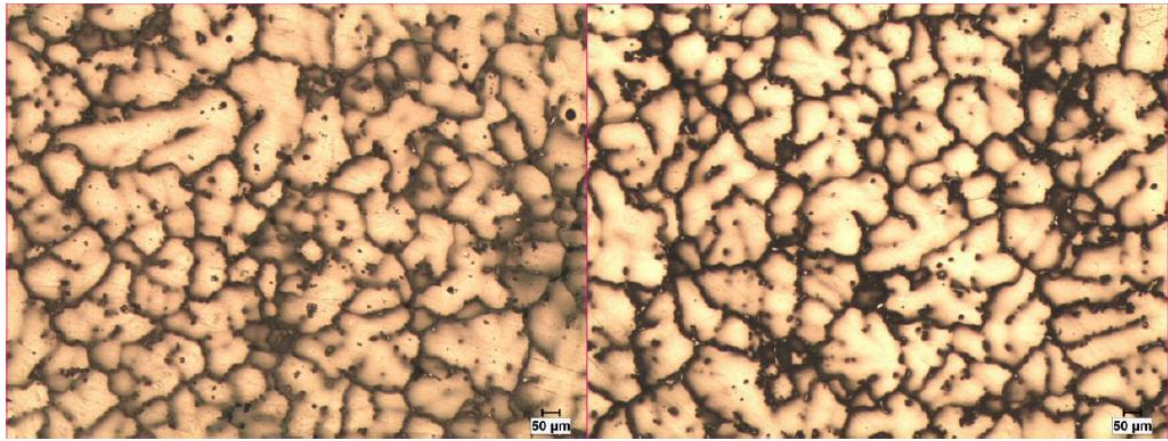


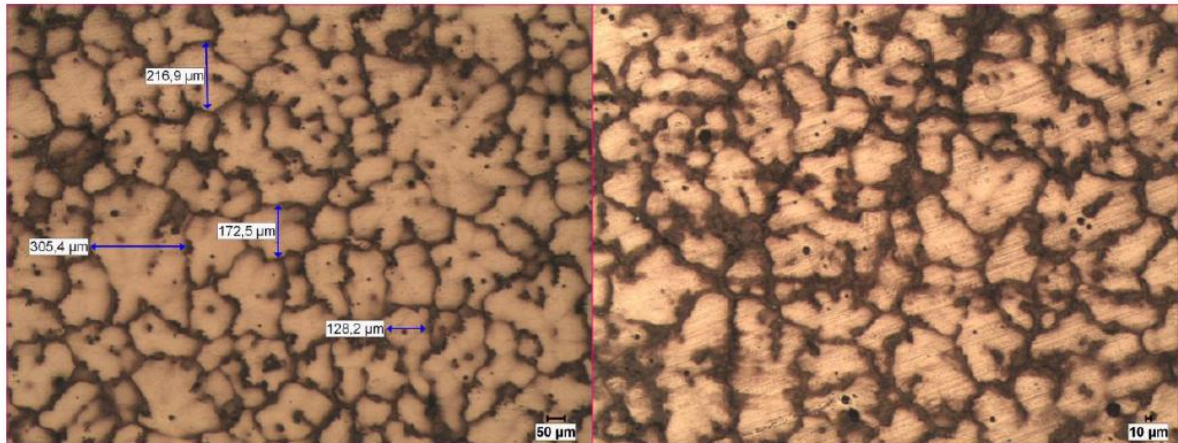
Figure 4.38 Microstructure of the age-tensioned sample at 150°C for 1hr under 40MPa stress from the a) sample middle section b) grip section



(a)

(b)

Figure 4.39 Microstructure of the age-tensioned sample at 200°C for 1hr under 40MPa constant stress from the a) sample middle section b) grip section



(a)

(b)

Figure 4.40 Microstructure of the age-tensioned sample at 250°C for 1hr under 40MPa constant stress from the a) sample middle section b) grip section

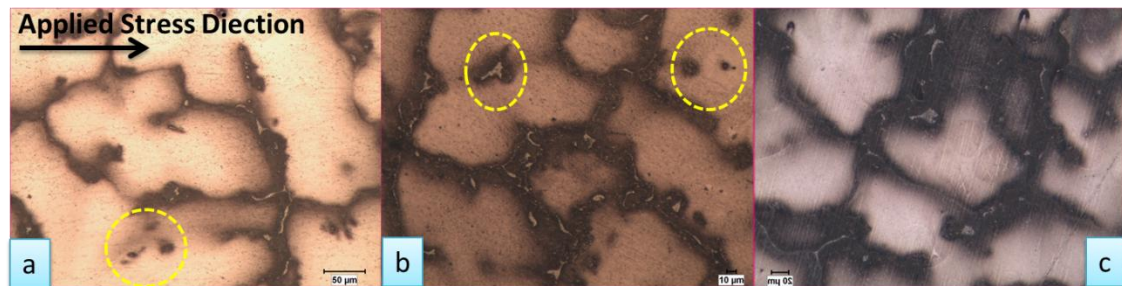


Figure 4.41 Microstructure of the age-tensioned samples at 250°C for 1hr under a) 40MPa b) 20MPa c) No Stress

Figure 4.42 shows a distribution of dislocations of the sample which was age-tensioned at 250°C for 1hr under 20MPa constant stress. It is believed that these might be the dislocations which are interacted and pinned by the precipitates in this age-tensioned sample. These dislocations were revealed at the stress induced section of the tensile coupon. It was shown that most of the dislocations were pinned by the precipitates.

As mentioned before, the precipitates are causing pinning effects and furthermore due to the pinning of the dislocations there is an increase in the strength of the materials. The precipitates stop dislocation movements and avoid the early fracture of the sample under lower stress levels. Tensile result for this sample shows better yield strength in comparison with the as-received and homogenized samples and interestingly, it shows better ductility comparing with the homogenized sample.

Revealing the dislocations in the microstructure of the samples using optical and/or scanning electron microscopy methods is a difficult task and we couldn't observe these dislocations in the microstructure of the other samples.

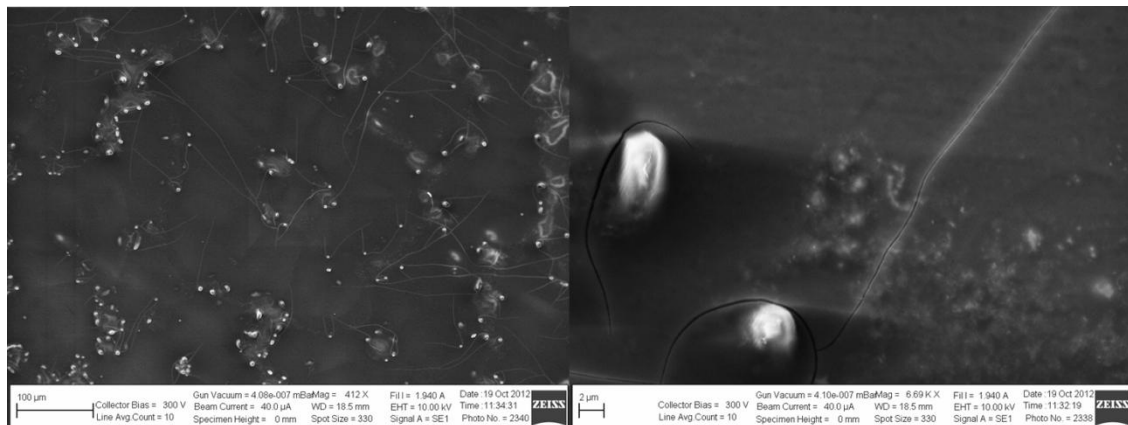


Figure 4.42 The dislocations and the precipitates in the microstructure of the sample which was age-tensioned at 250°C for 1hr under 20MPa constant stress

4.2.4 Tensile testing of AZ91

After all the aging and aging under stress experiments were performed and their microstructures were revealed, tensile tests were performed at room temperature to characterize the mechanical properties of thermo-mechanically treated samples.

Figure 4.43 shows the stress-strain curves of the samples aged at 150, 200 and 250°C for 1hr in comparison with the as-received and the homogenized samples. This figure shows that the strength and ductility of the homogenized sample decreased significantly in comparison with the as-received sample. This was because of the β precipitates in the matrix of the sample after performing homogenization heat treatment.

Later by performing the aging treatments, the strength and ductility of AZ91 tensile samples were improved again. For instance, the yield and ultimate tensile strength of aged samples at 150, 200 and 250°C for 1hr were increased significantly.

Optical microscopy images (please refer to Section 4.2.1 for more information) revealed the presence of high amount of continuous and discontinuous precipitates in the matrix of the AZ91 aged samples. Some of these precipitates were grown along the grain boundaries causing a great decrease in the elongation and a great increase in the amount of yield strength and UTS.

Figure 4.44 shows the tensile results of the samples aged for 1-5-24-50-100hrs and age-tensioned for 1hr at 150°C in comparison with the as-received and the homogenized samples. This figure shows that there is no need to age the AZ91 samples for long times to achieve higher strength and ductility. For instance, the age-tensioned sample under 60MPa constant stress showed close yield strength (140MPa) value to that of the 100hrs aged sample and the same ultimate tensile strength (250MPa) as well. Also, it showed higher ductility (11.83% strain) than that of the other aged and age-tensioned samples at this temperature.

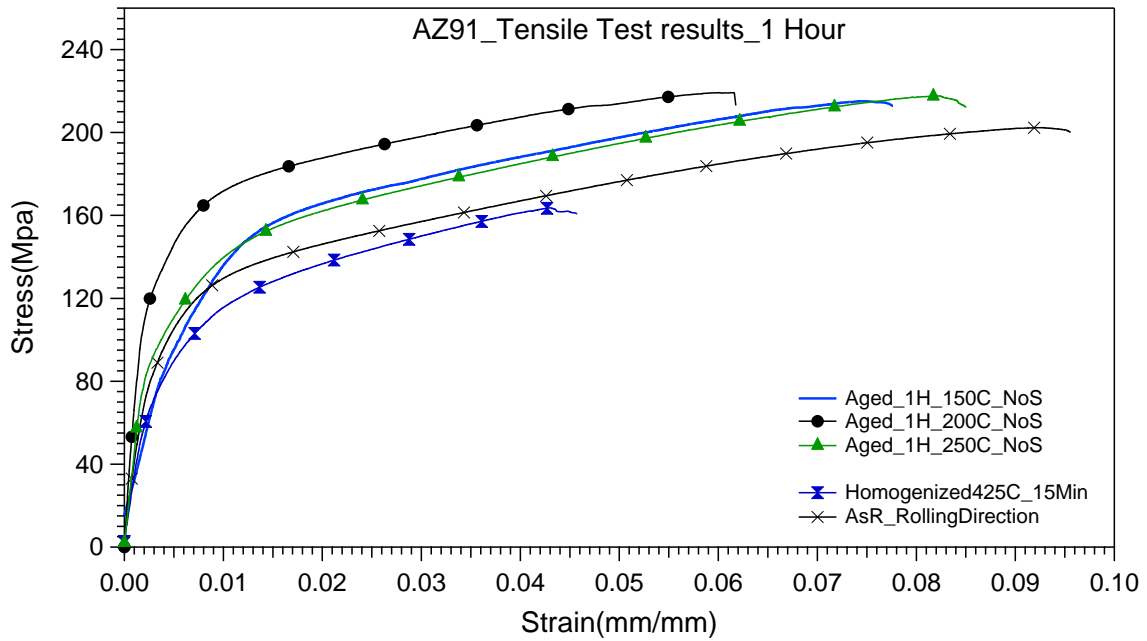


Figure 4.43 Tensile test results of the samples aged at 150, 200, 250°C for 1 hr, as-received and homogenized samples.

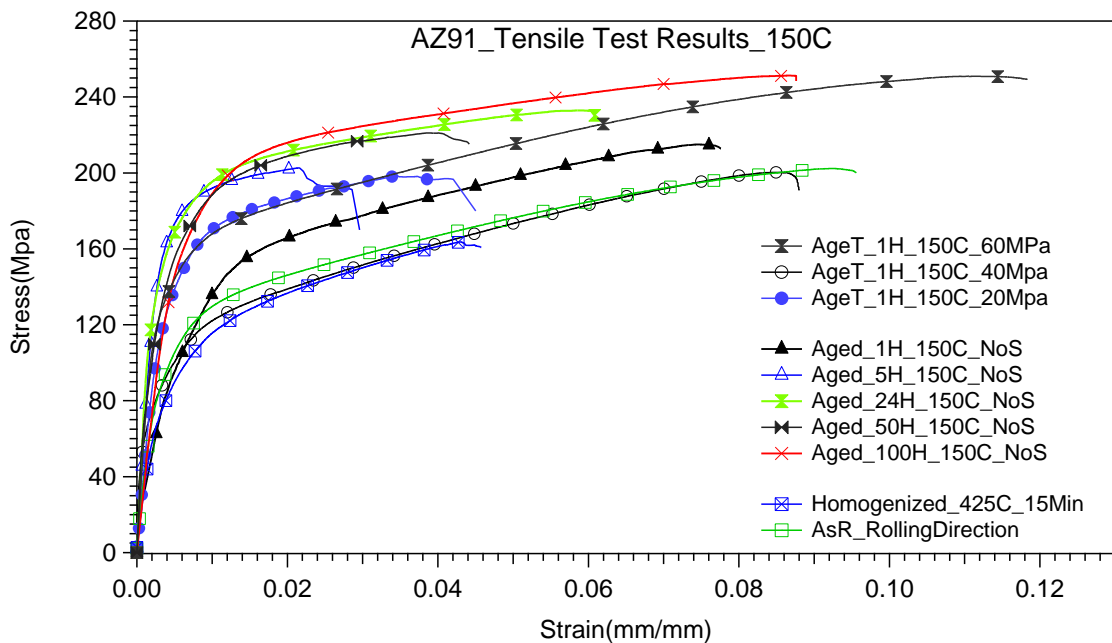


Figure 4.44 Tensile test results of the samples aged at 150°C for 1,5,24,50 and 100hrs under no stress and for 1hr under 20, 40 and 60MPa constant stress levels.

Figure 4.45 demonstrates the tensile results of the samples aged for 1-5-24-50-100hrs and age-tensioned for 1hr at 200°C in comparison with the as-received and the homogenized samples. The age-tensioned sample under 60MPa constant stress showed the highest yield strength and similar UTS like the 100hrs aged sample, however the ductility of the aged sample for 100hrs was 14% more than the age-tensioned sample.

Figure 4.46 presents the tensile results of the samples aged for 1-5-24-50-100hrs and age-tensioned for 1hr at 250°C. Again the age-tensioned sample under constant stress of 60MPa showed notable increase in the mechanical properties even among the samples which were thermo-mechanical treated at other temperatures. The elongation of this sample was the highest (13.44% strain) and its UTS was determined as 253MPa.

The increase in the mechanical properties of the age-tensioned samples might be because of possible precipitate orientations inside the matrix causing the increase in the strength and ductility of the samples, however this needs more investigations using advanced microstructure characterization methods such as transmission electron microscope.

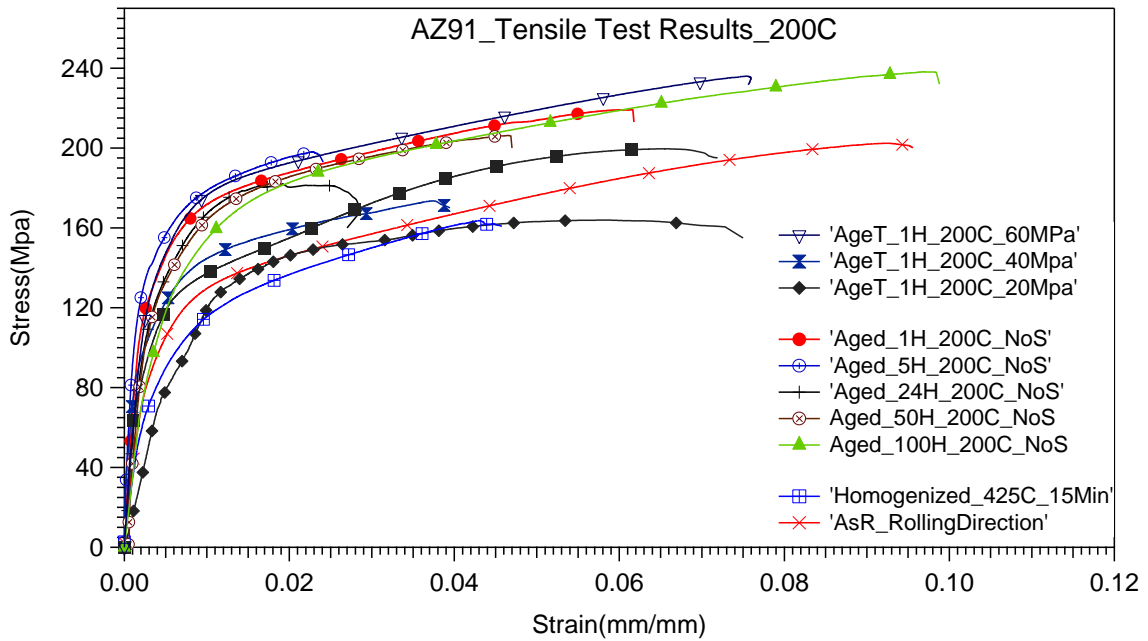


Figure 4.45 Tensile test results of the samples aged at 200°C for 1,5,24,50 and 100hrs under no stress and for 1hr under 20, 40 and 60MPa constant stress levels.

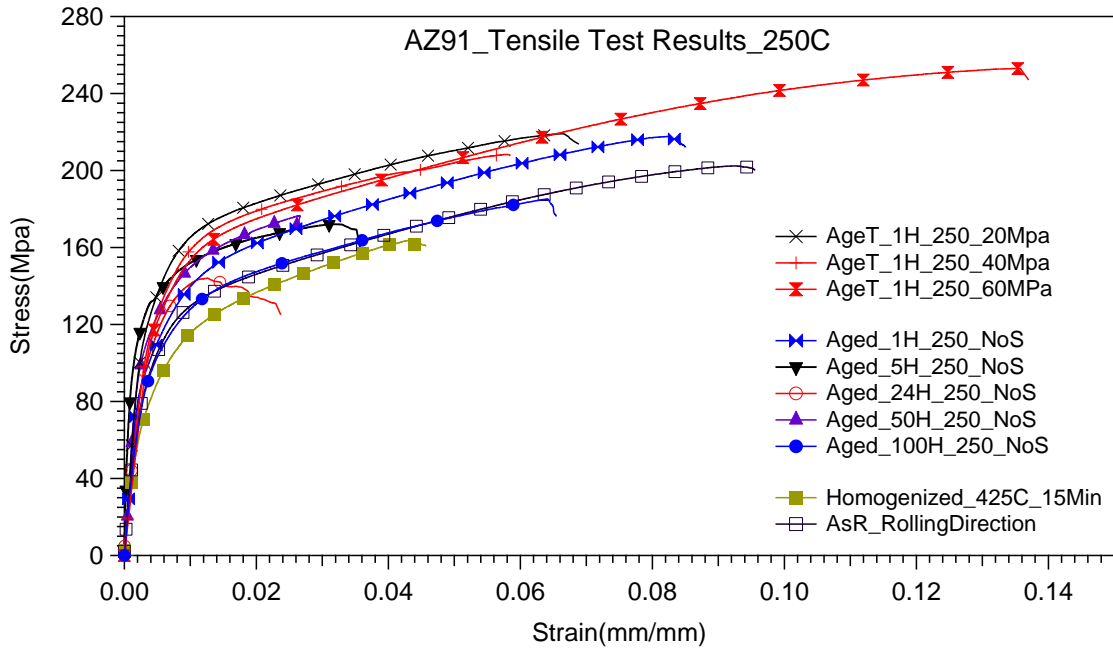


Figure 4.46 Tensile test results of the samples aged at 250°C for 1,5,24,50 and 100hrs under no stress and for 1hr under 20, 40 and 60MPa constant stress levels.

The analyses of the tensile curves of the AZ91 samples aged at different conditions were tabulated in Table 4.11, 4.12 and 4.13. The yield strength values from the curves were obtained using 0.2% offset method.

Table 4.11 AZ91 Tensile Properties for 150°C Heat Treatments

AZ91 Tensile Properties for 150°C Heat Treatments				
Heat Treatments	Elongation @ Fracture (%)	Yield Stress (MPa)	UTS (MPa)	ASM Metal Handbook Cast alloy, UTS : 230MPa, Elongation in 50mm: 3%
As-Received	9.6	96	202	
Homogenized	4.6	90	163.62	
1 Hour	7.76	91	215	
5 Hour	2.92	172	202.63	
24 Hour	6.1	160	232.87	
50 Hour	4.41	150	221.05	
100 Hour	8.66	165	251.31	
1 H – 20 MPa	4.50	109	198.99	
1 H – 40 MPa	8.80	86	200.21	
1 H – 60 MPa	11.83	140	250.91	

Table 4.12 AZ91 Tensile Properties for 200°C Heat Treatments

AZ91 Tensile Properties for 200°C Heat Treatments				
Heat Treatments	Elongation @ Fracture (%)	Yield Stress (MPa)	UTS (MPa)	ASM Metal Handbook Cast alloy, UTS : 230MPa, Elongation in 50mm: 3%
As-Received	9.6	96	202	
Homogenized	4.6	90	163.62	
1 Hour	6.2	137	219.2	
5 Hour	2.41	143	198.12	
24 Hour	2.87	130	180.97	
50 Hour	4.68	128.7	206.3	
100 Hour	9.64	133	238.15	
1 H – 20 MPa	7.5	100	163.81	
1 H – 40 MPa	3.9	110	173.5	
1 H – 60 MPa	7.61	145	236	

Table 4.13 AZ91 Tensile Properties for 250°C Heat Treatments

AZ91 Tensile Properties for 250°C Heat Treatments				
Heat Treatments	Elongation @ Fracture (%)	Yield Stress (MPa)	UTS (MPa)	ASM Metal Handbook Cast alloy, UTS : 230MPa, Elongation in 50mm: 3%
As-Received	9.6	96	202	
Homogenized	4.6	90	163.62	
1 Hour	8.5	105	217.6	
5 Hour	3.52	85.5	172.01	
24 Hour	2.29	114.5	144.07	
50 Hour	2.55	115.2	176.55	
100 Hour	6.49	97.5	185.21	
1 H – 20 MPa	6.8	131	219.03	
1 H – 40 MPa	5.8	133	208.3	
1 H – 60 MPa	13.49	127	253	

5 Summary of results, conclusions and future works

5.1 Summary of results and conclusions

In this work, we tried to enhance and examine the mechanical properties of the most conventional magnesium alloys by using two different methods. AZ31 and AZ91 alloys were aged at 150, 200 and 250°C for 1-5-50-100hrs and age-tensioned at 150, 200 and 250°C for 1hr.

The main purpose of this project was to enhance the low temperature deformation capability of the AZ31 and AZ91 alloys by considering three parameters (time, temperature, stress).

All of the related researches in the literature have shown that aging is being used to evolve the microstructure and properties of these alloys; however in this research we tried to examine the effect of a thermo-mechanical heat treatments (aging under stress) on the microstructure and the corresponding mechanical properties of the samples by conducting microstructure and phase characterization methods and also tensile tests at room temperature. Four constant stress values (20, 40, 60, 80MPa) at the elastic range of the material at room temperature were applied to the samples as the third parameter.

In the following paragraphs, the most important results will be summarized and discussed as well.

Even though the alloy compositions were very similar to each other, the microstructures of the alloys were different from each other. In AZ31, “ β ” precipitates were mostly growing inside the grains however in AZ91, precipitates were growing along the grain boundaries. In AZ91 the precipitates start to appear even at 1 hour aged samples along the grain boundaries due to higher percentage of Aluminum in this alloy.

XRD and optical examinations of the AZ31 showed that 150°C heat treatments didn't have so much effect on the precipitate growth. However, in the sample aged at 150°C for 50 hours, the precipitates have been observed. β precipitates have also been observed in the samples aged at 250°C. Therefore, for the β precipitate formation in AZ31 alloy, either longer aging duration or higher aging temperature is necessary. XRD and optical examinations of the AZ91 showed higher amount of

the β precipitate formation. The peaks of the β precipitates appeared clearly in the pattern of the samples aged at 200°C and 250°C for 24hrs.

Homogenization heat treatment in AZ31 broke out the dendritic and cast structure due to recrystallization of the grains. In AZ91, " β " precipitates were dissolved inside the matrix during the homogenization treatment. Therefore, the strength of the alloy decreased significantly. The decrease in the ductility can be attributed to the surface oxidation during homogenization treatment.

The tensile tests of the AZ31 samples showed that aging under stress heat treatment for 1hr gives better results and there is no need to age the samples for longer times. For instance, aging under 20MPa constant stress at 200°C and at 250°C caused a great increase in mechanical properties of AZ31. The increase in mechanical properties of the sample age-tensioned at 250°C for 1hr under 20MPa constant stress in comparison with the as-received material is listed below:

- Ductility: 147%,
- Yield strength: 30%
- Ultimate tensile strength: 6.2%

On the other hand, the tensile tests of the AZ91 samples showed a great decrease in ductility and strength after homogenization due to the formation of the precipitates inside the matrix. The aging treatments recovered the mechanical properties of the homogenized samples. However aging under stress heat treatment for 1hr showed better results and there is no need to age the samples for long times. Aging the samples at 150°C and 250°C under 60Mpa constant stress caused a considerable increase in the mechanical properties of this alloy. For instance, the increase in mechanical properties of the sample age-tensioned at 250°C for 1hr under 60MPa constant stress in comparison with the as-received material is listed below:

- Ductility: 40%
- Yield strength: 32%
- Ultimate tensile stress: 25%

The effect of thermo-mechanical heat treatment on the evolution of mechanical properties of both AZ31 and AZ91 was remarkable.

5.2 Future works and suggestions

Here is the list of the possible future studies to investigate the effect of thermomechanical treatments on the mechanical properties of AZ31 and AZ91. These studies might be useful to understand the microstructural evolution and the effect of these evolutions on the low temperature deformation capabilities of the conventional AZ Mg alloys.

1. It will be a good idea to perform the thermomechanical treatments under constant compressive stress levels at the same temperatures and for the same aging durations to see the effect of the compressive type loadings. Mg alloys are known to be brittle and there is a tension-compression asymmetry in these alloys.
2. It will be a good idea to age the samples under the same constant stress levels for longer durations especially considering AZ91.
3. Further analysis with transmission electron microscope (TEM) should be performed to examine the possible precipitate orientations in the material.

References

- [1] Mordike, B. L. and Ebert, T., 2001, "Magnesium: Properties — applications — potential," *Materials Science and Engineering: A*, vol. 302, pp. 37-45,
- [2] C. Blawert, N. H. a. K. U. K., 2004, "Automotive applications of magnesium and its alloys," vol. 57, pp. 397-408,
- [3] Housecroft, C. E. and Sharpe, A. G., 2012, *Inorganic chemistry*, 4th ed. Harlow, England ; New York: Pearson.
- [4] Ash, R., 2000, *The top 10 of everything 2001*. London: Dorling Kindersley.
- [5] Turekian, K. K., 1968, *Oceans*. Englewood, Cliffs, N.J.,: Prentice-Hall.
- [6] Mordike, B. L. and Kainer, K. U. E., 1998, *Magnesium alloys and their applications*. Frankfurt: Werkstoff-Informationsgesellschaft.
- [7] Polmear, I. J., 1995, *Light alloys : Metallurgy of the light metals*. London: Arnold.
- [8] Association, I. M., 2010, "Annual worldwide magnesium production at 2010", ed: International Magnesium Association.
- [9] Korea, P., 2008, "General forming processes for az31 alloy," ed. South Korea: Posco. .
- [10] Avedesian, M. M. and Baker, H., 1999, *Magnesium and magnesium alloys*. Materials Park, Ohio: ASM International.
- [11] Elvers, B. and Ullmann, F. E. o. i. c., *Ullmann's encyclopedia of industrial chemistry*, 7th, completely rev. ed. / [editor-in-chief, Barbara Elvers]. ed.: Weinheim : Wiley-VCH, c2011-.
- [12] Friedrich, H. E. and Mordike, B. L., 2006, *Magnesium technology : Metallurgy, design data, automotive applications*. Berlin ; [Great Britain]: Springer.
- [13] International, A., 1985, *Asm handbook: Formerly ninth edition, metals handbook. Metallography and microstructures*: ASM International.
- [14] Emley, E. F., 1966, *Principles of magnesium technology*, 1st ed. Oxford, New York,: Pergamon Press.
- [15] (1996). *Binary alloy phase diagrams* (1.0. ed.).
- [16] Friedrich, H. E. and Mordike, B. L., 2006, *Magnesium technology : Metallurgy, design data, applications*. Berlin ; New York: Springer.
- [17] Hono, K., Mendis, C. L., Sasaki, T. T., and Oh-ishi, K., 2010, "Towards the development of heat-treatable high-strength wrought mg alloys," *Scripta Materialia*, vol. 63, pp. 710-715,

- [18] Nakaura, Y., Watanabe, A., and Ohori, K., 2006, "Microstructure and mechanical properties of az31 magnesium alloy strip produced by twin roll casting," *Materials transactions*, vol. 47, p. 1743,
- [19] Zhao, H., Li, P., and He, L., 2012, "Microstructure and mechanical properties of an asymmetric twin-roll cast az31 magnesium alloy strip," *Journal of Materials Processing Technology*, vol. 212, pp. 1670-1675,
- [20] ASM International. Handbook Committee., 1990, *Asm handbook*, 10th ed. Materials Park, OH: ASM International.
- [21] Smallman, R. E. and Bishop, R. J., 1999, *Modern physical metallurgy and materials engineering : Science, process, applications*, 6th ed. ed. Oxford: Butterworths Heinemann.
- [22] Callister, W. D. and Rethwisch, D. G., 2008, *Fundamentals of materials science and engineering : An integrated approach*, 3rd ed. Hoboken, NJ: John Wiley & Sons.
- [23] Balasubramanian, S. and Anand, L., 2002, "Plasticity of initially textured hexagonal polycrystals at high homologous temperatures: Application to titanium," *Acta Materialia*, vol. 50, pp. 133-148,
- [24] Zhu, Y. T. and Langdon, T. G., 2005, *The langdon symposium : Flow and forming of crystalline materials*: Elsevier.
- [25] Bhattacharya, B., Science, M. U. D. o. M., and Engineering, 2006, *Plastic deformation behavior of pure magnesium in the temperature range 4.2k--300k*: McMaster University.
- [26] Nihon Kinzoku Gakkai., "Transactions of the japan institute of metals," ed. Sendai, Japan: Japan Institute of Metals.
- [27] Roberts, C. S., 1960, *Magnesium and its alloys*. New York,: Wiley.
- [28] Emley, E. F., 1966, *Principles of magnesium technology*. Oxford: Pergamon.
- [29] Schmid, E. and Boas, W., 1950, *Plasticity of crystals with special reference to metals*. London,: F.A. Hughes.
- [30] Polmear, I. J., 1995, *Light alloys : Metallurgy of the light metals*, 3rd ed. New York: J. Wiley & Sons.
- [31] Peckner, D., 1964, *The strengthening of metals*. New York: Reinhold ; London : Chapman and Hall.
- [32] Kelly, A. and Nicholson, R. S., 1971, *Strengthening methods in crystals*. Amsterdam ; London: Elsevier.
- [33] Kaya, A. A., Duygulu, O., Ucuncuoglu, S., Oktay, G., Temur, D. S., and Yucel, O., 2008, "Production of 150 cm wide az31 magnesium sheet by twin roll casting," *Transactions of Nonferrous Metals Society of China*, vol. 18, Supplement 1, pp. s185-s188,

- [34] Ebrahimi, G. R., Maldar, A. R., Ebrahimi, R., and Davoodi, A., 2010, "The effect of homogenization on microstructure and hot ductility behaviour of az91 magnesium alloy," *Kovove Materialy-Metallic Materials*, vol. 48, pp. 277-284,
- [35] Xu, S. W., Kamado, S., and Honma, T., 2011, "Effect of homogenization on microstructures and mechanical properties of hot compressed mg–9al–1zn alloy," *Materials Science and Engineering: A*, vol. 528, pp. 2385-2393,
- [36] Yakubtsov, I. A., Diak, B. J., Sager, C. A., Bhattacharya, B., MacDonald, W. D., and Niewczas, M., 2008, "Effects of heat treatment on microstructure and tensile deformation of mg az80 alloy at room temperature," *Materials Science and Engineering: A*, vol. 496, pp. 247-255,
- [37] Koike, J., Kobayashi, T., Mukai, T., Watanabe, H., Suzuki, M., Maruyama, K., and Higashi, K., 2003, "The activity of non-basal slip systems and dynamic recovery at room temperature in fine-grained az31b magnesium alloys," *Acta Materialia*, vol. 51, pp. 2055-2065,
- [38] Sasaki, T. T., Yamamoto, K., Honma, T., Kamado, S., and Hono, K., 2008, "A high-strength mg–sn–zn–al alloy extruded at low temperature," *Scripta Materialia*, vol. 59, pp. 1111-1114,
- [39] Singh, A., Somekawa, H., and Mukai, T., 2007, "Compressive strength and yield asymmetry in extruded mg–zn–ho alloys containing quasicrystal phase," *Scripta Materialia*, vol. 56, pp. 935-938,
- [40] Materials, A. S. f. T., 1917, *A.S.T.M. Standards: American Society for Testing Materials*.
- [41] Ebrahimi, G. R., Maldar, A. R., Ebrahimi, R., and Davoodi, A., 2011, "Effect of thermomechanical parameters on dynamically recrystallized grain size of az91 magnesium alloy," *Journal of Alloys and Compounds*, vol. 509, pp. 2703-2708,
- [42] Bulian, W. and Fahrenhorst, E., 1944, *Metallography of magnesium and its alloys*. [S.l.]: F. A. Hughes & Co Ltd.
- [43] Cook, R., Grocock, P. G., Thomas, P. M., Edmonds, D. V., and Hunt, J. D., 1995, "Development of the twin-roll casting process," *Journal of Materials Processing Technology*, vol. 55, pp. 76-84,
- [44] Kim, Y. M., Yim, C. D., and You, B. S., 2007, "Grain refining mechanism in mg-al base alloys with carbon addition," *Scripta Materialia*, vol. 57, pp. 691-694, Oct
- [45] Marya, M., Hector, L. G., Verma, R., and Tong, W., 2006, "Microstructural effects of az31 magnesium alloy on its tensile deformation and failure behaviors," *Materials Science and Engineering: A*, vol. 418, pp. 341-356,
- [46] Ben-Hamu, G., Eliezer, D., and Shin, K. S., 2007, "The role of si and ca on new wrought mg–zn–mn based alloy," *Materials Science and Engineering: A*, vol. 447, pp. 35-43,

- [47] Kim, Y. M., Yim, C. D., and You, B. S., 2007,"Grain refining mechanism in mg–al base alloys with carbon addition," *Scripta Materialia*, vol. 57, pp. 691-694,
- [48] Liang, P., Tarfa, T., Robinson, J. A., Wagner, S., Ochin, P., Harmelin, M. G., Seifert, H. J., Lukas, H. L., and Aldinger, F., 1998,"Experimental investigation and thermodynamic calculation of the al–mg–zn system," *Thermochimica Acta*, vol. 314, pp. 87-110,
- [49] Liu, S. W., Jiang, H. C., Li, X. Y., and Rong, L. J., 2010,"Effect of precipitation on internal friction of az91 magnesium alloy," *Transactions of Nonferrous Metals Society of China*, vol. 20, pp. S453-S457, Jul
- [50] Guan, Y. C. and Zhou, W., 2008,"Calorimetric analysis of az91d magnesium alloy," *Materials Letters*, vol. 62, pp. 4494-4496, Dec 15
- [51] Lin, L., Wang, F., Yang, L., Chen, L. J., Liu, Z., and Wang, Y. M., 2011,"Microstructure investigation and first-principle analysis of die-cast az91 alloy with calcium addition," *Materials Science and Engineering: A*, vol. 528, pp. 5283-5288,

Curriculum vitae

Personal Information:

Date & Place of Birth: 21 April, 1986, Miyandoab, IRAN

High School: Meshkat , major: Mathematics & Physics

B.Sc.: Tabriz Azad University

Honors & awards:

- ✓ TURKISH NSF 3501 Project Scholarship, Enhancement & characterization of Mg alloys
- ✓ Full Scholarship, for attending “Materials simulation across scales” winter school and join MESAM lab. at Texas A&M university
- ✓ Full Scholarship, to join LEMTA lab. at University of Lorraine as a visiting scholar student
- ✓ Being accepted at State/Public Exemplary School through a province-based exam

Publications:

- ✓ Attari V., Kockar B., “Stress and deformation analysis of NiTi and TiNb shape memory alloy mini-plate systems for the treatment of atrophic mandibular fractures” European Symposium on Martensitic Transformations (ESOMAT2012), Saint-Petersburg , Russia , Sep. 2012
- ✓ Attari V., Sorkhabi A.H., “Finite Element Study of effects of mechanical and physical specifications of 2.25 Cr-1Mo Steel in welding zones at Butt welding method” 10th National Conference on welding and inspection , Tehran , Iran , Oct 2009. (in Farsi)

Academic abroad research opportunities:

- ✓ Visiting scholar student at “Texas A&M University” , Fe-Based SMAs
- ✓ Visiting scholar student at “Université de Lorraine” , SMAs simulation

Language skills:

- ✓ Azerbaijani: Mother tongue
- ✓ Farsi: National Language
- ✓ Turkish(TÖMER Diploma)
- ✓ English
 - TOEFL®-IBT taken 06-15-2012
 - Total score: 90 (Reading 19, listening 27 , speaking 22, writing 22)
- ✓ French: Beginner
- ✓ Arabic : fair

Job history:

- ✓ Graduate Research Assistant, Hacettepe University, Ankara, Turkey
- ✓ R&D Engineer, Bonyan Diesel Co., Tabriz, Iran
- ✓ Vessels & Strainer Manager, Petrochemical Co., Tabriz, Iran
- ✓ Technical Office Employee, Khazar Kav Co., Tabriz, Iran